NASA Contractor Report 165660

NASA-CR-165660
19810011558

APPLICATION OF SUPERCONDUCTING COILS TO THE NASA PROTOTYPE MAGNETIC BALANCE

C. W. HALDEMAN, R. A. KRAEMER, S. W. PREY,
M. M. ALISHAHI AND E. E. COVERT

MASSACHUSETTS INSTITUTE OF TECHNOLOGY
Cambridge, Massachusetts 02139

NASA Grant NSG-1356
January 1981

National Aeronautics and
Space Administration

Langley Research Center
Hampton, Virginia 23665

PREFACE

This Final Report covers work performed on NASA Grant NSG 1356 between 1 January 1977 and 31 August 1980 under the Technical Cognizance of Mr. Richmond P. Boyden, Subsonic-Transonic Aerodynamics Division, NASA Langley Research Center.

The authors would like to thank Dr. J.E.C. Williams of the Francis Bitter National Magnet Laboratory for many discussions that helped their choice of conductors and experimental technique.

The use of trade names in this paper is essential to a proper understanding of the subject material; their use in no way constitutes official endorsement, either expressed or implied, by the National Aeronautics and Space Administration.

THIS PAGE IS BLANK

TABLE OF CONTENTS

LIST OF FIGURES

LIST OF TABLES

Chapter I. INTRODUCTION

Magnetic model suspension and balance systems for wind tunnel use (1) have been designed, tested and used at M.I.T.'s Aerophysics Laboratory for over eighteen years. These research programs which have been funded by the USAF, NASA, Army Ballistics Research Laboratory and the Army Research Office among others have led us to explore the many unique capabilities of the magnetic balance for aerodynamic testing. Among these are the precise measurement of forces (2,3,4); the measurement of wakes behind cones (5,6), spinning bodies at angle of attack (7), and waverider type bodies (8); the accurate measurement of Magnus force on spinning bodies (9), and ring airfoils (10); as well as the production of forced simultaneous spinning and coning model motion in a subsonic flow (11).

Despite this background, which demonstrates the utility and durability of the magnetic model suspension and balance systems, no large-scale system has yet been constructed for use anywhere in the world.

Recently the National Aeronautics and Space Administration has moved in the direction of cryogenic working fluids which increases the Reynolds number by a factor up to 7. Hence it becomes possible to envision wind tunnel testing of models at near full scale Reynolds numbers. The existence of such a tunnel makes it plausible to consider the use of superconducting or supercooled magnetic coils. It is possible in this way to either reduce the bulkiness of coils for a fixed force level, or to increase the force limits for a fixed coil volume. This application depends upon the perception of superconductors as useful technologies rather than a technological curiosity.

With the emergence of D.C. superconductors* as engineering materials for a number of large magnet applications, they should be considered for use in magnetic suspension systems not only for the reasons stated above but also because their use should greatly reduce the required operating power.

This report presents the results of a three and one-half year study of the feasibility of using superconductors for a general-purpose magnetic balance and suspension system.

Because superconductors lose their property of zero resistance when heated or when exposed to intense magnetic fields, successful application depends on careful understanding of each specific use, conductor design and physical environment. Because motion of

*A superconductor is one of a series of metals or compounds which when cooled to cryogenic temperatures near $4^{o}K$ offers no resistance to the flow of electric current. The physics of superconductors will be described briefly in Chapter II as needed to understand their application to magnetic balances.

magnetic fields through superconductors results in energy loss and local heating to some extent, only steady, direct current conduction can be maintained at fields above .1 Tesla without resistance. At the present time the design of superconductors for pure direct current applications is well understood. Applications for alternating current or changing field situations are still being evolved at a rapid rate. For magnetic balance operation the coils must supply a D.C. field to sustain steady loads. When model motion is encountered or is induced deliberately for dynamic measurements, the field must change rapidly.

The effort reported, therefore, evolved in four areas: study of superconductors to choose those types most suited for this application (12,13); construction and test of sample coils to compare conductors and verify methods of calculating A.C. losses in such coils (12); tests of two coupled coils to verify losses in one coil induced by changing current in another coil (13); and sample preliminary design of a superconducting coil array for the NASA prototype magnetic balance to provide a benchmark for comparison with the iron core normal coils in current use (14).

The results of the reported research indicate: that superconductors are highly feasible for magnetic balance and suspension systems; that large numbers of parallel fine individually insulated wires should be used as a conductor (superconducting litz cable); that these windings should be mechanically confined to provide LHe circulation and a plausible coil arrangement for such a balance is presented.

This study did not include determination of the best wire cross section for a given design nor the economic trade-off to determine for what combination of design parameters wholely superconducting coils, wholely normal coils, or a combination of superconducting and normal coils would be most economical.

Methods are presented for calculating magnetic fields and A.C. losses that appear suitable for magnetic balance design purposes.

Chapter II. SUPERCONDUCTORS AS APPLIED TO THE MAGNETIC BALANCE PROBLEM

Superconductivity

The superconducting state arises in certain materials through a pairing of electrons. These electron pairs interact with the crystal lattice through which they travel in a manner that produces zero resistance to the flow of electrons (15). This pairing of electrons is disrupted by temperature induced lattice vibrations. Internal voltage gradients caused by magnetic flux penetration accelerate electrons and also disrupt the pairing interaction.

Pure elements which exhibit the property of superconductivity are called Type I superconductors. Type I superconductors show no resistivity to A.C. or D.C. current and steady or varying magnetic fields unless extremely high frequencies are applied. However, the superconducting state is extinguished in Type I superconductors by the flux penetration caused by a field on the order of 0.1 Tesla or less. This makes Type I superconductors unsuitable for magnetic suspension systems.

Type II superconductors are metallic compounds and alloys which exhibit the property of regular magnetic subdivision into effectively normal and superconducting regions below about 21^{o}K. The superconducting regions are small enough so that they can be fully penetrated by magnetic flux without extinguishing the superconducting state. A transport current induced Lorentz force would cause viscous, steady and dissipative motion of flux quanta in a uniform lattice. Thus, a pure annealed Type II superconductor will not carry a transport current and is not suitable for magnet wire.

In real crystal lattices the network of imperfections in the form of vacancies, grain boundaries and impurities provide low energy sites for quanta of magnetic flux called fluxoids. These low energy sites produce a mechanism called flux pinning, which resists the movement of fluxoids in the superconducting matrix. Type II superconductors properly heat treated or cold worked to provide a large quantity of high pinning strength flux pinning sites can carry large transport currents and will do so under the influence of large magnetic fields.

Present Technology

The development of Type II superconductors for application to high field D.C. magnets and more recently for high field pulsed magnets and energy storage devices has led to the present day

superconducting coil wire technology. Type II compounds have higher flux pinning strengths than alloys and thus can support larger current densities under the influence of higher magnetic fields. However, the compounds lack ductility, making them difficult to work and susceptible to mechanical damage in handling. Such compounds such as Nb_3S_N provide the only conductors usable above 10 Tesla and for such applications the other difficulties are warranted.

Type II alloys such as Nb-Ti are tough and ductile, simplifying magnet construction. Their lower pinning strength (lower critical field and current density) is partially compensated for by higher filling factors in small wires, 30 percent to 60 percent being common. The alloy most successfully applied to engineering applications below about 8 Tesla is Niobium -- 47 percent Titanium alloy NbTi. These wires are made by co-drawing NbTi rods in a copper matrix.

Type II superconductors display zero resistance under D.C. conditions. The applied magnetic field can be varied through external means or by variations in the transport current of magnet coils. During changes in the applied magnetic field energy dissipation occurs within the superconductor and throughout the copper matrix of most modern wire configurations. This energy must be removed from the wire to prevent a significant temperature rise that would extinguish the superconducting state.

At present the most common means of accomplishing energy removal is through the boiling of the liquid helium bath surrounding the conductor which cools it to and maintains it at a superconducting temperature. 42.5 watts will vaporize 1 liter per minute of liquid helium at its boiling temperature of $4.2^{O}K$ under one atmosphere. Almost 38,000 watts are required to boil 1 liter of water per minute at its 1 atmosphere boiling temperature. When a cost of several dollars per liter for liquid helium is considered, the economic aspects become apparent.

The physical limitation of liquid helium to carry away energy is the onset of film boiling which occurs at about 0.75 watts/cm^2. This presents no difficulties for the most part, except on a transient basis, since in a large coil this heating rate represents excessive boil-off.

When subjected to a magnetic field, a superconductor behaves quite differently from a theoretically perfect conductor. Consider a sample in a magnetic field, initially at zero strength. As the field strength is gradually increased, currents will begin to flow on the surface of the sample in a manner that maintains the field at zero strength in the bulk of the sample. This is true of both the superconductor and a "perfect" conductor. At

a certain critical field strength, designated H_c, the superconducting state is extinguished, and the ambient field penetrates the bulk of the sample. Assume also that the perfect conductor's perfect conducting state was also extinguished. Now begin to lower the field strength until H_c is reached from above. At this point the superconductivity and perfect conductivity are switched on again. As the field is further lowered, the perfect conductor will set up surface currents to oppose any change in the field within itself. Thus the field in the bulk will remain at H_c. The superconductor,* however, will immediately expel its interior field as soon as it becomes superconducting (Meisner effect).

Thus for a specimen in the superconducting state, the magnetic field in the interior is zero, independent of the history of the specimen. It behaves like a perfect diamagnet.

Penetration Depth and Coherence Length

The superconductor sets up current at its surface to exclude any fields present. These currents extend into the bulk of the sample a short distance λ. Typically this depth for exponential decay of a one-dimensional magnetic field is 20-200 nm (200-2,000 Å).

Detailed models of this field decay process depend on the quantum mechanics of the lattice, the simplest being the London equation (16,13) for the London penetration depth.

$$\lambda_L = \left(\frac{mc^2}{4\pi n_s e^2}\right)^{1/2} \qquad 2.1$$

where n_s is the number density of superconducting electrons in the lattice. m,c and e have their usual meanings.

If n_s is expressed in terms of V_F, the Fermi velocity and N the total number of electrons and T is assumed=0, an expression for the smallest depth is obtained as

*True only for Type I superconductors. Because of the mixed state of Type II superconductors, field penetrates the bulk of the material in normal regions between the superconductor microstructure.

$$\lambda_L = \frac{3c^2}{8\pi N(0)V_F^2 e^2}^{1/2} \qquad 2.2$$

There is another length of importance in describing superconductors. This is the length over which the electron wave functions are coherent in the solid. This is called the coherence length ξ_0. For the London equation to be valid we must have $\lambda_L >> \xi_0$.

where $\xi_0 = .18 \frac{hV_F}{KT}$ 2.3

in terms of the thermal energy KT and Planck's constant.

These two lengths lead to the distinction between the two types of superconductors. For Type I superconductors $\lambda_L << \xi_0$. This means that the London equation is not valid and the penetration depth is given by Pippard (13) as

$$\lambda = \frac{3}{2\pi}^{1/3} \xi_0^{2/3} \lambda_L^{1/3} \qquad 2.4$$

Basic Properties

Type I superconductors are pure metals. In these the effective mass m is close to the free electron mass and λ_L is short, on the order of 20 nm (200 Å). Also, V_F is high, making ξ_0 long.

Type II superconductors include chemical compounds and high concentration alloys. These are characterized by longer penetration depths, around 200 nm (2,000 Å) and shorter coherence lengths, about 5 nm. Type I and Type II superconductors behave very differently in the presence of magnetic fields.

Type I superconductors behave like ideal superconductors. The Meisner effect is total up to H_c and below H_c they show zero resistance to either alternating or direct currents. Above H_c there is no retention of superconducting properties. Unfortunately, H_c, the thermodynamic critical field is low for all superconductors. This makes Type I superconductors unsuitable for use in magnet coils.

As the magnetic field surrounding a Type II superconductor increases, the Meisner effect is total until the field reaches the first critical field H_{c_1}. This field is smaller than the thermodynamic critical field H_c defined for all superconductors by:

$$\frac{H_c^2(T)}{8\pi} = F_n(T) \cdot F_s(T) \qquad 2.5$$

where F_n and F_s are the free energies of the normal and superconducting states. Below H_{c_1} a Type II superconductor behaves exactly as a Type I superconductor.

As the external field, H, is increased above H_{c_1}, flux gradually penetrates the sample, but the field in the interior remains less than if the sample were normal. An array of supercurrent vortices forms on the surface, penetrating the bulk of the superconductor. These vortices are called fluxiods and each contains one quantum of magnetic flux. This is often referred to as the "mixed state" as the superconductor has subdivided itself into effectively normal and superconducting regions.

If the field is increased further, there exists a field, called H_{c_2} at which the superconducting state is extinguished. H_{c_2} is generally quite high.

Thus there are three distinct ranges of magnetic field for the behavior of a Type II superconductor. For $H < H_{c_1}$ magnetic flux is totally excluded and behavior is ideal. For $H_{c_1} < H < H_{c_2}$, there is some flux penetration and behavior is less than ideal. For $H > H_{c_2}$ the sample is normal.

For most engineering applications the superconductor will be operated in the second range, $H_{c_1} < H < H_{c_2}$. This takes advantage of the high value of H_{c_2} for most superconductors. In this range the superconductor is in the "mixed state", the material is divided into a filamentary structure of normal and superconducting regions, and flux has penetrated in the form of the supercurrent vortices or fluxiods.

In a wire, a transport current flowing along the wire axis is perpendicular to the fluxiods and exerts a Lorentz force upon them. Where they are able to move, their movement will cause a dissipation of energy. Fortunately, grain boundaries and imperfections in the crystal lattice provide favorable sites for the fluxiods. In order for the fluxiod to move, the Lorentz force must be greater than some finite value. The ability of a Type II superconductor to resist fluxiod movement is called "pinning strength". Type II superconductors with high pinning strength are called "hard superconductors". Where fields are steady below H_{c_2} the fluxiods once pinned remain stationary and dissipate no energy. In a changing field, however, fluxiods must adjust to new field levels. As the field rises from zero initially, flux is excluded for a short time until the applied field equals H_{c_1}. Then the field begins to penetrate. Thus energy is taken from the changing field to move fluxiods from one site to another and shows up at the terminals much as ferramagnetic hysteresis does in iron core magnets.

This is referred to as hysteresis loss in superconductors and is the dominant loss mechanism in low loss fine wire bundles where transverse eddy currents cannot flow.

Calculation of A.C. Losses

Kraemer (12) has surveyed the literature for methods of calculating A.C. losses in superconductors. These methods vary widely and depend in the specific application because multiple loss mechanisms are present and only one or two are dominant in each engineering application. Kraemer found that at frequencies from D.C. to 30 Hz where magnetic balances operate copper matrix multifilament Nb-Ti or Nb_3S_n superconductors will have excessive eddy current losses.

The dominant loss mechanism in this regime is hysteresis, which can be reduced by fine filaments of superconductor. Since eddy current loss can be eliminated by using small individually insulated wires, a cable of copper stabilized insulated wires each having a superconducting core (superconducting litz cable) was selected for evaluation. The following methods of loss calculations were found to give reasonable results for this application.

The critical current is the lowest current that will drive the sample normal, and is greatest in low fields, and goes to zero at H_{c_2}. We will use the Kim (17) approximation:

$$J_c = \frac{J_0 B_0}{B+B_0} \qquad 2.6$$

J_c is the critical current density. B is the strength of the magnetic field. B_0 and J_0 are constants related to the self field of the conductor and the pinning strength.

A changing field perpendicular to the superconductor penetrates to a depth (18).

$$X = \frac{2\pi\Delta B}{\mu_0 J_c} \qquad 2.7$$

The interior field lags the changing exterior field until the field has fully penetrated the conductor. Thereafter, changes in applied fields appear instantaneously across the conductor. Thus the area of the hysteresis loop depends on whether the field can fully penetrate the wire.

For a wire of diameter d, the perpendicular field which fully penetrates is (19)

$$B_p = \frac{\mu_0 J_c d}{\pi} \qquad 2.8$$

while for a field parallel to the wire,

$$B_p = \frac{\mu_0 J_c d}{2} \qquad 2.9$$

For a cycling field $B_a \sin \omega t$, Carr (18,20) shows the loss in joules per cycle per m^3 of superconductor as,

$$\frac{W}{V} = \frac{256}{9\pi} \frac{B_a^3}{\mu_0^2 J_c d}, \quad B_a < B_p \qquad 2.10$$

When a transport current $I_a \sin \omega t$ is present, the loss should be multiplied by $(1+F^2)$, where $F=(I_a/I_c)$. $I_c=J_c \cdot A$, A = area of superconductor.

When B_a is greater than B_p (the changing field fully penetrates the wire), Carr (21) gives,

$$\frac{W}{V} = \frac{2}{3} B_a J_c d, \quad B_a > B_p, \text{ parallel} \qquad 2.11$$

and

$$\frac{W}{V} = \frac{8}{3\pi} B_a J_c d, \quad B_a > B_p, \text{ transverse} \qquad 2.12$$

Thus using the above equations, and given currents and coil configurations, the losses can be calculated. First, the local fields due to each coil must be calculated, then applied to Equations 2.10 and 2.12. For a large coil array this will require long but straightforward machine calculation.

Chapter III. CABLE CONSTRUCTION

Because the loss models available (12) indicated the superiority of fine, separately insulated strands of individually stabilized superconductor, the litz type cable was chosen for construction of sample coils. The size cables selected for test were chosen to provide a coil of similar size and field level encountered in the NASA prototype magnetic balance. Cable design must permit reasonably good packing factor combined with a means for penetration of the LHe into the bundle of wires. Several geometrical possibilities exist for construction of large cables. These will be discussed later. First the cable chosen for use on sample coils will be described.

Cables were constructed of sufficient strands of superconductor to provide a working design point of .6 Tesla central coil field at 200 amperes. To provide a margin of safety and allow for the local field concentration near the inside turn a superconductor area was chosen to provide a nominal short sample critical current of 600 amperes. Performance data on the superconductor is shown in Figure 1 from the manufacturer's data. All cables were fabricated by New England Electric Wire, Division of the Montgomery Co., in Lisborn, New Hampshire, for Supercon Inc. of Natick, Massachusetts, who manufactured the superconducting wire. Three cable designs were chosen:

Cable 1 - 220 strands .064 mm (2.5 mil) O.D. copper with .037 mm (1.4 mil) core of niobium titanium superconductor, 11x4x5 construction with polyurethane film insulation on individual wires, with nylon braid overall.

Cable 2 - Same as above except cabled from 55 strands of .122 mm (5 mil) O.D. copper, .074 mm (2.8 mil) diameter superconductor core, 11x5 construction.

Cable 3 - Same as above except cabled from 55 strands of .121 mm (5 mil O.D.) copper matrix with 54 filament superconducting core Cu/SC+2.1 with strand twist of 2 per inch.

Cable Construction

All cables were 5 bundle rope lay construction. In both 55 wire cables the cabling pitch was .5 inch and direction of lay was reversed between bundle and rope. An individual strand was measured and was found to be 2.4 percent longer than the final cable.

In the 220 wire cable the outer rope pitch was 1/2 inch. The intermediate bundle pitch was 1/4 inch and the inner bundle pitch was 1/2 inch. For this cable the wire length was 5.2% longer than the cable length.

Actual performance of the cables (from Supercon's data) is summarized in Table 1. This data is replotted along with the manufacturer's published performance in Figure 2. The wide variation in the two short samples of coil 4 multifilament cable wires caused Supercon to test longer (10 ft) samples. The long samples of the multifilament wire showed values of critical current approximately one-third below the specification data point at low fields. The wire had been degraded by broken filaments during drawing. Broken filaments were found when the copper was etched from samples of the wire to measure the filament diameter. Multifilament composite superconductors are not used in diameters as small as .12 mm (5 mil). Supercon had never before drawn this material into a wire this fine. This points to possible technical difficulties in attempting to adapt a high resistivity mixed matrix multifilament composite superconductor to dynamic magnetic suspension system requirements. The magnitude and rate of change of transport current and external fields will require small diameter wires for efficiency and stability. Tested values of critical current for the other two conductors were very close to the published specifications at low fields and were higher than specifications at high fields.

D.C. critical current measurements verified the reported critical current data. The highest magnitude of field in the coils exists in the center turn of the inner winding. This value of field was computed at various coil currents and is plotted in Figure 3 with the Supercon sample critical current data for the cable wire. The straight line interpolation between cable data (dashed lines) shows coils 3, 5 and 4 going normal at .88, .84 and .92 of test sample critical current respectively. A curve fit to the lowest three data points (dotted line) would raise the value for coil 5 to 92 percent of sample critical current while it would not affect the others much.

The failure to meet sample critical current may indicate that the coils exhibited degradation due winding motion. There was a significant amount of noise and one or two percent of 60 Hz A.C. ripple in the D.C. current that was used for critical current tests. These transients may have caused the early superconducting to normal transition. Also, the critical current had to be approached fairly rapidly (.5 to 1.0 amp per second above 350 to 400 amps) because the lead in wires were

Table 1

Critical Current Data on 3 Superconducting Litz Cables
Based on Nominal Superconductor Dimensions
I_{SC} in Amperes (10^3 A/sq mm)

Cable Construction	A_{SC} sq mm	1	2	3	4	6	8
2.5 mil 220 strand short sample	.219	740 (3.38)	495 (2.26)	-	440 (2.01)	330 (1.51)	-
5 mil 55 strand short sample	.218	731 (3.35)	561 (2.57)	-	346 (1.59)	313 (1.44)	-
5 mil 54 filament 55 strand short sample 1	.217	-	-	-	510 (2.35)	338 (1.56)	-
short sample 2		-	-	-	352 (1.62)	275 (1.27)	176 (.812)
(3m) long sample 1		462 (2.13)	352 (1.62)	313 (1.44)	297 (1.37)	-	-
long sample 2		412 (1.90)	286 (1.32)	264 (1.22)	220 (1.01)	198 (.912)	110 (.507)

not designed to carry critical current. This was because the excess heat leak into the helium dewar from the high conductivity copper wire was not wanted. The relatively rapid and unsteady (hand controlled) approach to critical current may also have contributed to the early transition.

Another possibility is that the actual field strength at the central turn of the inner coil winding was higher than estimated. This could very well be because the model used to estimate the field at points in the coil cross section assumed an even distribution of current density throughout the coil cross section and the self field of the wire was not considered. This is believed to be the cause of the discrepancy. The later calculations of Alishahi (14), Chapter V, use a more accurate current filament model.

The two coils (3 and 5) that actually failed during critical current tests did so at the center turn of the inner winding. This is where the field is the highest and thus indicates the extinguishing of superconductivity by reaching the critical field for the transport current density and not due to any instabilities, local training or poor cooling. The coils were easily repaired and the cables spliced and rewound. The performance of coil 3 after this procedure was exactly the same as before, indicating the ability of superconducting cable to be repaired after failure or damage. This is important for actual engineering use of the materials.

Photomicrographs of the cross section of the three conductors used in the test coil cables are shown in Figures 4 and 5. Samples of each kind of wire were chemically stripped of their electrical insulation and their diameters were measured. The copper was etched away and the filament diameters were measured. These same dimensions were measured under a microscope and from the photomicrographs. There was a significant difference between the dimensions obtained by these two methods. The magnification scale in the photomicrographs was suspected as the cause. The ratios of dimensions within the same conductor were taken from the photomicrographs but the absolute dimension scale was taken from an average of the outer diameter measurement from both methods. The geometries used for calculations are shown in Table 2.

Both solid conductor cables behaved as expected with respect to short sample critical current. The 54 filament wire, however, exhibited a large discrepancy in critical current between two short samples, as can be seen in Table 2. This was determined to be a result of breaks in the superconductor during drawing.

Table 2

Geometry of Superconducting Litz Cables

Dimensions in mm and sq mm
based on Micrographs of Cross Section

Cable	O.D. over Varnish	Bare O.D.	Nb-Ti Filament Diameter	Core Area	Copper Area	Cu:Sc	Cable Total S.C.	Cable Overall Diameter	Coil Number
220 strand solid core	.0711	.0605	.0367	1.059×10^{-3}	1.816×10^{-3}	1.71:1	.233	1.78	5
55 strand solid core	.135	.1223	.0737	4.261×10^{-3}	7.487×10^{-3}	1.76:1	.234	1.60	3
55 strand 54 filament core	.132	.121	.0097	4.031×10^{-3}	7.47×10^{-3}	1.85:1	.222	1.60	4

Because of the larger diameter of the 220 strand cable, coil 5 was wound with slightly fewer turns (378 turns) than coils 3 and 4, which had 390 turns. Fields were calculated using the actual numbers of turns after construction.

Cooling of Superconducting Litz Cable

In addition to providing low A.C. losses a mechanically constrained cable of fine wires provides an excellent heat transfer medium for transpiration or percolative cooling. This cooling process was tested using a test coil wound with normal copper litz cable. To compare the effect of epoxy impregnation another identical coil was wound, impregnated with epoxy resin and drained completely before curing. This left the cooling passages open but filled the voids between individual wires in the cable.

These normal copper coils were wound with four layers of 300/42 litz wire having an overall diameter of .062 inch. Coil 1 was dry wound and coil 2 was impregnated with epoxy resin.* Coil layout and winding detail are the same as the superconducting coils described in Chapter IV except for the number of layers which is six for the superconducting coils and four for the normal coils. Measurements in liquid nitrogen provided thermal conductivity data. Measurements in liquid helium provided boil-off data for flowmeter calibration. Resistivity data in helium could not be used because of the vanishing slope of the resistivity temperature curve for copper below 10°K (22). Studies since this experiment have indicated that Manganin or Constantan litz wire could be used and would give accurate temperature data (23). Data for coil resistance versus input power for the copper coils, Numbers 1 and 2, are given in Table 3. These data were plotted to permit smoothing the data before reading off values for calculations of the thermal conductivity using the following model.

As shown below in Figure 6, a long cylindrical litz cable of radius r_o is subject to a heat dissipation Q watts per unit length.

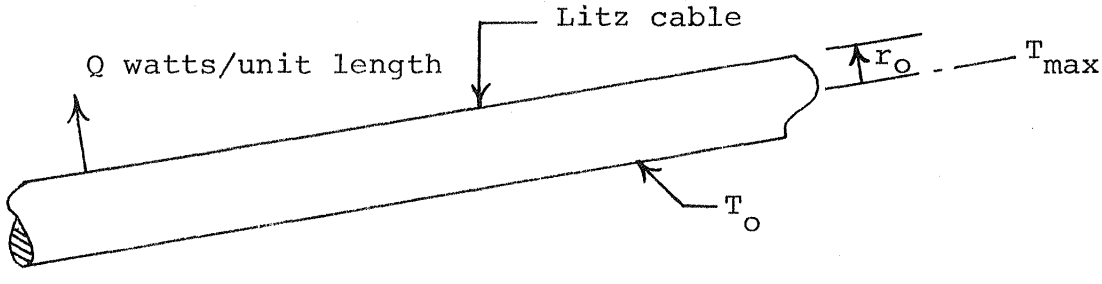

Figure 6 Litz Cable Cooling Model

*Emerson and Cuming's Eccoseal 1207.

Table 3

Power - Temperature Data for Copper Coils in Liquid Nitrogen

Coil 1 - Dry Wound

Power Watts	Watts/m	Watts/ft	R/R_{77}	R	$10^9\rho$	$\frac{[R/R_{77}-1]/.034}{\Delta T=(T_{av}-77^{\circ})}$	k Watts/$m^2/^{\circ}K/m$
30	.308	.095	1	.284	1.7	0	
450	4.62	1.42	1.0035	.285	1.706	.104	1.76
1000	10.27	3.16	1.0070	.286	1.712	.206	1.98
2000	20.54	6.32	1.0176	.289	1.73	.518	1.57
4000	40.95	12.6	1.0475	.2975	1.781	1.397	1.17

Coil 2 - Epoxy Impregnated

Power Watts	Watts/m	R (ohms)	$\frac{R}{R_{77}}$	$\frac{[R/R_{77}-1]/.034}{\Delta T=(T_{av}-77^{\circ})}$	k
3	.031	.360	1	0	
10	.103	.364	1.011	.323	.0127
40	.411	.373	1.036	1.059	.0154
150	1.54	.387	1.075	2.206	.0278
600	6.17	.405	1.125	3.676	.0668
1200	12.34	.426	1.183	5.382	.0912
3000	30.85	.500	1.389	11.44	.107
6000	61.71	.630	1.750	22.06	.111

Assume that:

1) The litz cable strands are perfectly transposed so that regardless of the temperature distribution, the resistance of each strand of the complete coil will be the same. This implies that the current density will be uniform across the cross section and that the measured resistance of the cable will be the resistance determined by the volume average temperature.

2) Cable outside temperature is uniform and equal to the coolant boiling point.

3) The cable can be modeled thermally as an isotropic material with thermal conductivity k and thus only radial temperature gradients will exist. (In fact, this means that the axial conduction down individual transposed wires which will take place will be included in the equivalent value measured for k.)

4) The radial temperature gradient is sufficiently small that variation of thermal conductivity across the cable can be neglected.

In the steady state the temperature is determined by

$$\frac{\partial^2 T}{\partial r^2} + \frac{1}{r}\frac{\partial T}{\partial r} + \frac{Q}{k\pi r_o^2} = 0 \qquad 3.1$$

Since wire resistance, $R=R_o\left[1 + \varepsilon(T-T_o)\right]$ to a linear approximation, the generation term will depend on T.

3.2

$$\text{Then } Q = I^2 R_o \left[1 + \varepsilon(T-T_o)\right] \qquad 3.3$$

$$\text{Let } Q^* = I^2 R_o / k\pi r_o^2 \qquad 3.4$$

Jakob (24) gives the solution for this case which is Bessel's equation for $(T-T_o)$.

$$T=T^{o} + \frac{1}{\varepsilon}\left[\frac{J_o \frac{r}{r_o}\sqrt{\varepsilon Q^* r_o^2}}{J_o(\sqrt{\varepsilon Q^* r_o^2})} - 1\right] \qquad 3\text{-}5$$

$$T_{max} = T_o + \frac{1}{\varepsilon}\left[\frac{1}{J_o(\sqrt{\varepsilon Q^* r_o^2})} - 1\right] \qquad 3.6$$

$$T_{av} = T_o + \frac{1}{\varepsilon}\left[\frac{2 J_1\left(\sqrt{\varepsilon Q^* r_o^2}\right)}{\sqrt{\varepsilon Q^* r_o^2}\, J_o(\sqrt{\varepsilon Q^* r_o^2})} - 1\right] \qquad 3.7$$

In the case where $\varepsilon \to 0$, the dissipation across the cross section is uniform and equal to Q^* evaluated with R_o determined at the average temperature. The solution in that case gives a parabolic temperature distribution

$$T=T_o+(1/4)Q^* r_o^2 \left[1-(r^2/r_o^2)\right] \qquad 3.8$$

$$T_{av} = T_o + (1/8)Q^* r_o^2 \qquad 3.9$$

$$T_{max} = T_o + (1/4)Q^* r_o^2 \qquad 3.10$$

In order to calculate k from experimental data the following steps are necessary:

1. Calculate T_{av} from voltage, current and R vs T for pure copper. Use the ratio R/R_{77}.

2. Calculate k_1 from 3.9 and the measured power dissipation. Substitute k_1 into 3.7 and calculate T_{av}.

3. Repeat with a new guessed value of k_1 until the measured value of T_{av} is matched.

Referring to the data (22), we can calculate ε between $50^{o}K$ and $100^{o}K$ as .0339. This is sufficiently small to use equation 3.9 for determination of conductivity. This has been done and the results are given for both coils in Table 3.

These results are very significant. Note that the effective thermal conductivity of the litz wire matrix is between 10 and 100 times higher when wetted by liquid nitrogen than when impregnated by epoxy resin. It should be noted that the 1207 resin used was unfilled and drained completely off the coil, leaving only a very thin coating, but filling the spaces between wires. Clearly, a mechanism exists for the liquid to penetrate and the vapor to escape from the cable during heating, since in liquid nitrogen 20 watts per meter of cable were dissipated with only a $.5^{o}K$ temperature difference between center and outside of the cable. It is believed the behavior in liquid helium was similar since no temperature rise could be detected up to about 2 watts per meter where boil-off was excessive.

These experiments indicate that superconducting magnetic balance coils should be constructed of mechanically-supported bundles of fine wires and should not be impregnated with resin. Thus the cable designs in Figure 7 having coolant pumped down the center of the litz cable appear to be a good approach for large magnet systems.

Individual Wire Cross Section

The sample cables tested showed the benefits of litz cable construction. Wire cross sections, however, were simply limited to solid core copper stabilized Nb-Ti and were sized at the smallest that could be obtained by current drawing techniques.

An alternate configuration appears capable of producing the same or lower A.C. losses than the smallest wire tested while requiring a drawn individual wire no smaller than 8 mills. This strand geometry is shown in Figure 8. Here the wire cross section consists of 6 copper stabilized Nb-Ti segments separated by 6 spokes of high resistance material such as cupro-nickel or Ti-Va-Al. This has the advantage of providing small filaments of Nb-Ti for low hysteresis loss, intimate contact with the stabilizing copper, high resistance transverse to the wire axis, and good external copper area for making solder joints.

Since the cost of making superconducting litz cable increases by a large factor for each reduction in strand diameter, this design would probably provide substantial savings over the solid core wire.

Since Nb-Ti is limited to those applications where fields are below about 8T, there is a need to apply litz cable techniques to Nb_3Sn superconductors which are useful up to 14T (25). The difficulty lies in providing strand insulation that will withstand the 700°C heat treating temperature after winding.

It appears that a cable similar to those evaluated in this report could be constructed using wires of the design shown in Figure 9 in a bundle with a quartz fabric braid. This is similar to Figure 8 with the urethane insulation replaced by Al_2O_3 formed by anodizing an aluminum cladding. Nb_3Sn would be formed by the bronze matrix technique (26) inside the copper sections. To achieve finer filaments of superconductor the Nb tubes could be replaced by bronze rods with Nb wires inside them with each rod wrapped in tantalum foil before inserting in the copper block for drawing. This type of cable might be required for magnetic balance coils to be used at Q=50 psi or above.

This Page Intentionally Left Blank

Chapter IV. SUPERCONDUCTING LITZ CABLE COIL TESTS

In order to measure the A.C. and D.C. performance of the proposed superconducting litz cable construction three coils were constructed using the three conductors described in the previous chapters. These were chosen to provide a comparison between two sizes of single filament wire .122 mm and .06 mm O.D. and between multifilament and single filament wire, both .122 mm O.D.

Coil Construction

Winding geometry was determined from tables of the field components for short axial coils (27) and the required central field of .6 Tesla at 200 amps. This field and current are approximately the design values for the NASA prototype.

Balance Magnetizing Coils

The outer dimensions of the coil were designed so that a commercially available 15.24 cm inside diameter silvered, evacuated, double wall glass dewar could be used as the liquid helium container during testing. Winding layers were separated by 2.38 mm to provide a passage for the flow of liquid helium and the escape of gas bubbles evolved during power dissipation. During cable design the cross section of the litz cables was estimated using graphs of packing factors based on experience with copper cables (28). The coil parameters were varied within the physical constraints required until a coil that would produce a 0.6 Tesla field at 200 amps and fit the physical restraints was obtained. The design coil had 390 turns in six layers of 65 turns each. The inner winding radius was 47.5 mm and the outer winding radius was 69.34 mm. The axial length of the design coil was .114 m. The spacing between the windings was designed to be 2.54 mm. The coil cross section is shown in Figure 10 and an axial section in Figure 11.

The coil form is machined out of G-10 fiberglass laminate with splines to provide cooling passages for the inner winding. Layer spacing is provided by spacer bars, also machined from G-10, which are retained by G-10 radial pins that thread into the coil form, Figure 11. The coils are wound with 27 NT (6 lb) tension on the wire. Figure 12 shows a completed coil with a 1.52 mm thick G-10 support sleeve to provide radial support outside the windings. The internal construction can be seen from Figure 13 taken during repair of a damaged coil.

The lead in cables are made from 11 parallel, 80 strand number 36, single polyurethane coated round braids. These were chosen because of their high flexibility and large heat transfer area for regenerative cooling by the boil-off helium.

When the actual cable was delivered it was determined that coils 3 and 4 could be wound with a row of G-10 spacers between the outer winding and the support sleeve. The cable for coil 5 was so large that only 63 turns could be wound on each layer and only .125 mm Mylar spacers would fit between the outer winding and the support sleeve. No failures ever occurred in the outer layer, however, despite its lower cooling.

Test coils were suspended by a section of G-10 fiberglass support pipe from a plywood platform 2M above the floor. The 130 mm I.D. pipe had a removable fiberglass separator down its center which cut the cross section into two electrically insulated semicircles. The separator was formed around two thin 15.87 mm I.D. G-10 fiberglass pipes. One of these off axis tubes provided support and guidance for inserting and withdrawing cryogenic fluid transfer tubes. The other off axis pipe was a guide pipe for the liquid level, indicating system and its wiring. This setup is shown in Figure 14.

The coil forms were attached by nylon screws to the end of the 1 m section of pipe so the coils were physically suspended from above. 25.4 mm diameter holes were milled into the portion of the coil form that would be above the liquid helium level. These allowed the gaseous helium to leave the experiment through the inside of the support pipe. All power and other electrical connections entered and left the helium dewar through the holes in the coil form and the interior of the support pipe. The coil and helium dewar assembly are shown in Figure 15.

A Teflon helium dewar cover was made and clamped around the support pipe. The outer radius of the cover had an annular sleeve which fit over the lip of the glass helium dewar to provide a gas seal and structural attachment. The glass dewar was clamped so it could not slip out of the Teflon sleeve and this hung by the sleeve from the support pipe without touching the coil form or the liquid nitrogen outer dewar. The Teflon cover was covered with several layers of .0127 mm aluminized Mylar superinsulation.

The outer nitrogen dewar shown in Figures 14 and 15 was made of 50.8 mm thick sections of Styrofoam, pressed and glued together with Epon 815 epoxy resin and Epon V-40* curing agent mixed in equal weight proportions. The dewar was lined with three layers of .0127 mm aluminized Mylar for liquid seal. The coil power cables were brought in through the nitrogen dewar to maintain the power leads at liquid nitrogen temperature. It was estimated that this reduced the overall tare boil-off of liquid helium by almost 50 percent. The copper braid leads inside the support pipe were also lengthened and run part way up the pipe on either side of the fiberglass insulation separator. This was to provide a longer path and more area for regenerative boil-off cooling to further reduce the heat leak into the helium dewar through the high conductivity copper leads.

The top cover of the nitrogen dewar remained with the G-10 support pipe and the bottom part of the dewar was raised or lowered to assemble or disassemble the dewar system. The Styrofoam collar around the support pipe provided thermal insulation for this pipe and forced the gaseous nitrogen to exit along a thin passage all the way up the support pipe for regenerative cooling of the support pipe on the outside. The helium boil-off cooled the pipe on the inside. The 6.35 mm thick support pipe was milled to a thickness of 2 mm above the power lead in bolts and was insulated on its outside with several layers of superinsulation. The unconventional use of non-metallic materials for structural support and dewars was to reduce the outside electromagnetic effects on the magnitude of the losses of the test coils.

A Pyrex glass junction at the top provided O-ring sealed flanges for connection to the flowmeter tube and electrical connection flange. This tube and another threaded to it provided a two-meter section which had a flowmeter orifice plate and radiation shielded thermocouple in its center. The top flange had Swagelock fittings with O-ring seals instead of the metal ferrules. This furnished pressure or vacuum seal for the level indicator and cryogenic fluid transfer tubes while allowing the tubes to be raised and lowered.

*Miller-Stephenson Co.

Experimental Measurements

Coil power was provided by eight motor driven generators. The generators were connected in various series and/or parallel combinations, depending on whether A.C., D.C., voltage or current was desired. The generator field amplifiers were excited by a Spectral Dynamics SD 104A signal generator for A.C. and by potentiometer varied battery voltage for D.C.

The current in the coil power leads was measured with a 200 amp or a 500 amp 50 mv shunt. These shunts were calibrated with a 300 amp .04% Honeywell calibrated shunt. The power supply excitation was adjusted by monitoring the shunt voltage on an oscilloscope. The shunt voltage was recorded for each run as one of three traces on a 6 channel Model 650 Sanborn Recorder. The peak shunt voltage was taken from the Sanborn record and corrected for shunt calibration to obtain the run current reading. These corrected current readings were used in data reduction.

The voltage across the coil was obtained from voltage tap wires connected to each electrical connection between superconducting and normal wire. This provided an average voltage for all the connections. The voltage tap leads were twisted together and run up the support pipe to feed through bolts on the electrical connections' flange. From the outside of the flange the voltage sensing was routed through 2 amp fuses and B.N.C. coaxial shielded connectors to a power meter input, oscilloscope input and Sanborn Recorder input. Although the coil voltage was also recorded by the Sanborn Recorder, the phase angle between the voltage and current could not be determined accurately enough to determine coil power dissipation. (Losses were so low that this angle was usually indistinguishable from 90 degrees).

This was expected and an electronic multiplier to measure the coil power dissipation was devised. This is discussed in Appendix A. While the meter worked well with LN_2 cooled coils, and at D.C. for superconductors, the lower signal-to-noise ratio with superconducting coils and A.C. fields rendered the performance unreliable. Time and effort level did not permit development of this very promising instrument. Its further development is a promising area for continued research.

Coil power dissipation was therefore measured from the mass flow rate of helium boil-off. For these experiments a 19.05 mm diameter orifice flowmeter was constructed in accordance with Kent's Mechanical Engineer's Handbook (29) from which charts for this orifice were constructed. The charts use the pressure across the orifice and the temperature of the gas to find the helium mass flow rate in equivalent liters per minute of liquid helium at 4.2°K. A correction factor for the flowmeter was determined by using the copper sample coils and a calibrated D.C. input while measuring He boil-off with the flowmeter (12,13).

For very low boil-off rates the flowmeter readings were compared with liquid level indicator readings from an American Magnetics Inc level indicator.

Dewar system tare boil-off tests were conducted by noting the time it took the surface of the liquid helium to drop a unit length inside the helium dewar when the experiment was fully assembled. The rate of tare boil-off varied between 0.1 and .025 liters per minute, depending on the height of the liquid when the timed reading was taken. This large variation was due to the fact that to keep the coil submerged in liquid helium the liquid had to be very near the top of the glass dewar. The relative length of the path from the liquid to other higher temperature sink areas in the system changed by large amounts as the liquid level moved up and down. After many test runs an average figure of 0.05 liters per minute tare boil-off was chosen and this amount was subtracted from the data that was plotted or compared with computed coil losses.

Test Procedure

The apparatus was assembled and checked for pressure leaks. Pressures ranged between 1.5 atm and 100 torr. However, leakage would prevent liquid nitrogen precooling or accurate helium boil-off measurements. The apparatus was then filled with liquid nitrogen which was then forced out with a transfer tube into the outer nitrogen vessel. A vacuum pump was then connected to the system and it was evacuated to below 250 torr. This evaporated the residual LN_2 and lowered the temperature from 77°K to about 67°K. The vacuum was then broken by admitting helium gas and LHe was transferred into the system. Two people could take a fully assembled experiment from room temperature to liquid helium temperature in about 45 minutes for the price of only four liters of boiled-off liquid helium.

Once the system was filled with helium the liquid transfer was halted and testing begun. Tare boil-off measurements were made by timing the drop in liquid level with the level indicator and recording the flowmeter temperature and pressure readings at the same time. Three people were required to operate the experiment and take data. One person operated the Sanborn Recorder. Another person read the Baratron flowmeter pressure and kept track of the helium liquid level while guarding the manual coil power knife switch. This person pulled the knife switch if the helium liquid level got too low, if the coil gave indications of going normal and between runs. The third person adjusted the power generator field excitation amplifier input frequency and amplitude, adjusted the power meter range, recorded the power meter setting and reading, the digital voltmeter thermocouple reading, the Baratron pressure reading given by the second person, the run number, frequency, approximate current shunt reading, voltage attenuators being used on power meter or Sanborn inputs, and the speed of the Sanborn recorder chart.

When the level indicator meter indicated liquid passage below approximately 2.5 cm above the coil, the experiment was stopped. The helium storage dewar was pressurized and liquid helium was transferred into the experiment. This process took about two minutes. Then the experiments were continued.

The experiment proceeded from a frequency of 1 Hz to 5 Hz, 10 Hz, 15Hz, 20 Hz anf finally 30 Hz. At each frequency 50 amps, 100 amps and 200 amps peak current readings were attempted. Due to limitations on the output of the generator field excitation amplifiers, 200 amps could not be attained above 15 Hz and only a maximum of 70 amps was attained at 30 Hz. The data is summarized in Table 4.

After the A.C. tests were made, the generators were connected in parallel and D.C. critical current tests were made. Under the D.C. conditions, the power meter gave ample warning that the coil was going normal; however, two coils were burned out during critical current tests; once because the power meter was not connected and once because the monitor was reading the liquid level indicator when the power meter gave the warning.

Coil 3, which had the .122 mm single core wire cable, was tested twice. The first time each separate superconducting wire was connected to its own separate bundle of copper lead wires so that there would be several feet of normal wire before the filaments were connected at the lead in lug. The second time after the coil was burned out, repaired and rewound, five superconducting wires at a time were all connected at the same joint on the coil form to the appropriate number of lead in

Table 4

Single Coil Test Data

Coil 3 (Bc = 2.9255×10^{-3} x Amps)

Run Number	Freq. Hz	Ia Peak Amps	Bc Tesla	$\dot{B}_{max}$ Tesla/sec	He Flow Liquid Liters Minute
3	1	38	.111	.70	.117
4	1	106	.31	1.95	.11
5	1	242.5	.7094	4.45	.193
6	5	41.5	.1214	3.8	.166
7	5	112	.3276	10.3	.225
8	5	180	.5266	16.5	.385
9	10	40	.117	7.35	.138
10	10	110	.322	20.2	.335
11	10	188	.55	34.6	.98
12	20	42	.123	15.5	.151
15	30	84.6	.2475	46.6	.65
16	30	44.5	.1302	24.5	.19
18	20	103	.3013	37.8	.42
19	15	179	.5237	49.4	1.2
20	10	198	.5792	36.4	.97
21	D.C. critical current 535 amps				

Coil 4 (Bc = 2.9255×10^{-3} x Amps)

24	30	45	.1316	24.8	.47
25	30	52.3	.153	28.8	.53
27	20	51.5	.15066	18.9	.32
28	10	166	.4856	30.5	.84
30	10	192	.5617	35.3	1.22
31	10	194	.5675	35.66	1.34
35	1	92	.2691	1.69	.114
36	1	176	.5149	3.24	.115
37	1	176	.5149	3.24	.147

Table 4 (continued)

Coil 4 (Bc = 2.9255 x 10^{-3} x Amps) -- continued

Run Number	Freq. Hz	Ia Peak Amps	Bc Tesla	$\dot{B}_{max}$ Tesla/sec	He Flow Liquid Liters Minute
38	1	92	.2691	1.64	.125
39	1	64	.1872	1.18	.138
40	1	101	.2955	1.86	.138
41	1	209	.6114	3.84	.14
42	5	45	.1316	4.15	.125
43	5	95	.2779	8.75	.197
44	5	168	.375	11.76	.375
45	10	45.5	.13311	8.4	.170
46	10	90	.2633	16.5	.375
47	10	197	.5763	36.19	.98
48	15	91	.2662	24.7	.62
49	15	188	.55	51.84	1.4
50	20	84	.2457	30.9	.74
51	20	129	.3774	47.05	1.21
52	30	70.5	.2062	38.87	.86
53	30	45	.1316	24.8	.4
54	20	145	.4242	53.3	1.35
55	D.C. critical current 400 amps				

Coil 5 (Bc = 2.731 x 10^{-3} x Amps)

59	1	96	.2622	1.65	.096
60	1	188	.5134	3.22	.10
62	5	98	.2676	8.4	.128
63	5	202.5	.5530	17.4	.225
68	5	50	.1366	4.29	.114
69	10	50	.1366	8.55	.117
70	10	96	.2622	16.46	.224
71	10	182	.497	31.23	.407
72	15	46.6	.1273	11.97	.125
73	15	99	.2704	25.48	.295
74	15	99	.2704	25.48	.330
75	15	181	.4943	46.56	.59
76	20	49	.1338	16.81	.166
77	20	103	.2813	35.31	.42
78	20	99	.2704	33.9	.407
79	20	140.5	.3837	48.25	.66
85	D.C. critical current 510 amps				

wires. This was to determine if the normal lead separation between superconducting filaments would reduce any eddy current loops that might link wires through the connections. Because no difference in losses was noticed between the two connection configurations, the other coils were connected with the less time consuming multiple wire joints and were only tested once.

It was determined by trial that excess liquid helium could be returned to the storage dewar from the experiment. This was accomplished by lowering the helium transfer tube to a position about 2.5 mm from the bottom of the glass dewar. The other end of the transfer tube was raised until it was only about two-thirds of the way into the helium storage dewar and the storage dewar cap seal was removed to allow excess gas to escape. The experiment was then pressurized with gaseous helium, which forced the liquid helium remaining in the experiment back into the storage dewar.

Comparison with Calculated Losses

Measured coil physical geometry and wire cross sectional areas were used with NASA TR 170 (27) to predict coil central field Bc for applied current and to find the local field at every turn of wire. Coils 3 and 4 were identical except for the type of conductor. Coil 5 was slightly larger in radius and had two less turns on each row of windings. Since all three coils filled almost the same winding area, the axial and radial field magnitudes as a percentage of coil central field were about the same. The two different areas were averaged and only one detailed calculation of radial and axial field was done.

Since radial and axial field components are both perpendicular to the winding wire axis, the vector sum was taken as the magnitude of the transverse field at the point in question. By multiplying the value of the percentage of central field times the length of wire in a turn at that position and summing over all the wires the volume average fraction of the coil central field was obtained. By squaring the fraction of central field before multiplying by the length of turn, and cubing, the volume average fraction of central field^2 and field^3 were also obtained.

Coil	Bc = central Field (Tesla)	Vol Avg Field	Vol Avg Field	Vol Avg Field
3	2.9255×10^{-3} x amps	.4887 Bc	.3295 Bc	.2582 Bc^3
4	2.9255×10^{-3} x amps	.4887 Bc	.3295 Bc	.2582 Bc^3
5	2.731×10^{-3} x amps	.5011 Bc	.3405 Bc^2	.2996 Bc^3

Because the maximum current used in the coil tests (200A) only produces a .585 Tesla central field, the Kim relation for critical current was used for calculations. Equation 2.6 was fitted to the two lowest field points in the .1 mm specification data in Figure 2. The curve of this derived relation fits the specification data very well up to about 6.0 Tesla. For the volume average of the 200 amp field, the value of Jc from Equation 2.6 is 5.35×10^2 a/m^2. Using this in Equation 2.8 the value of Bp is .16 Tesla, indicating that most of coils 3 and 5 are fully penetrated with flux. Applying the full penetration hysteresis loss, Equation 2.12, to coils 3 and 5 gives the graph lines in Figure 16. The actual data for 200 amps is about 20 percent too high but clearly the linear frequency dependence of full penetration hysteresis loss is present.

At 50 amps the volume average field is .073 Tesla, giving $Jc = 6.4 \times 10^9$. Bp from Equation 2.8 is now .188T for coil 3, indicating that the coil is undergoing partial penetration hysteresis loss. If the volume average field cubed is applied to the partial penetration hysteresis loss, Equation 2.10, the calculated value is 9.76×10^3 Joules/m^3 cycle, which is within the data, as shown in Figure 17. Assuming the multifilament conductor has decoupled filaments, the eddy current loss asymptotes were calculated by Kraemer (12). They are shown along with the coil 4 data in Figure 18. The loss data does not follow these asymptotes nor the usual transition from one to the other.

The hysteresis loss assuming the filaments are fully coupled and are acting like a 93 μm solid core is also shown in Figure 18. This is very close to the experimental data. Thus theory and experiment show that there is no advantage and in fact, a disadvantage to using copper matrix multifilament composite superconductors for application to the highly varying field portions of a dynamic magnetic suspension system. In fact, the losses of the semistock single core conductor used in coil 5 are one-half the losses of the multifilament composite. Thus it appears that small diameter wires with one or a very few superconducting cores in each is the proper direction to seek low A.C. loss superconducting coils for dynamic magnetic balance applications.

Losses were reported by Kuwasawa, et al. (30) from Japan for a portion of a coil that was constructed similarly to the single core cables used in these experiments. The superconducting filament in these wires was about the same as that in coil 3

in the present experiments. The losses reported show the expected transition from an H^3 dependence to an H^1 dependence characteristic of partial and full penetration hysteresis loss. There were two major differences between the Japanese experiments and those conducted here. One was that the Japanese cable was twisted and not fully transposed. More importantly, the Japanese carefully wound their coil in three sections so that the central section was in a moderately strong uniform bias field besides having the gradients of a coil. The only losses reported were for the portion of the coil in the bias field. The bias field insured that none of the affected parts of the coil operated at low field levels where the critical current is high. At low fields a drop in field is more than compensated for in the full penetration hysteresis loss formulas by a rise in critical current. The full penetration losses dominate the calculation whenever they exist.

In Figure 17 the Japanese data curve is superimposed on the losses of the three coils tested in this program. Although coil 3 had a filament diameter only 5 percent larger than that of the Japanese wire, the losses are more than proportionally higher. It is believed that this is due in part, if not all, to the fact that the coils tested in the current experiments had large portions exposed to low field strengths and thus high critical currents for all or large portions of the cycle, causing larger full penetration hysteresis losses.

The theory used by Kuwasawa, et al. (30) could not be used here because the present experiment was carried out at a much lower field level. It thus appears that Equations 2-10 to 2.12 can be used with an accuracy of about 20% to estimate losses in single magnetic balance coils. By multiplying those losses by 1.2 the error can be reduced further, probably to about $\pm$ 10 percent.

Interacting Coil Tests (13)

Because magnetic balance systems involve many different coils which operate in each other's fields, the single coil tests described above do not represent the entire class of loss which may occur. In addition to the self field losses caused by the current through a given coil, there will be losses caused in a coil by fields due to currents in another coil. The tests reported in this section using two of the coils described above tested simultaneously under various conditions.

With two different coils, three configurations were tested. The first configuration was with the coils side by side, axes parallel. The second configuration had coil 5 held perpendicular

to coil 3, coil 5's axis pointing at coil 3. Reversing their respective positions produced the third configuration.

Experimental Apparatus

The experimental setup had to support the coils in liquid helium in all three configurations, provide power and instrumentation connections to the coils, provide for measurement of helium boil-off and minimize heat leak into the liquid helium. This required a much larger liquid helium volume than the single coil tests and many practical difficulties were encountered in scaling of the experiment.

Liquid helium was contained in a 35.6 cm (14-inch) diameter 83.8 cm (33-inch) high double walled evacuated glass dewar (Pope #8596). The inner walls of the dewar were silvered except for a one-half inch strip down the side, across the bottom and back up the side. This was to minimize eddy-current losses in the silver film. The glass dewar was supported on a styrofoam pad at the bottom of a cylindrical bucket made from .8 mm thick, G-10 sheet wound around a 38 cm disk of 6.4 mm thick G-10. The side sheet was both glued and bolted to the disk. This bucket held a bath of liquid nitrogen around the glass dewar and was in turn placed in a larger styrofoam bucket to provide insulation for the nitrogen bath, as shown in Figure 19.

A cap was made for the glass dewar to constrain the helium boil-off. The cap was constructed of a G-10 fiberglass top disc with a 5 cm wide band of .8 mm G-10 sheet wrapped and glued around the disk. A Viton "0" ring between the glass and the G-10 side band provided a seal and was retained with a hose clamp. An initial attempt to use a scaled-up version of the Teflon dewar cap, Figure 15, failed because of thermal cracking in the thicker section of the larger cap.

The relationship of the coils in the perpendicular setup is shown in Figure 20 and the entire arrangement in Figure 21. In addition to the litz cable power leads each coil had a shielded twisted pair of wires connected to each end. These voltage taps extended up the pipe to attack to the electrical connection flange. In addition, four wires from a liquid helium sensor went up the pipe to the flange to be connected to the American Magnetics' Model 110 liquid helium level indicator. The voltage taps and output from the level indicator were used as inputs to a safety circuit, involving the power meter.

The power meter controlled a relay controlling a contactor through which the coils received their power. Should the power reading peg (due to the coils going normal) or the helium level drop below a set value, the power meter could cut power to the coils. This was intended to prevent the earlier accidents which necessitated the repairs to the coils.

As mentioned earlier the power meter operated satisfactorily as a protection device but was not quantitatively accurate as constructed. General operation of the experiment was the same as for single coil tests except the times to fill and precool were somewhat larger because of the larger mass of dewar involved. Data was taken first with the coils perpendicular and coil 5 powered. It was powered at 1 Hz, 5 Hz, 10 Hz, 15 Hz, 20 Hz and 30 Hz. At each frequency peak currents of 50, 100 and 200 amps were attempted. Due to limitations in the motor generators, the higher currents could not be attained at the higher frequencies. At each frequency-current setting, three loss readings were taken. First with the unpowered coil open, then with it shorted, and finally with 100 amps D.C. going through it. Loss readings were taken by reading the flow meter and thermocouple.

After this was completed, the external power leads were switched so that coil 3 was connected to the motor generators and coil 5 could be held open, shorted, or fed 100 amps D.C. The above procedure was repeated with coil 3 being powered at the same frequencies and currents as coil 5 had been. Coil positions were then interchanged and the process was repeated. The process was repeated again with the coil axes parallel. To change coil configurations the system had to be disassembled, then reassembled. It was then cooled down and the data taken. The data is presented in Table 5.

The results in Table 5 indicate two things. First, as expected, the boil-off is much lower with coil 5 than with coil 3. This confirms earlier results showing the marked superiority of very fine wire. Second, a small reduction in dissipation due to lowering of Jc by the 100 amp D.C. current did not materialize. This is probably due to the low level of the interaction loss due to the fixed loss and the relative insensitivity of the boil-off technique for measuring loss.

Interaction Loss Calculation

A computer program was written to predict the performance of the coils in the various configurations (see Appendix B). The results are found in Table 6. To find the predicted loss the

Table 5

Coil Interaction Test Data

Perpendicular; Coil 3 over Coil 5

Run Number	Frequency Hz	Current Peak Amps	He Flow l/min	Watts	Joules per Cycle	Predicted Watts
Coil 5 powered						
1	5	46	.012	.527	.105	.245
2	5	46*	.012	.527	.105	-
3	5	95	.054	2.281	.456	1.709
4	5	170	.176	7.480	1.496	5.304
5	5	170*	.204	8.670	1.734	-
6	10	48	.018	.764	.076	.489
7	10	124	.141	5.984	.598	4.241
8	10	220	.442	18.770	1.877	12.483
9	15	49	.025	1.080	.072	.734
10	15	98	.156	6.620	.441	5.126
11	15	175	.446	18.945	1.263	16.384
12	20	48	.027	1.133	.057	.978
13	20	97	.167	7.106	.355	6.834
14	30	48	.029	1.238	.041	1.467
15	30	48*	.029	1.238	.041	-
Coil 3 powered						
16	5	48	.020	.863	.173	.519
17	5	97	.162	6.882	1.376	4.662
18	5	189	.517	21.973	4.395	16.781

Run Number	Frequency Hz	Current Peak Amps	He Flow l/min	Watts	Joules per Cycle	Predicted Watts
19	10	50	.028	1.190	.238	1.038
20	10	101	.334	14.175	1.418	9.323
21	10	211	1.066	45.305	4.531	33.561
22	15	48	.039	1.636	.109	1.557
23	15	48*	.039	1.636	.109	-
24	15	96	.416	17.690	1.179	14.563
25	15	96*	.416	17.690	1.179	-
26	20	47	.055	2.350	.118	2.076
27	30	33	.046	1.934	.064	.895

*Denotes 100 amps D.C. on unpowered coil

Parallel Coils

Run Number	Frequency Hz	Current Peak Amps	He Flow l/min	Watts	Joules per Cycle	Predicted Watts
Coil 3 powered						
1	5	49	.019	.788	.158	.424
2	5	96	.124	5.273	1.055	4.030
3	5	201	.477	20.26	4.052	16.842
4	10	51	.025	1.056	.106	.847
5	10	102	.290	12.305	1.231	8.060
6	10	210	1.078	45.80	4.580	33.683
7	15	47	.027	1.131	.075	1.271
8	15	101	.444	18.850	1.257	12.090
9	20	49	.032	1.339	.067	1.694
10	30	33	.012	.491	.016	.730
Coil 5 powered						
11	5	47	.010	.422	.084	.245
12	5	102	.063	2.693	.539	1.710
13	5	198	.193	8.217	1.643	6.250
14	10	50	.012	.527	.053	.489
15	10	99	.096	4.077	.408	3.419
16	10	197	.346	14.716	1.472	12.499
17	15	52	.025	1.054	.070	.734
18	15	98	.141	5.984	.399	5.129
19	15	170	.426	18.119	1.208	15.938

Run Number	Frequency Hz	Current Peak Amps	He Flow l/min	Watts	Joules per Cycle	Predicted Watts
20	20	48	.053	2.240	.112	.978
21	20	96	.223	9.462	.473	6.838
22	30	49	.066	2.819	.094	1.467

Table 6

Measured Loss compared to Calculated Loss

Calculated Loss and Error of Calculation in Parenthesis

CONFIGURATION	Loss, Ave Joules per Cycle at		
Coil 3 Powered	50 amps	100 amps	200 amps
Parallel Coils	.102 (.085, 20%)	1.186 (.806, 47%)	4.207 (3.368, 25%)
Perpendicular Coil 3 Upper	.160 (.104, 54%)	1.323 (.932, 42%)	4.472 (3.361, +33%)
Coil 5 Powered			
Parallel Coils	.083 (.049, 69%)	.456 (.342, 33%)	1.512 (1.250, 21%)
Perpendicular Coil 3 Upper	.071 (.049, 44%)	.465 (.342, 36%)	1.485 (1.248, 19%)

appropriate unpowered coil loss is added to the powered coil's self-field loss (the same for all configurations).

The results show that the interactive losses are never expected to be great compared to self-field loss. At its greatest, the interactive loss is only 10-15 percent of the self-field loss and is less than 1 percent for the smallest case.

The greatest predicted interactive losses occur when the unpowered coil is located underneath the powered coil perpendicular to it. This configuration exposes the interacting coil to the strong field lines coming out of the center of the powered coil. Thus when the interacting coil is in the area of the strongest field surrounding the powered coil, the interaction is greatest, though still small.

The field surrounding the powered coil is much weaker alongside of it. When the interacting coil is in this area, the interactive losses should be smaller. The program predicts that for the interacting coil adjacent to the powered coil, either parallel or perpendicular, the interactive losses will be negligible, less than one percent.

In general, the actual currents in the test data differed from the 50, 100, 200 amps used by the computer. In most cases the difference was small. When the difference was greater than 10 percent the loss was corrected by a factor of $(200/I)$, for 200 amp data, $1/2\ (100/I) + (100/I)^3$ for 100 amp data, and $(50/I)^3$ for 50 amp data. This assumes full penetration loss and linear field dependence for 200 amps, partial penetration and cubic field dependence for 50 amps, and a mixture for 100 amps.

Each loss value in watts was then divided by the frequency in cycles per second. This yielded loss in Joules per cycle. For each configuration the Joules per cycle was averaged over the frequencies for each amperage level. The results are tabulated and compared with the computer predictions in Table 6.

Analysis of Results

When the data is compared to predictions large discrepancies are seen at low current levels, but agreement comparable to the earlier research is seen at 200 amperes. There are, however, good reasons to expect less agreement at lower current.

Low flow rates are difficult to read on the flow meter. Low flow rates take the longest to reach a steady pressure reading and calibration readings indicated a need for large corrections. At the low flows orifice Reynolds number is very low, causing calculations for orifice constant to be in error (29) and experimental difficulties at low flow also cause calibration error. This inaccuracy is indicated by the scatter in the 50 and 100 amp data, 50% and 30% respectively, compared to only a 10% scatter in the 200 amp data.

Since the longer wait to get low current readings gives more time for the normal copper leads heat up, their contribution to boil-off will be greater. Also, even in the steady state lead losses will be more significant at low currents because hysteresis losses go down with the cube of the current while normal metal losses decrease quadratically with current.

The interaction tests thus support findings from single coil tests that for low loss coils of superconducting litz wire the losses can be calculated based on the models of Chapter II with due regard being taken to include the total field from all coils. This field and the local transport current are used to compute losses in each differential volume element of superconductor and the resulting loss is summed over all superconductors.

Chapter V. COIL ARRANGEMENTS

The first demonstration of feasibility for the use of superconductors in a magnetic balance and suspension system depends on the existence of a feasible geometry for the requisite number of coils. This requires decisions about which coils should be placed in a common dewar and which coils should be placed inside of other coils. Such decisions cannot usually be justified until the entire design has been solidified and detailed calculations have been performed for each coil. Iteration can then be performed to more closely approach the desired performance.

Alishahi (14) developed a computer program to perform coil calculations and proceeded through several iterations to produce a geometry for superconducting coils which should be a viable technical alternative to the normal copper coils of the NASA prototype balance.

No estimates of whether or not these superconducting coils pose a viable economic alternative have been made.

A two-step path was followed to arrive at a suitable superconducting coil arrangement. First a geometry for the lift and side force gradient coils was sought which would eliminate the use of iron. Second, other coils were added and the shapes of the lift coils were modified to produce a workable, compact array.

In order to take the first step an existing computer program for field calculation by Adams (31) as modified later by Way (32) was adapted for computing the magnetic field from a series of line current elements. This was used to compare various lift coil geometries. To provide a benchmark for performance, coils were sought that would reproduce the maximum design fields of the NASA prototype magnetic balance at its maximum current.

The present NASA-MIT balance at the MIT Aerophysics Laboratory uses three main groups of copper coils, cooled with water, with iron poles for controlling and producing forces and moments in different directions (33). The three groups of coils are as follows:

a) Helmholtz-coil system (controls $\bar{B}_x$, $\bar{B}_{xx}$)*

b) Saddle-coil system (controls $\bar{B}_y$, $\bar{B}_z$)

c) Side and lift force system (controls $\bar{B}_{zx}$, $\bar{B}_{yx}$)

*Here the first subscript denotes the vector component and the second denotes the derivative; i.e., B_{zx}=partial derivative with regard to x of z component of B.

Figure 22 shows the arrangement of these coils. Besides these, there is an Electromagnetic Position Sensor Coil System, which measures the position of the model for controlling it.

Since the main sources of power consumption are coils in groups (a) and (c) and the iron poles of group (c) limit the field and make scaling unreliable, it was decided to design coils (a) and (c) using superconductors and no iron.

Because the high frequency fields of both the roll system and EPS system penetrate the EPS coils and saddle coils (b) above, these were left as normal copper in the proposed design. This choice eliminated the need for windowed or dielectric dewars since all superconducting coils could be confined to two, axially separated, short, annular dewars radially outside the EPS coil. Thus a copper shield outside of the normal coil package could shield the EPS from the extraneous effects of stainless steel or inconel dewars. The main constraints for such a design are:

a. All superconducting coils should be in one or two warm bore dewars.

b. Enough light passage to watch the model or use optical measuring devices such as a laser velocimeter or transits should be provided.

c. The saddle coils and position sensor coils should remain in their position. This assumes that new LN_2-cooled coils for these purposes could be housed in this volume. The remaining space is shown in Figure 23.

Computer Program

The computer program (TABLE) (14,31,32) tabulates the magnetic field components due to a series of straight line elements or a series of circular line current elements. In the straight line current element mode it is limited to the shapes which could be approximated by straight lines. Figure 24 shows a sample winding that can be handled by TABLE (see Appendix C for listing).

The number of turns used in the computer program is controlled by M and N (number of layers and turns per layer in winding cross section). Alishahi (14) has shown that for smaller than 16 wires per layer the correct number should be used but that for larger numbers a less time consuming approach is to substitute an equivalent 16 by 16 array for this particular configuration. The error is below 2 percent.

Testing Computer Program

A model coil similar to the designed lift coil system was made and the transverse field component on the axis was measured and compared with TABLE predictions for the same coil system. The model coil is shown in Figure 25.

Figure 26 shows the results of TABLE together with measured results. The computer program overestimates by about 10 percent. This is probably a result of the departure from the ideal shape. Winding edges are not perfectly square and the corners of individual turns are rounded where they go over the form.

Finding the Best Configuration

The present side and lift coil system with iron poles (Figure 22) has a measured performance of:

$$\overline{B}_{zx} = 1.4\ I_{zx}$$

Taking I_{zx} = 385A, the gradient should be 540 gauss/in. This is the basic requirement chosen for each different configuration of air core superconducting side and lift coils.

As a first step a model coil with the coil form shaped like the iron poles was tested as Model I (Figure 27). Since the performance was not satisfactory and winding was expected to be difficult (the winding plane is not perpendicular to the core form axis so wires will slip during winding), Model II with the same core shape but with the winding plane perpendicular to the core axis was tried (14). The disadvantage with this model was that due to its acute angle of winding with the axis plane, it does not use the available volume efficiently.

Figure 28 shows Model III. This model came about as an approximation to Model II and since it uses all available space, it is a better choice in most cases. The test coil array (Figure 25) is a two coil version of this geometry.

Choosing a configuration depends on the magnitude of gradient which is needed. For a low transverse field gradient ($\overline{B}_{zx}$ < 200 gauss/in). Model I and Model II are comparable to Model III but at field gradients as high as ($\overline{B}_{zx}$ = 500 gauss/in).

Model III is considerably superior. For producing 500 gauss/in. gradient, Model II at 60^{o} core axis angle should have 5000 turns in each of 8 coils whereas Model III with three-stage optimized coils needs 3900 turns in each of eight locations. This should be clear since for extending Model III upper stages would be closer to the center than upper stages of Model II.

Model III can be optimized easily if the effect of each stage is studied separately. Such an investigation shows that at a definite radial position the highest gradient may be obtained from one stage. Table 7 shows the $\bar{B}_{zx}$/(ampere turn) for each stage in Figure 28 and a fourth stage that might be added. Stage one was discarded after such a study because it is far from the optimum radius and its contribution to total gradient is negligible. Table 7 shows that the optimum radius is about the place where stage 3 is. It seems the optimum radius depends on the axial spacing of the two sets besides the geometrical parameters of the winding.

It is interesting to note that due to symmetry, computation of the field of one coil of each stage is enough to compute the total field for points on the x axis (axis of symmetry). This can save a lot of CPU time in preliminary calculations.

Comparison of results for the three models shows that Model III is the most advantageous since

a) It can produce the desired field gradient $\bar{B}_{zx}$ = 540 gauss/in. with the least volume of space and superconductor.

b) It could be extended for higher field gradients.

c) Construction of such a coil system would be less troublesome since winding is straightforward and the methods of Kraemer could be used for coil construction.

Figure 29 shows the B_z component of magnetic field for points on the x axis. The B_{zx} gradient at the center is 586.8 gauss/in. with gradient uniformity 12% over a sphere of radius 3 in. The average gradient is $\bar{B}_{zx}$ = 619 gauss/in. over a distance from x = -3 to x = 3.

Magnetizing and Drag Coils

After the dimensions of side and lift coil system were found, the magnetizing and drag coil system (Helmholtz coils) could be designed according to the following considerations:

Table 7

Transverse Field Gradient of Different Stages of the Side and Lift Coil Model

Stage	Mean Radius in.	Gradient $\bar{B}_{zx}$ gauss/in.	Ampere Turn*	$\bar{B}_{zx}$/Ampere Turn
1	5.5	15.6	18x24x260	1.39×10^{-4}
2	8.5	102.	36x24x260	4.54×10^{-4}
3	11.5	190.6	54x24x260	5.66×10^{-4}
4	14.5	189.88	72x24x260	4.23×10^{-4}

*260A cable current is assumed for design purposes. 18x24, 36x24, etc. are the turns per layer and number of layers of each lift coil; i.e., half the total available number of turns. Program details are in Appendix C.

a) Magnetizing and drag coils should produce B_x = 7700 gauss/in. and $\overline{B}_{xx}$ = 655 gauss/in. according to the measured performance:

$$B_x = 20\ I_x$$

$$\overline{B}_{xx} = 1.7\ I_{xx}$$

for present M.S.B. and $I_x = I_{xx}$ = 385A.

b) Drag coils should be inside the magnetizing coils to minimize inductance, so the inner diameter is the outer diameter allowed by side and lift coil system.

c) Magnetizing and drag coils should be optimized for the least volume or least inside field, since several dimensions are possible in a trade-off. This should be done in conjunction with loss computation. Note that A.C. losses were not computed in this part of the study for the proposed coil arrays.

Computations for drag and magnetizing coils were carried out by using the circular current element program POINT, Appendix B. Figures 30 and 31 show B_x vs. axial distance for magnetizing and drag coils. Magnetizing coils have a field component, B_x = 7448 gauss/in. with a uniformity of .92 percent over a sphere of radius 3 in. and corresponding values for the drag coils are B_{xx} = 634.7 gauss/in. at the center with gradient uniformity 6.5 percent over a sphere of radius 3 in.

Figure 32 shows the overall designed coils with present saddle and position sensor coils. All superconducting coils were designed for 260A operation. Note that the Helmholtz coils are not separated by the theoretically ideal distance. This is also true of the NASA prototype Helmholtz coils, which are approximately positioned. A more detailed picture of this coil arrangement can be found in Figures 39a,b,c,

Magnetic Field inside Coils and the Conductor Size

For choosing the proper diameter of conductor the magnetic field due to all coils inside the windings is needed. From these the current density should be determined to be less than J_c from Figures 1 or 2. Computer program TABLE (Appendix C) was used for this purpose and the field at different wire locations was obtained. The wire self field, which depends on conductor diameter, was added to this. Table 8 includes the maximum field inside each stage of side and lift coils, drag and magnetizing coils and the percentage contribution of each set of coils to the overall field. This field is the magnitude of B; i.e., $(B_x^2 + B_y^2 + B_z^2)^{1/2}$, which is perpendicular to the wires. The maximum field is found from a comprehensive study for each set of coils. Figures 33 through 36 show the magnitude of the magnetic field inside respective coils. Figure 35 shows the field distribution in two drag coils, since prediction of the worst one is difficult. In each computation the absolute value of each field component due to side and lift coils was added to the absolute value of the same component of the drag and magnetizing field.

One can define the appropriate conductor size either by the maximum field in the worst coil, or by the maximum field in each coil locally. This procedure could be repeated for each single coil; i.e., dividing each coil into several parts and defining the proper conductor size for each segment based on maximum field in that segment. The second method would be advantageous in reducing superconductor volume but would require the purchase of more types of cable.

One can check the initial assumed cable size on which the field calculations were based by noticing that for every cable size trial, the current density in the superconductor should be less than the critical current density obtained from a J_c vs. B relation, such as one in Figure 1. Checking this condition leads to a new conductor size and new coil dimensions. Therefore, the field calculation must be repeated until $J < J_c$. It is worth noticing that the field does not change with cable size a great deal if one keeps the number of turns constant. This may cut down the number of iterations.

After such an attempt for the proposed configuration, the proper cable dimensions are presented in Table 9. The computed maximum fields were increased 20 percent to take into account the possible computer error and other factors.

Table 8

Maximum Magnetic Field Inside Coils
with Percentage of Contribution of each Set

Coil Description	% Self Field	% of Cont. of S&L 1st	% of Cont. of S&L 2nd	% Mag-netizing	% Drag	Max Field Tesla
S & L Coil 1st stage	27.5	2.6	31.2	11.8	26.8	3.71
S & L Coil 2nd stage	35.1	23.6	5.3	11.1	24.9	3.71
Drag Coil	41.	1.	2.	51.1	4.1	3.56
Magnetizing Coil	34.	8.	15.4	4.9	37.7	2.81

Table 9

Final Cable Dimensions
for Different Coils

Side and Lift, 1st stage					
Cable	Dia_{mm}	$S_{SC_{mm^2}}$	J_{A/mm^2}	Maxfield x 1.2 Tesla	J_{C} A/mm^2
7x6x5	1.73	.222	1170	4.52	1250
Side and Lift, 2nd stage					
7x6x5	1.73	.222	1170	4.52	1250
Drag Coil					
8x5x5	1.69	.212	1229	4.35	1338
Magnetizing Coil					
6x5x5	1.46	.159	1639	3.46	1700

The proposed conductor is a cable of solid NbTi core filaments. .0367 mm in diameter with copper/superconductor ratio = 1.71/1. This conductor, the smallest tested in this program, appears to be the best conductor solution available without development for the present application. Possible improvements were mentioned in Chapter III.

Saddle Coil Geometry

While the design of Figure 32 using planar rectangular winding side force and lift coils is a feasible geometry and is the simplest to design and construct, it is large. Using the normal copper coils with an outside dimension of 33 inches as a benchmark, the 61.5 inch dimension of Figure 32 represents an increase of 86 percent or about six times the volume. It was therefore suggested to wrap the side and lift coils around the central volume in a saddle stage as shown in Figure 37.

As this type of coil is composed of both circular and straight line current elements, a new computer program was necessary. The chosen procedure is to divide each circular current element into a number of definite angle increments and approximate each arc with its chord. The subroutine SADDLE, which computes the coordinates of the endpoints of circular elements and the supplementary Fortran statements, is presented in Appendix D along with an evaluation of the error resulting from the chord approximation.

In addition to use of saddle side and lift coils additional volume saving can be made by moving the drag and magnetizing coils to the inside of the side and lift coils in the volume axially outside of the inner saddles. The saddle coil results show no great field gradient loss over the previous design if one keeps the same number of turns. However, the advantage of saddle coils is somewhat offset by the fact that less turns can be located in the same region because the volume is smaller. This design assumes the needed improvement of about 30 percent in packing factor can be realized. Time was not available to pursue this in more detail.

Figure 38 demonstrates this configuration together with the Figure 32 design (dashed lines). The reduction in outer radius is quite noticeable, 12 inches, thus saving 78 percent in superconductor volume. The transverse field gradient B_{zx} at the center is 542 gauss/in. with uniformity 11.4 percent over a sphere of radius of 3 inches. The field from the magnetizing coils is B_x = 7026 gauss/in. with uniformity 18 percent and for the drag coils is B_{xx} = 678 gauss/in. with uniformity 15 percent over a sphere of radius 3 inches.

The internal field in one coil of each set due to the lift force current was computed. Table 10 shows these results with the percentage contribution of each set of coils. Table 11 shows the appropriate cable size using the results of Table 10. If we choose the cable size in the worst case, when one lift coil set comes to full power and the other is off (i.e., computing the field due to two upper coils of each set with twice the former ampere turns) instead dividing the lift coil current, we will end up with a 17 percent increase in cable diameter.

This design is more advantageous than the previous one in being more compact and using less conductor. However, it has the disadvantages of requiring a more complex dewar design; a more complicated mechanical support; and a more difficult winding procedure.

In order to better visualize how these two possible geometries could be implemented, Figures 39 and 40 were made. These are assembly views of the two geometries showing winding layout and possible coil support structure. Figure 39a shows the coil array in end view with location for winding support rings and clamping bolts. Figures 39b and 39c show vertical and 45 degree longitudinal sections. Figures 40a,b and c show the alternate saddle coil arrangement to the same scale. It is also possible to use the drag-magnet coil position from Figure 40 with the planar side and lift coils of Figure 39. This would provide some size reduction along with easier construction.

Table 10

Percentage Contribution of Each Coil Set

Coil Description	% Contribution					Max. Field Tesla
	Self Field	Upper Left S & L*	Upper Right S & L**	S & L Rest Coils	Mag. and Drag	
1st stage S & L	25.9	74.8	3.2	5.8	16.2	2.94
2nd stage S & L	41.5	82.6	2.7	5.2	9.5	3.11
3rd stage S & L	51.1	85.5	2.5	4.9	7.1	2.79
Magnetizing	57.6	13	8.4	7	71.6	3.77
Drag	24.6	12.5	8.6	7.6	71.3	3.5

*Including 1st, 2nd and 3rd stage S & L coils at X(+) Y(-) Z(-).

**Including 1st, 2nd and 3rd stage S & L coils at X(+) Y(+) Z(-). The field in this column should be subtracted from the previous column.

Table 11

Cable Diameter

Cable	Dia_{mm}	$S_{Sc_{mm}^2}$	J_{A/mm^2}	Max Field x 1.2 Tesla	Jc_{A/mm^2}
1st stage S & L					
10x4x4	1.51	.169	1537	3.61	1550
2nd stage S & L					
11x5x3	1.53	.174	1490	3.81	1500
3rd stage S & L					
11x7x2	1.48	.163	1597	3.43	1600
Magnetizing					
10x5x4	1.69	.211	1299	4.52	1266
Drag					
9x7x3	1.64	.200	1301	4.2	1333

This Page Intentionally Left Blank

Chapter VI. CONCLUSIONS

The conclusion of the study reported is that use of superconductors for magnetic balance coils is technically feasible and advantageous, particularly so for large systems at high dynamic pressure.

This is a result of the fact that superconducting coils without iron can be directly scaled to larger sizes and higher force levels needed in large cryogenic wind tunnels. In the configuration of Figure 40 a coil array is suggested which does not use iron and which is nearly the same size with the same force capability as the present NASA prototype normal copper coil system which uses iron cores.

This study determined that use of superconductors is feasible for a magnetic balance system. It did not determine for what design conditions superconducting coils are the best choice. A detailed study of each proposed application will be required to determine what the optimum trade-off will be between superconductors and normal conductors considering both initial cost and operating cost.

Specific recommendations are made for cable designs and superconductor choice and two coil arrangements for a multi-purpose magnetic suspension and balance system are suggested. Specifically, for a benchmark comparison conductor sizes and winding sizes are presented based on achieving the same maximum design conditions as the present NASA-MIT prototype magnetic balance.*

For the magnetic balance application where frequency response from D.C. to 20 Hz is required and desired for some cases up to 40 Hz the best conductor is a bundle of fine copper stabilized superconducting wires which are individually insulated. For fields below 6 Tesla, Nb-Ti appears to be the best material. This is the type of cable tested in the present study. For fields up to 10 or 12 Tesla Nb_3-Sn bronze process superconductor appears best. Additional development, however, is required to produce the required insulated fine wire in this material.

---

*Note: Since funds never permitted construction of the originally planned power supplies, all operation to date has been limited to 100 amps or roughly one-ninth design power.

In the coil geometries selected, Figures 39 and 40, the position sensing coils and saddle coils for pitch, yaw and roll are normal copper and are located in the center of the balance volume. Since these coils operate in the strongest fields, have high frequency signals 400 to 20,000 Hz and are closest to the optical access, there is nothing to be gained and much to be lost by making them superconducting. With this approach two metal (stainless steel or Inconel) annular dewars can be used to house the other coils and the central region is kept clear for optical access.

Also, in order to make these coils superconducting a dielectric dewar assembly would be required. An attempt to construct a fiberglass dewar for the coil interaction experiments indicated that this is a difficult practical problem which will require significant effort for solution. The use of the suggested geometries avoids the need for the dielectric dewar.

REFERENCES

1. Covert, E E, M Finston, M Vlajinac and T Stephens, "Magnetic Balance and Suspension Systems for Use with Wind Tunnels", Progress in Aerospace Science, 14, Pergamon Press, 1973, pp 27-107.

2. Vlajinac, M and E E Covert, "Sting-Free Measurements of Sphere Drag in Laminar Flow", Journal of Fluid Mechanics, 54, Part 3, Aug., 1972, pp 385-392.

3. Judd, M M, M Vlajinac and E E Covert, "Sting-Free Drag Measurements on Ellipsoidal Cylinders at Transition Reynolds Numbers", Journal of Fluid Mechanics, 48, Part 2, July, 1971, pp 353-364.

4. Vlajinac, M, T Stephens, G Gilliam and N Pertas, "Subsonic and Supersonic Static Aerodynamic Characteristics of a Family of Bulbous Base Cones Measured with a Magnetic Suspension and Balance System", NASA Contractor Report, 1932 National Aeronautics and Space Administration, Washington, D.C.

5. McLaughlin, D K, J E Carter, M Finston and A J Forney, "Experimental Investigation of the Mean Flow of a Laminar Supersonic Cone Near Wake", AIAA Journal, 9, Sept, 1969, pp 479-484.

6. Blankson, I M and M Finston, "Measurements in the Laminar Near-Wake of Magnetically-Suspended Cones at M=6.3", AIAA Journal, 13, No. 12, December, 1975, pp 1562-1567.

7. Finn, D M, C W Haldeman and E E Covert, "Wake Measurements behind a Magnetically-Suspended Spinning and Non-Spinning Ogive Cylinder at Angles of Attack", BRL CR 331, Feb., 1977.

8. Solomon, M, M Finston and C W Haldeman, "Wake Studies Related to Reentrant Pyramids", MIT Aerophysics Lab. TR 205, AFOSR-TR-79-0984, Aug., 1979.

9. Birtwell, E P, J B Coffin, E E Covert and C W Haldeman, "Reverse Magnus Force on a Magnetically-Suspended Ogive Cylinder at Subsonic Speeds", AIAA Journal, Feb., 1978.

10. Bisplinghoff, R L, J B Coffin and C W Haldeman, "Support Free Measurements of Aerodynamic Characteristics of a Spinning 2-1/8 inch Diameter Ring Airfoil using the Magnetic Balance", BRL CR 317, Sept., 1976.

11. Covert, E E and C W Haldeman, "Initial Wind Tunnel Tests of a Magnetically-Suspended Spinning and Coning Ogive Cylinder", MIT Aerophysics Lab. TR 201, DAAG29-75-C-0001, March, 1978.

12. Kraemer, R A, "Low A.C. Loss Superconducting Coils for a Wind Tunnel Magnetic Suspension and Balance System", S.M. Thesis, Dept of Aeronautics and Astronautics, Sept., 1978.

13. Prey, S W, "A.C. Losses in Interacting Superconducting Magnetic Coils", S.M. Thesis, Dept of Aeronautics and Astronautics, Sept., 1979.

14. Alishahi, M M, "Preliminary Design of a Superconducting Coil Array for NASA Prototype Magnetic Balance", S.M. Thesis, Dept of Aeronautics and Astronautics, May, 1980.

15. Williams, J E C, "Superconductors-Their Properties and Applications, Past, Present and Future", Francis Bitter National Magnet Laboratory Publication, 1977.

16. London, H, "Alternating Current Losses in Superconductors of the Second Kind", Phys. Lett., Vol 6, 1963.

17. Kim, Y B, C F Hempstead and A R Strand, "Magnetization and Critical Supercurrents", Phys. Review, Vol 129, No. 2, 1963.

18. Carr, W J, Jr., "Longitudinal and Transverse Field Losses in Multifilament Superconductors", IEEE Trans. on Magnetics", Vol MAG-13, No. 1, 192, Jan, 1977.

19. Murphy, J H, M S Walker and W J Carr, Jr., "Theory of Alternating Field Losses in Cylindrical Twisted Multifilamentary Superconductors", IEEE Trans. on Magnetics, Vol MAG-10, 1974, p 868.

20. Carr, W J, Jr., "A.C. Loss in a Twisted Filamentary Superconducting Wire. I", J. Appl. Phys. 45, No. 2, Feb, 1974.

21. Carr, W J, Jr., "A.C. Loss in a Twisted Filamentary Superconducting Wire. II", J. Appl. Phys. 45, No. 2, Feb, 1974.

22. Handbook on Materials for Superconducting Machinery, Battelle Report MClC-HB-04, Nov., 1975.

23. Cieloszyk, G S, P J Cote, G L Salinger and J C Williams, "Thermal and Electrical Properties of Evanohm and Other Resistance Alloys below 4°K", Rev. Sci. Instr., 46 No. 9, Sept., 1975, pp 1182-1185.

24. Jakob, M, Heat Transfer, 1, J Wiley & Sons, New York, 1957.

25. Walker, M S, J M Cutro, B A Zeitlin, G M Ozeryansky and R E Schwall, "Intermagnetics General Corp.; C E Oberly, Wright-Patterson Air Force Base; J C Ho, Wichita State University; and J A Wollam, NASA-Lewis Research Center, "Properties and Performance of Fine-Filament Bronze-Process Nb_3Sn Conductors", IEEE Trans. on Magnetics, Vol MAG-15, No. 1, Jan., 1979.

26. Murase, S, M Koizumi, O Horigami, H Shiraki, Y Koike, E Suzuki, M Ichihara, F Nakane and N Aoki, "Multi-filament Niobium-Tin Conductors", IEEE Trans. on Magnetics, Vol MAG-15, No. 1, Jan., 1979.

27. Brown, G V, L Flax, E C Itean and J C Laurence, "Axial and Radial Magnetic Fields of Thick, Finite-Length Solenoids", NASA TR R-170, Lewis Research Center, Cleveland, Ohio, Dec., 1963.

28. Haldeman, C W and J Sullivan, "Engineering Aspects of Electromagnetic Energy Addition to a Gas by a Traveling Magnetic Field", MIT Aerophysics Lab TR 156, F33615-68-C-1380, Sept., 1969.

29. Salisbury, K J, "Kent's Mechanical Engineer's Handbook", Twelfth Ed., Power Volume, J Wiley & Sons, 1950.

30. Kuwasawa, Y, T Ando and S Nakano, "Hysteresis Losses in Superconducting Coil", IEEE Trans. on Magnetics, Vol MAG-13, No. 1, Jan., 1977, pp 556-560.

31. Stephens, T and R Adams, "Wind Tunnel Simulation of Store Jettison with the Aid of Magnetic Artificial Gravity", NASA CR 1955, Feb., 1972.

32. Way, P, "TABLE Program Modifications", MIT Aerophysics Lab. Internal Memo AR 1031, Nov., 1977.

33. Stephens, T, "Design, Construction and Evaluation of a Magnetic Suspension and Balance System for Wind Tunnels", MIT Aerophysics Lab TR 136, NAS1-4421, Nov., 1969.

34. Stratton, J A, "Electromagnetic Theory", McGraw-Hill Book Co., New York, 1941.

35. Hastings, C, Jr., "Approximation for Digital Computers", Princeton University Press, 1955.

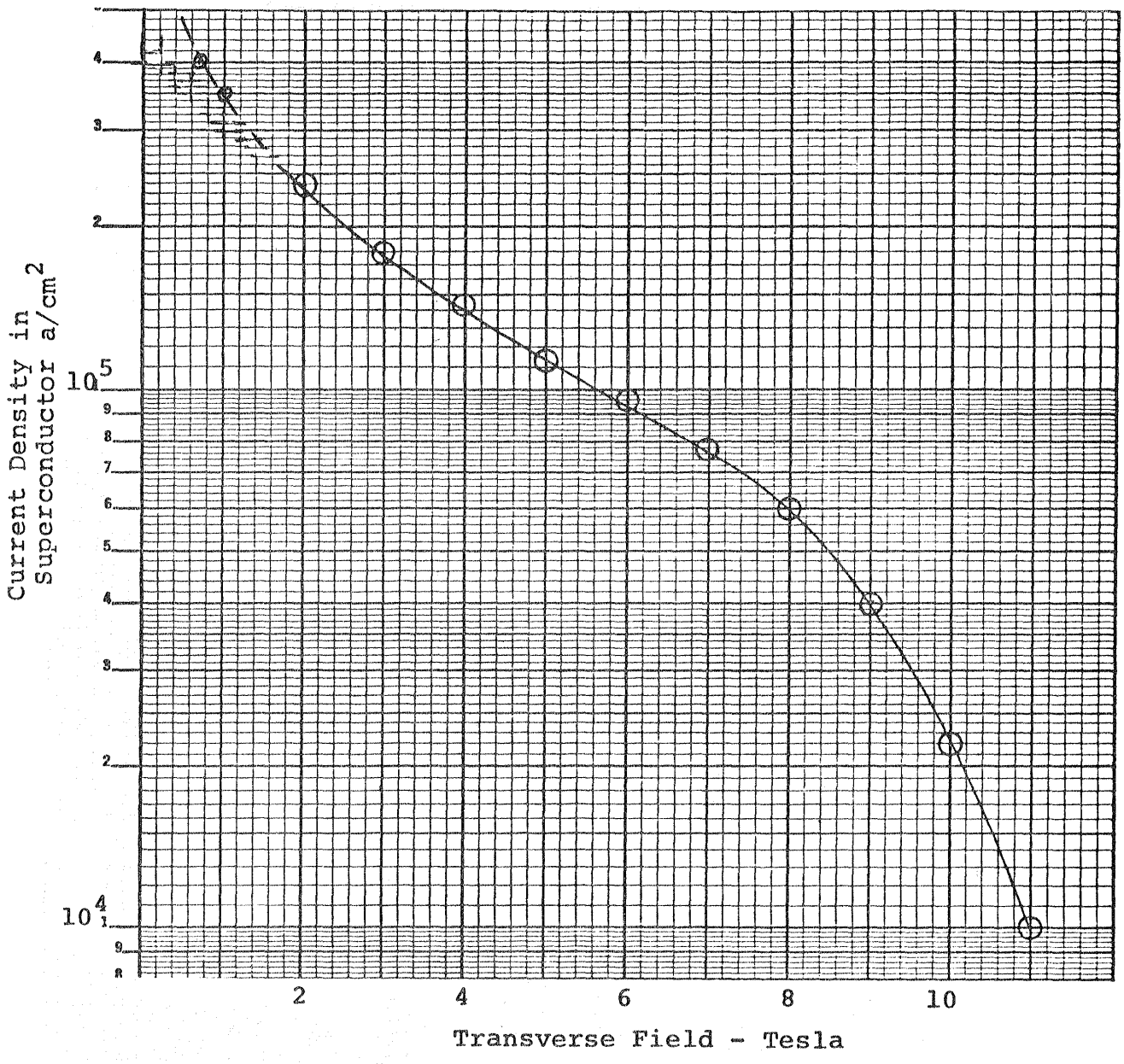

Figure 1 Critical Current Density in Copper Stabilized Nb-Ti Wire .1 mm Diameter (SuperCon Inc.)

Figure 2

Critical Current Density in Copper Stabilized
Nb-Ti Wire and Litz Cables (Supercon Inc.)

- O Published Spec .1 mm Wire
- Δ Cable for Coil 5 Short Sample
- ▭ Cable for Coil 3 Short Sample
- ⊖ ⊕ Cable for Coil 4 Short Sample
- × † Cable for Coil 4 10 ft. Sample
- •—•- Calculated: $Jc = \frac{Jo\ Bo}{Bm+Bo}$ $Jo = 6.81885 \times 10^{+9}\ \frac{A}{M^2}$

$Bo = 1.05124T$

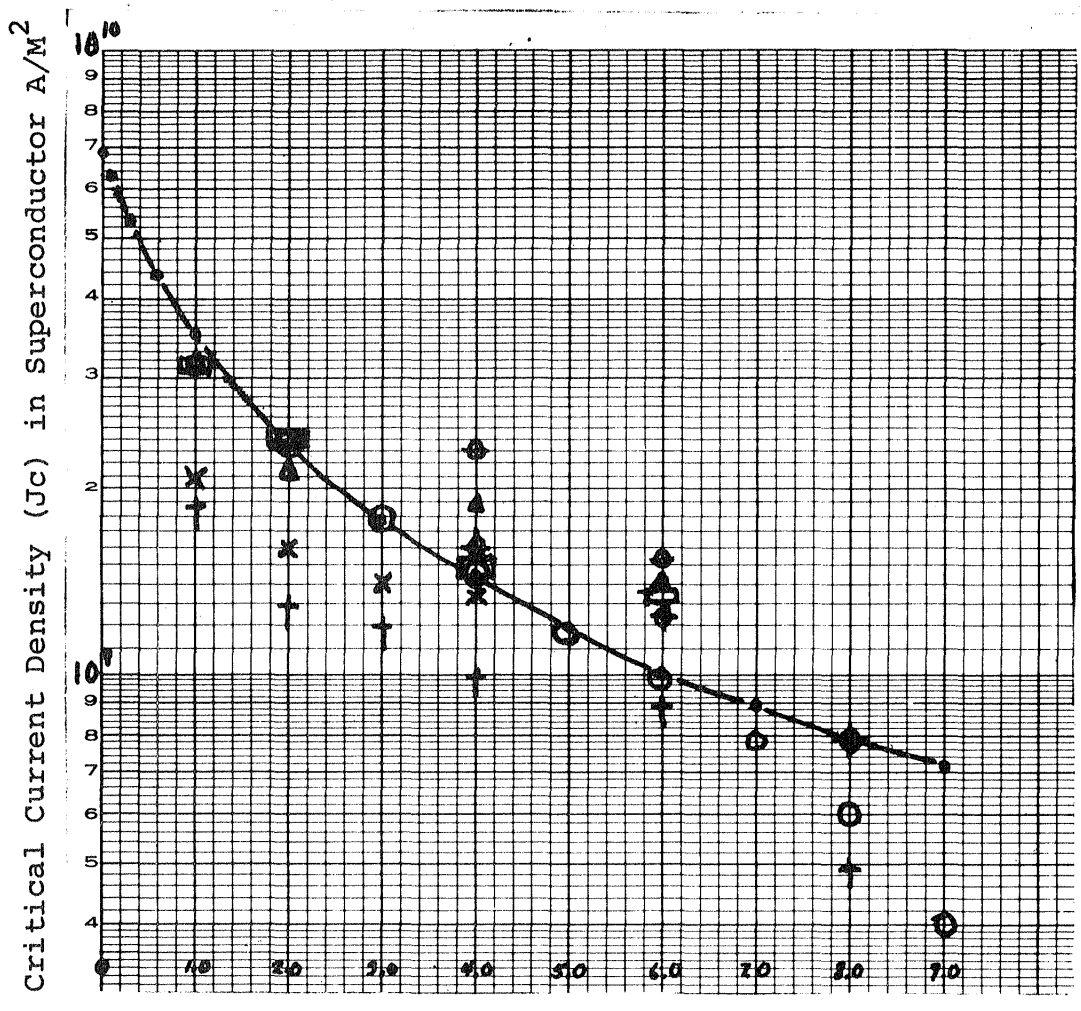

Figure 3.

Measured Critical Current
vs. Flux Density for Superconducting
Litz Coils compared to Cable Data.

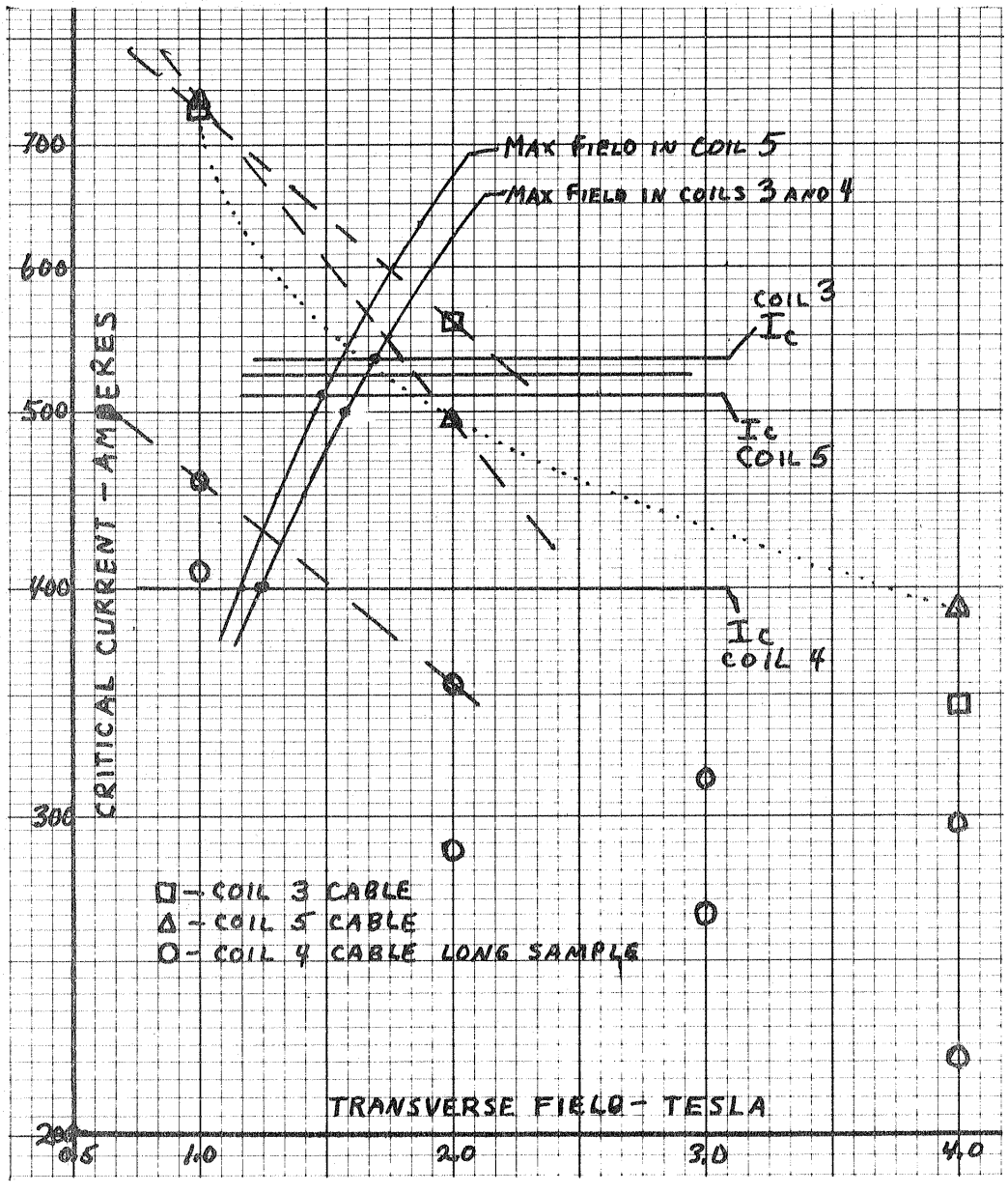

500X

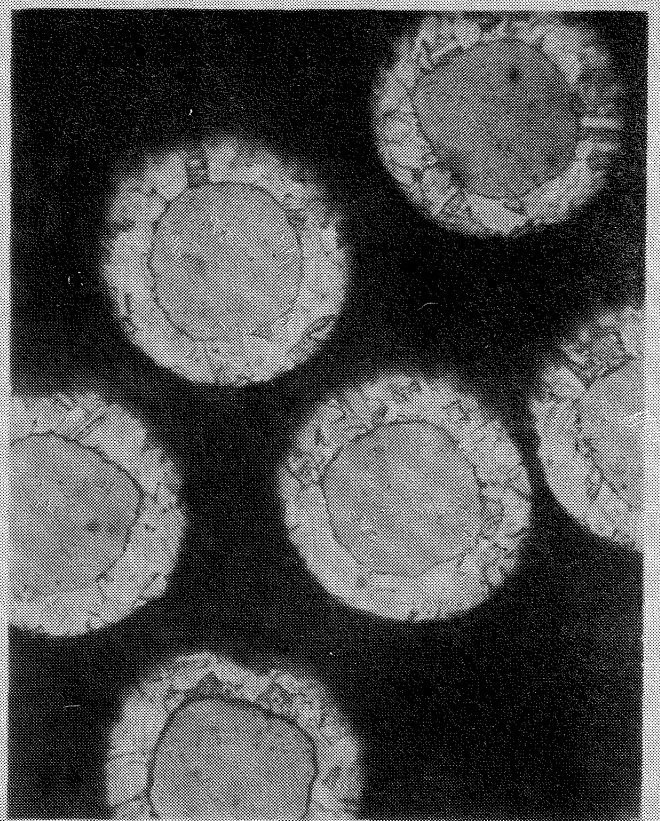

500X

Figure 4. Coil #3 (Larger) and Coil #5 (Smaller) Cable Wire. Single Nb-Ti Core Stabilized with Copper Outer Sheath.

500X

1000X

Figure 5 Coil #4 Cable Wire. Nb-Ti 54 Filament.
Multifilament Composite in Copper Matrix.

Alternate Superconducting Litz Cable Constructions

Figure a

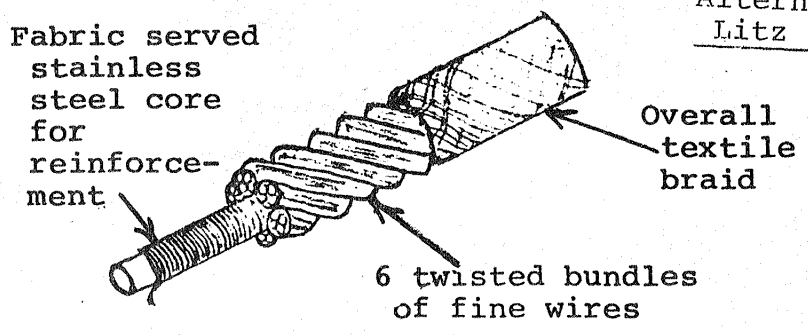

Figure b

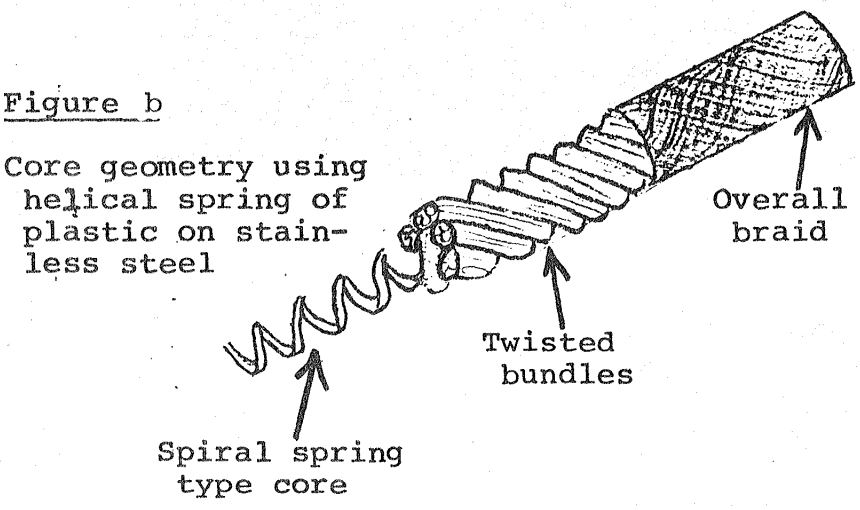

Figure c

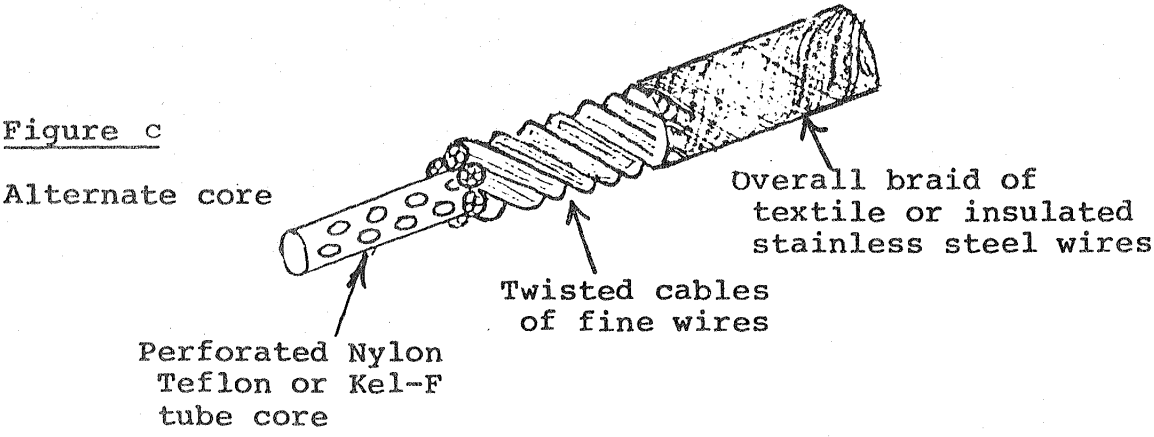

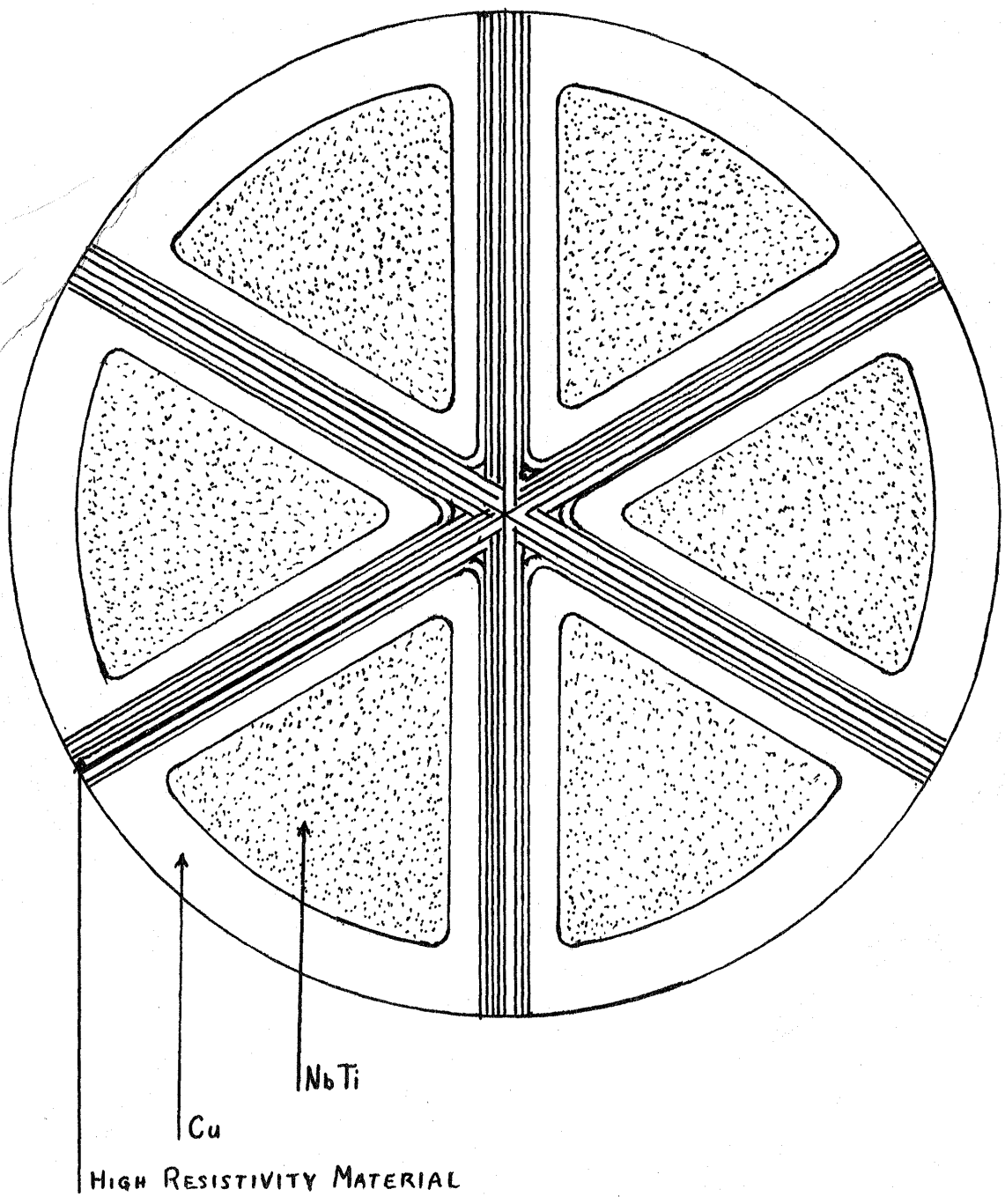

Figure 8

Multifilament Shielded Superconductor

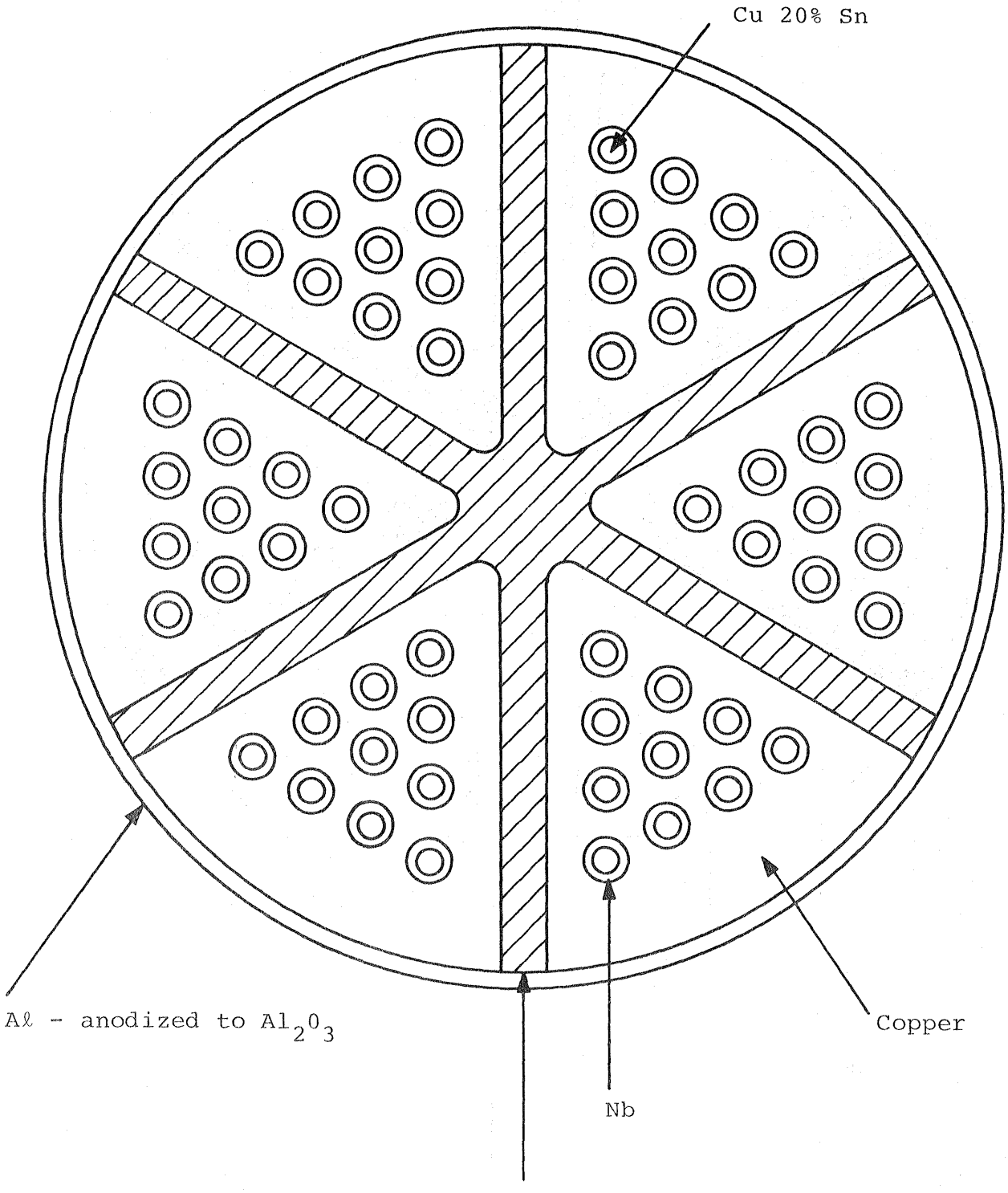

Figure 9 Nb_3Sn Litz Wire Strand

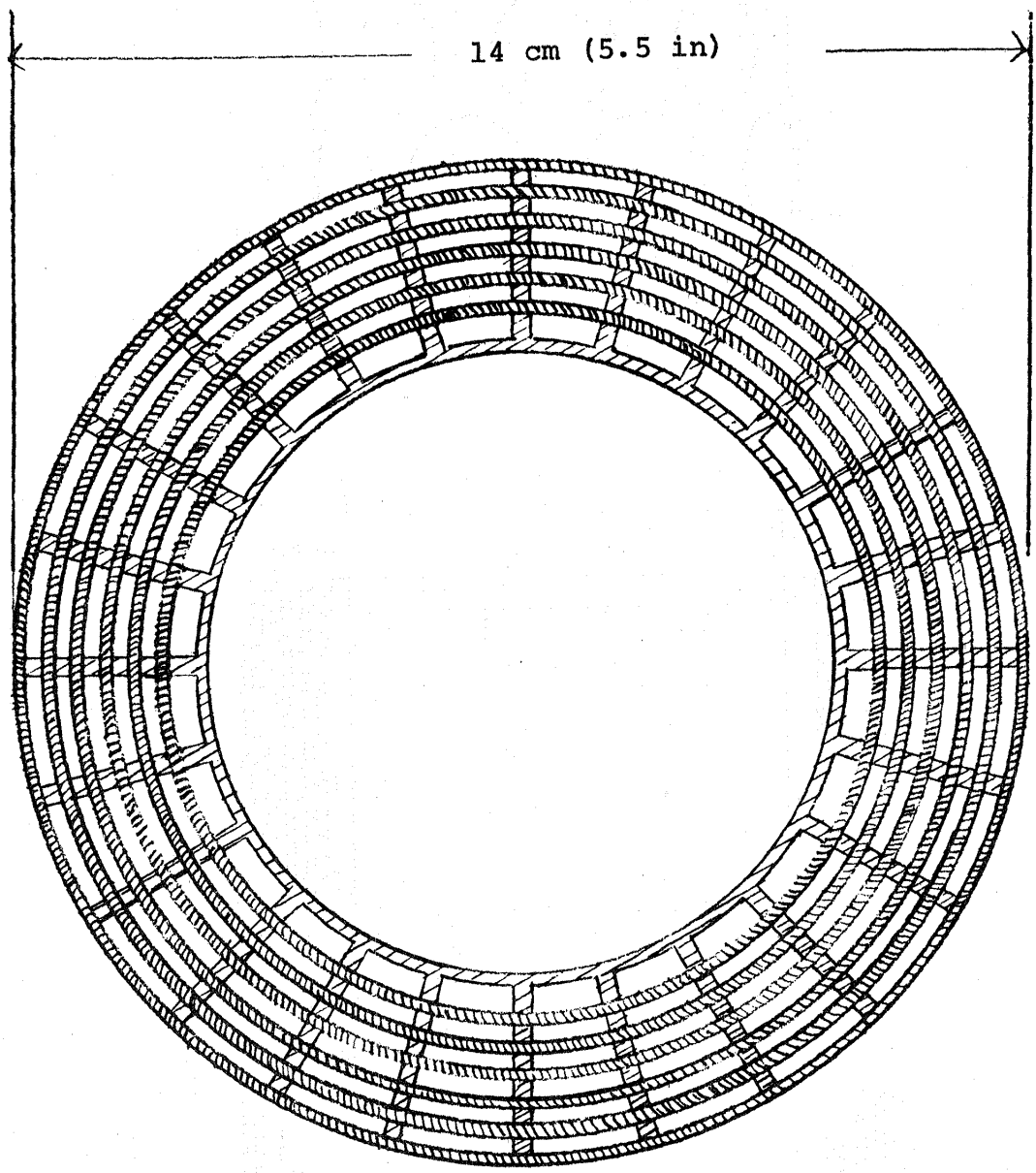

Figure 10 Sample Coil Cross Section

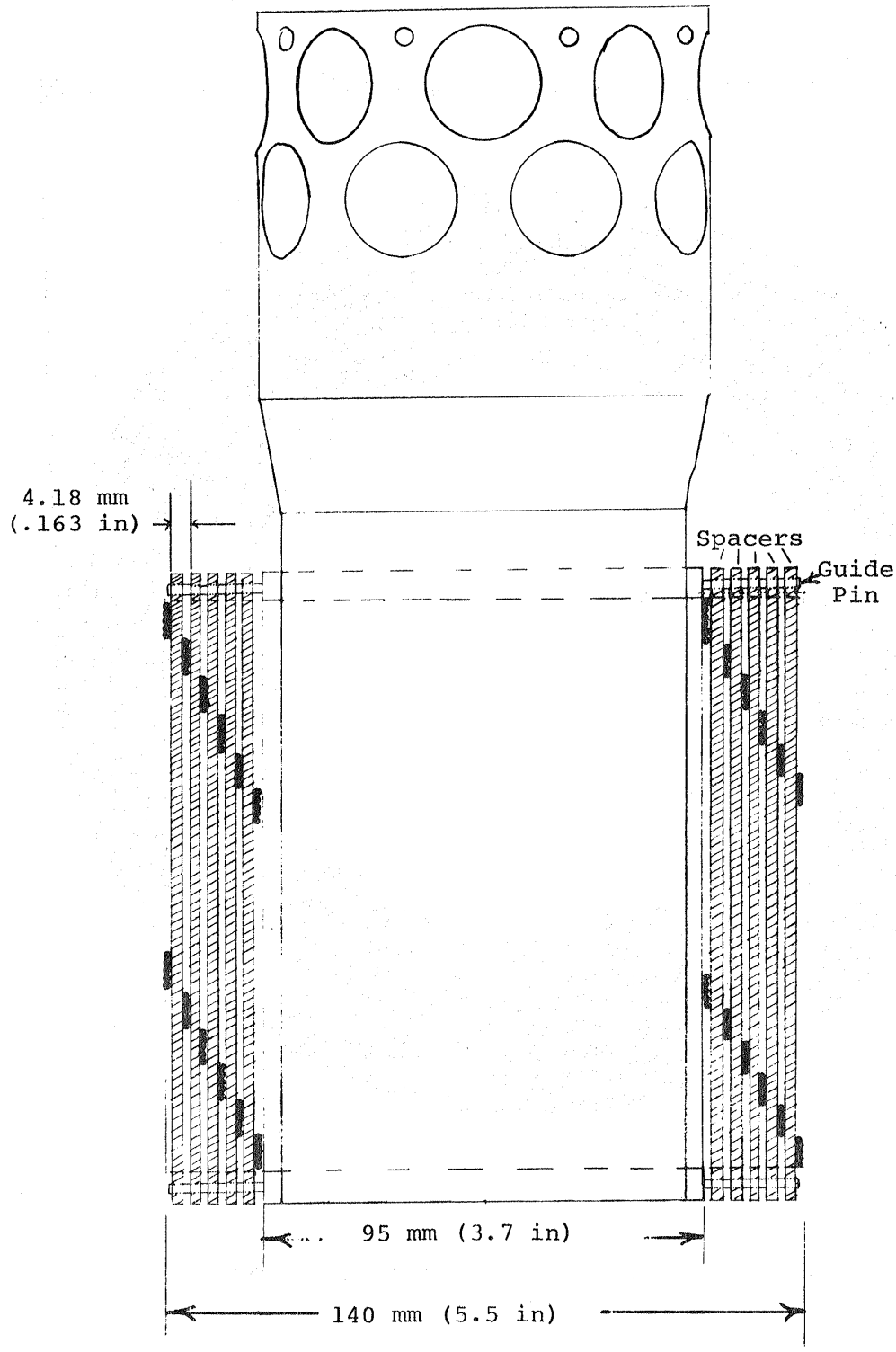

Figure 11 Sample Coil Axial Section

Figure 12

Test Coil 4 Assembled
with Electrical Connections

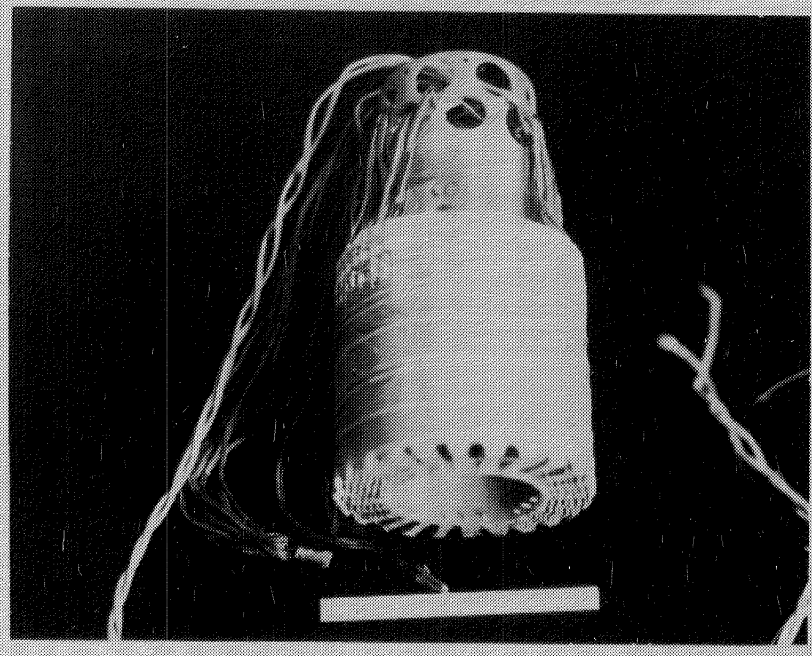

Figure 13

Test Coil Construction showing wire being wound over cooling channel spacers. This coil is being rewound after failure and a cable splice is shown.

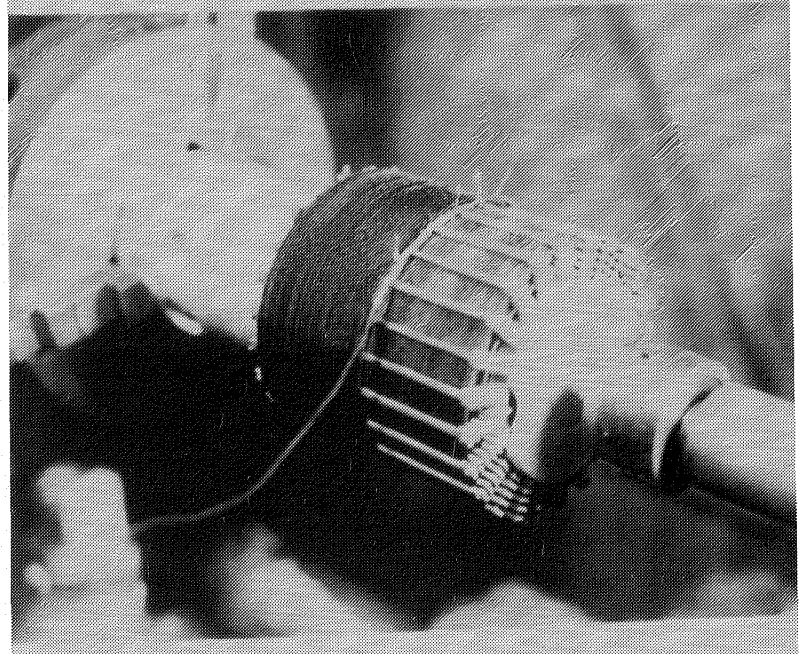

Figure 14 Experimental Setup

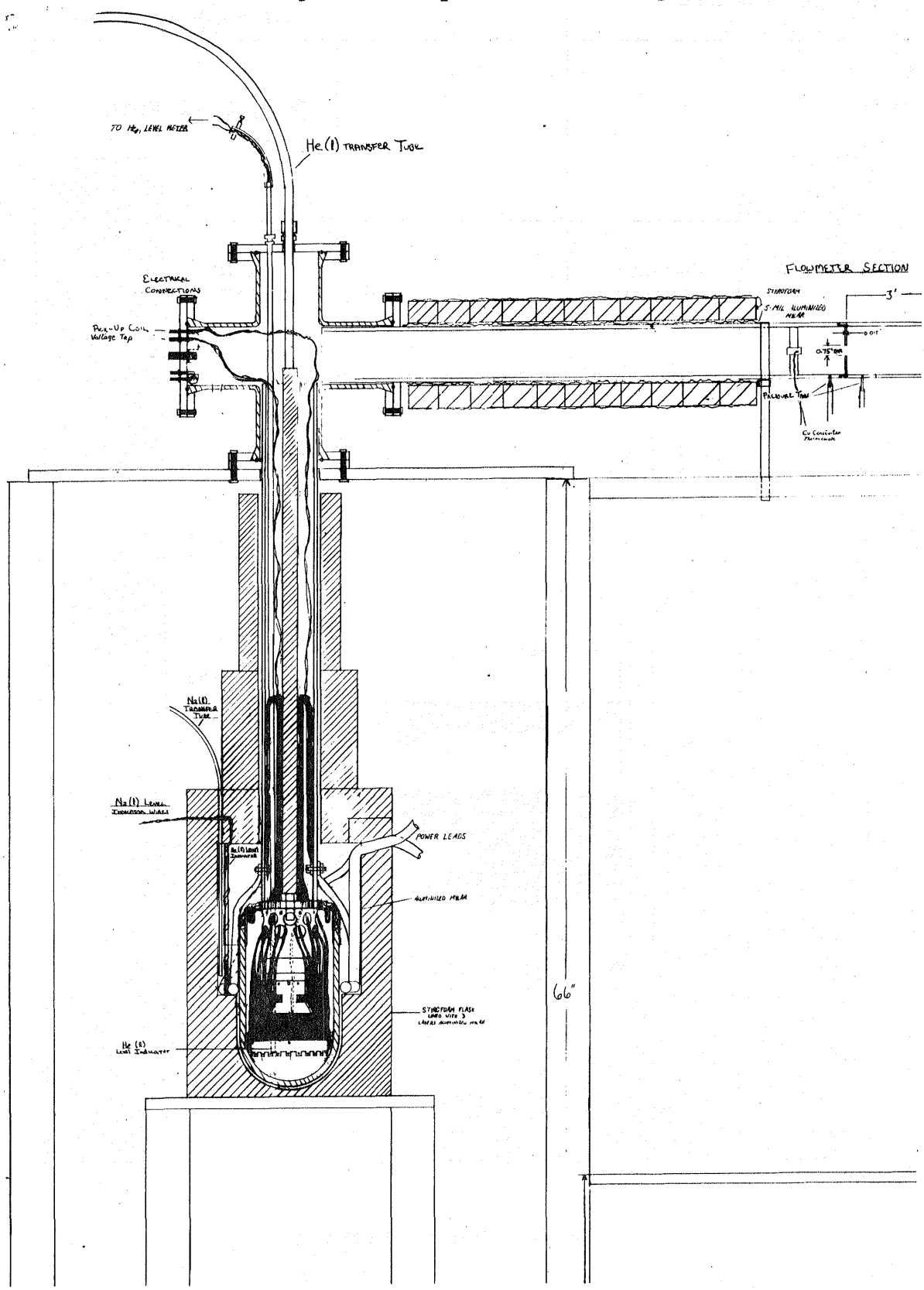

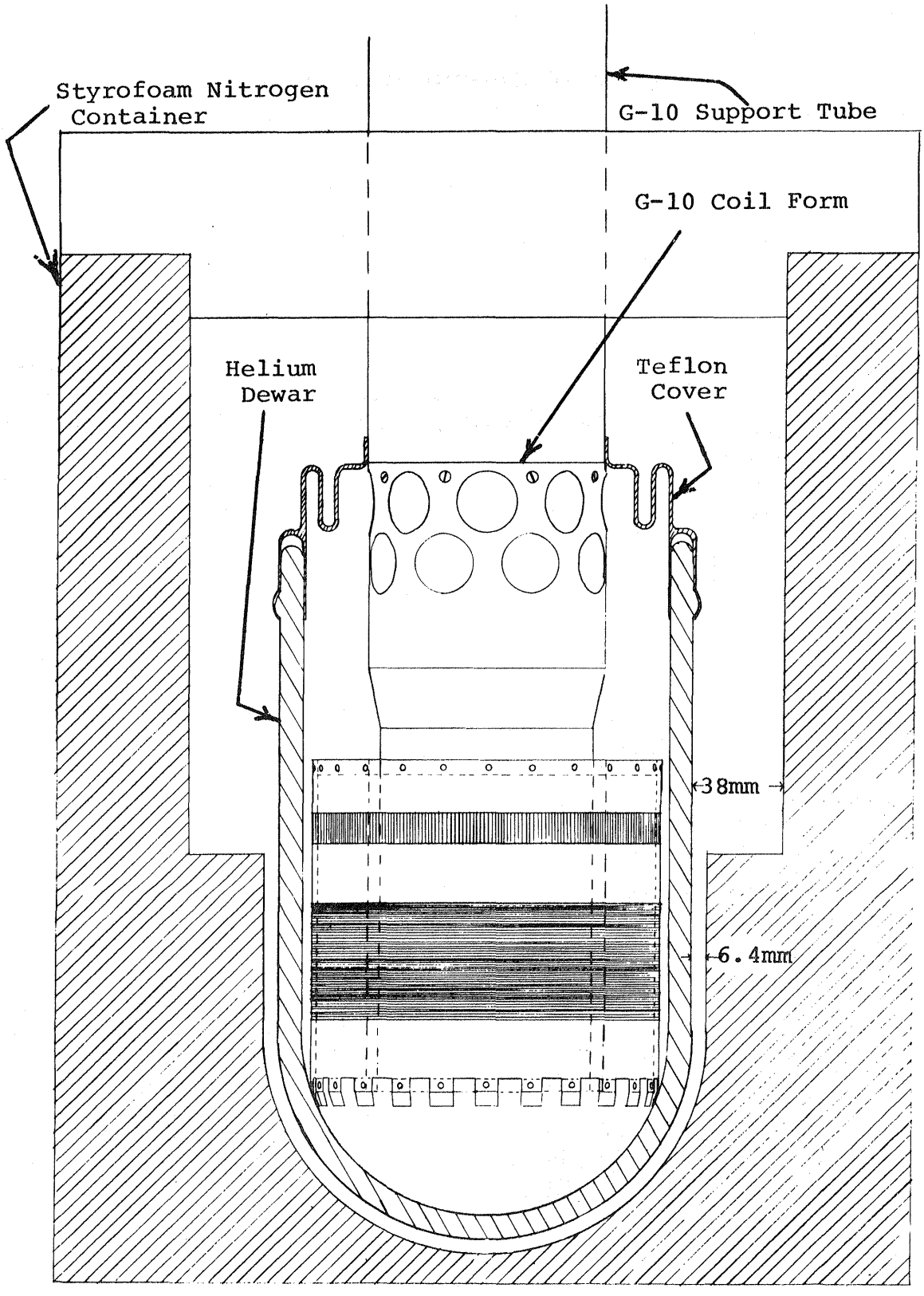

Figure 15 Dewar Assembly

Figure 16

Single Core Wire Coil Losses Measured at 200 Amp Peak Sinusoidal Current. Lines are calculated from:

$$\frac{\text{Watts}}{M^3 \text{ s.c.}} = \frac{8\ Bm\ d\ f}{3\pi} \left(\frac{Jo\ Bo}{Bm+Bo}\right)$$

$Jo = 6.81885 \times 10^9 \frac{A}{M^2}$ $\quad Bo = 1.051724T$

f = Freq. Hz.

□ Coil #3: $d = 7.37 \times 10^{-5} M$ $\quad Bm = .268T$

△ Coil #5: $d = 3.67 \times 10^{-5} M$ $\quad Bm = .257T$

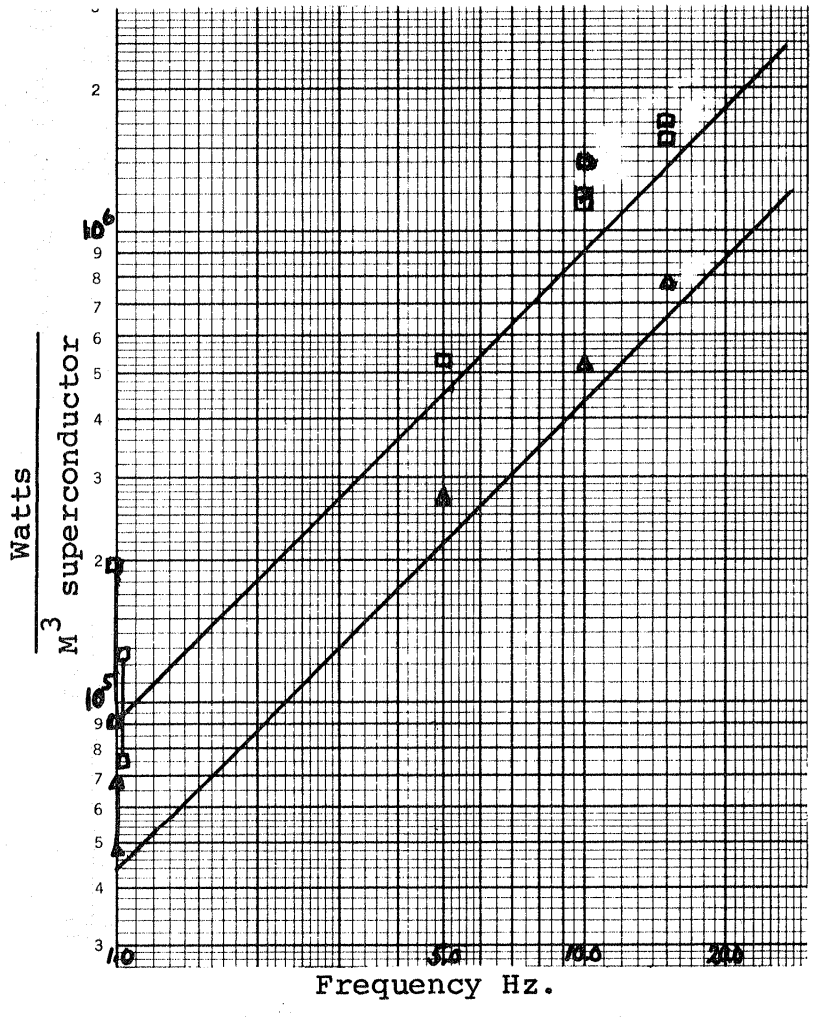

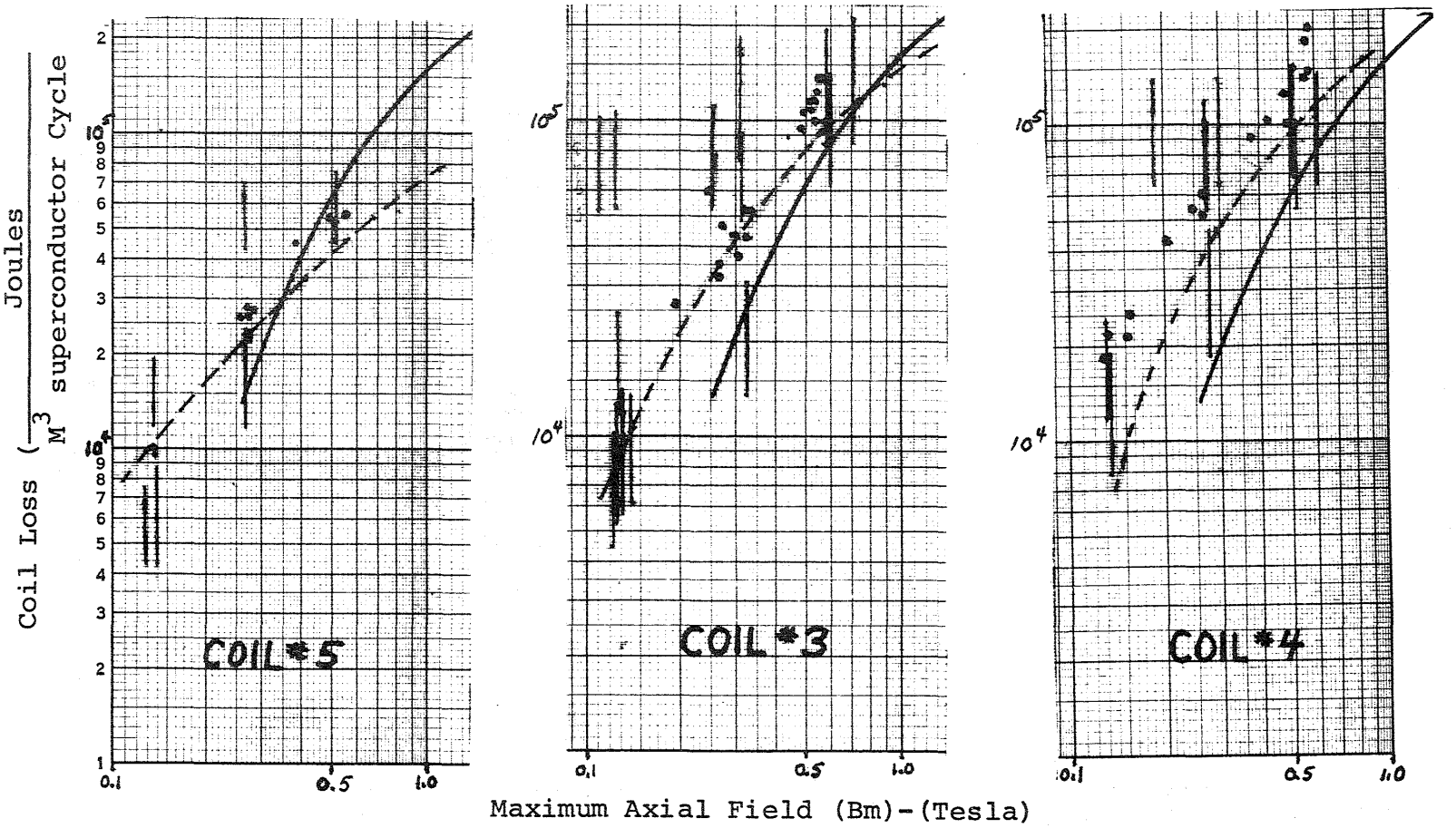

Figure 17. Coil Loss per Cycle vs. Maximum Field at Coil Axis
———— compared to Published Coil Losses (30)
— — — — computed for these coils.

Figure 18

Multifilament Wire Coil Losses Measured at 200 Amp Peak Sinusoidal Current. Line is calculated from:

$$\frac{\text{Watts}}{M^3\ \text{s.c.}} = \frac{8\ Bm\ d\ f}{3\pi}\left(\frac{Jo\ Bo}{Bm+Bo}\right)$$

$Jo = 6.81885 \times 10^9 \frac{A}{M^2}$ $Bo = 1.051724T$

f = Freq. Hz.

● Coil #4: $d = Ro = 9.3 \times 10^{-5} M$ $Bm = .271T$

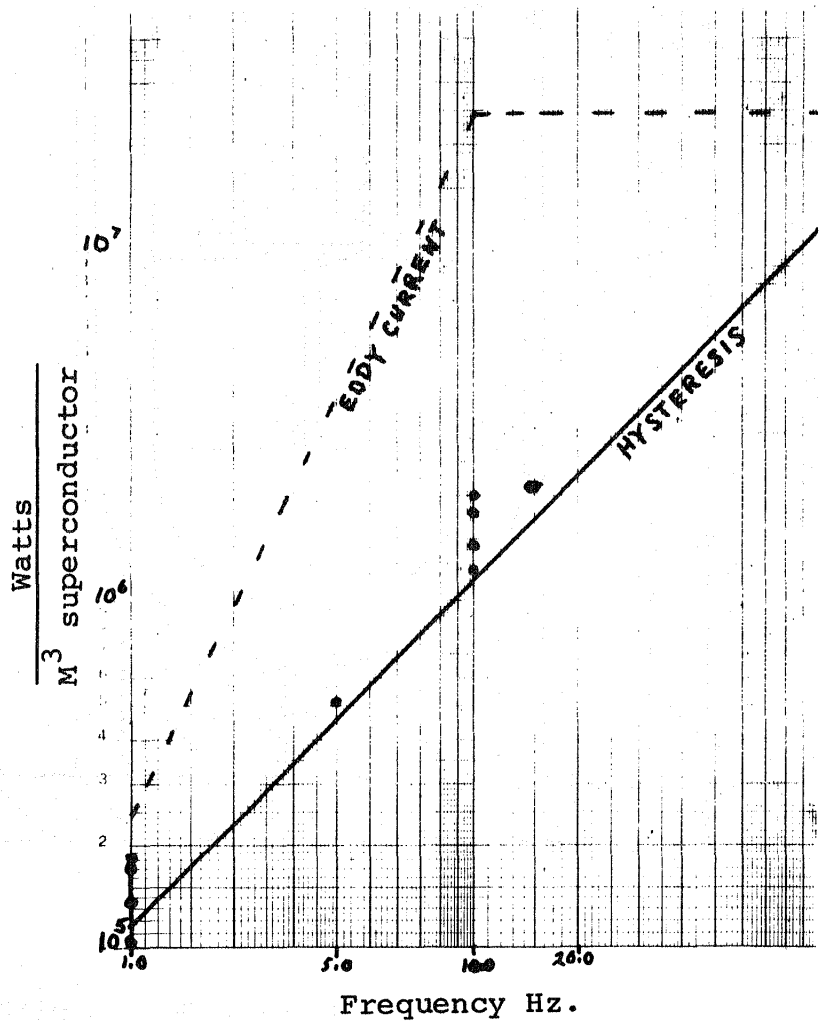

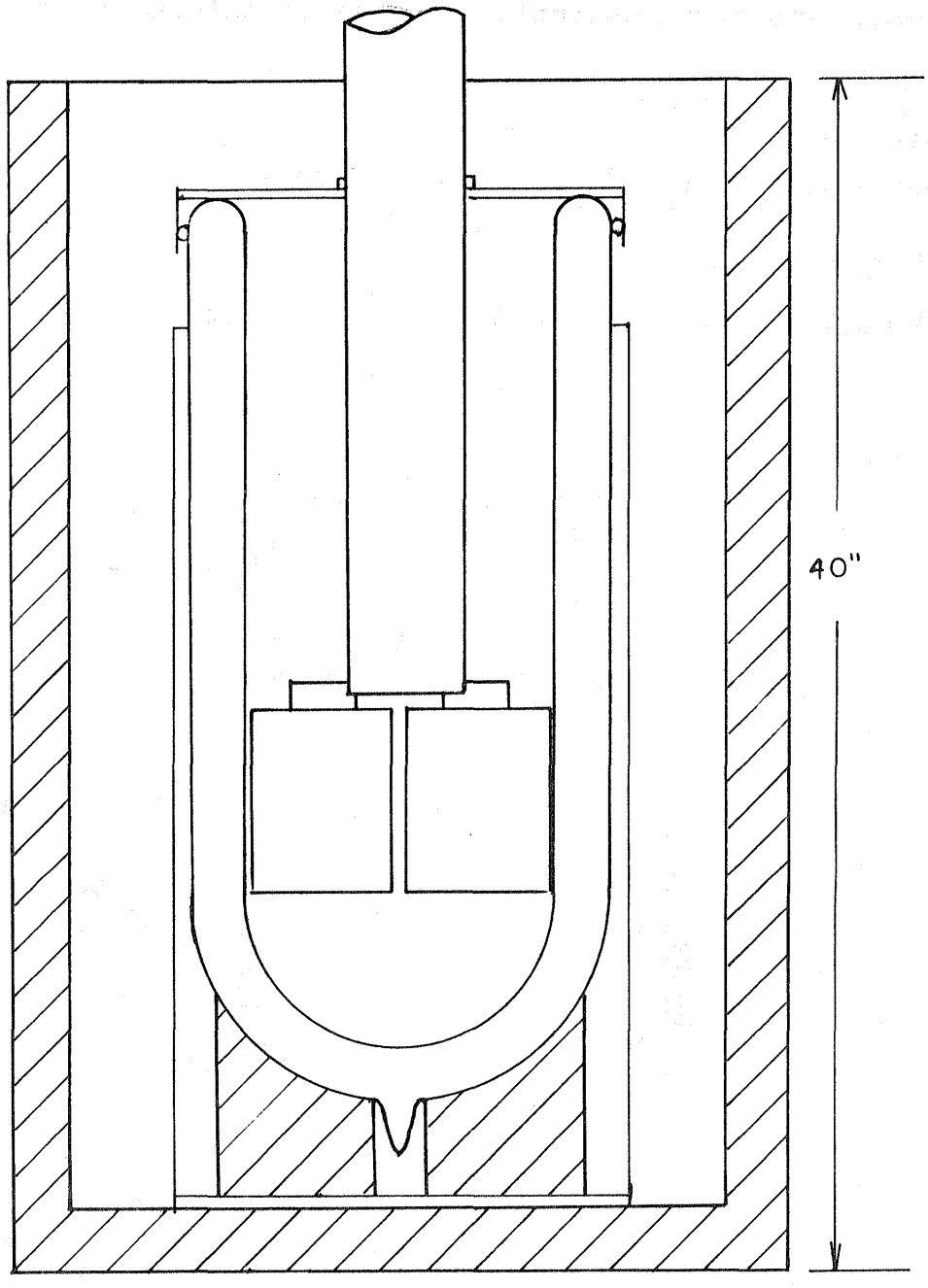

Figure 19 Dewar Set-up with
Parallel Coil Arrangement

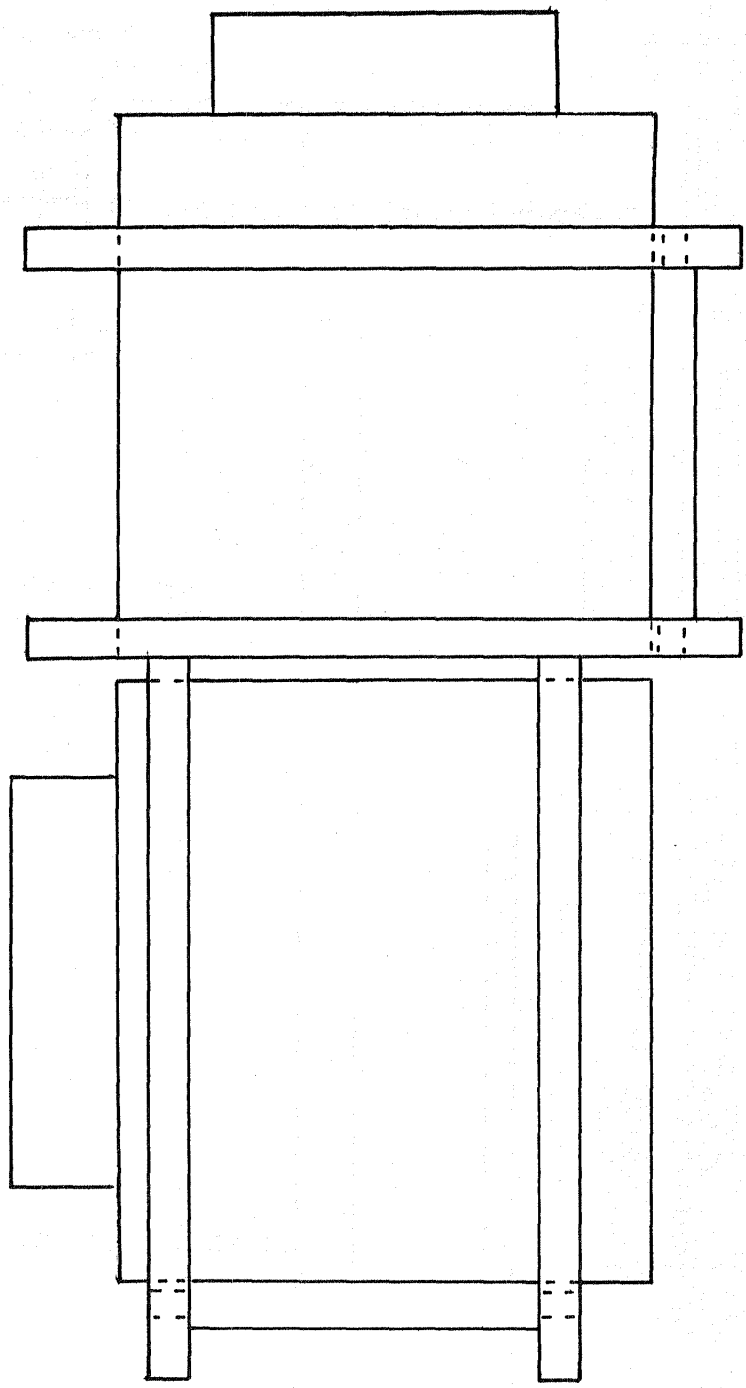

Figure 20 Test Coils in Perpendicular Bracket

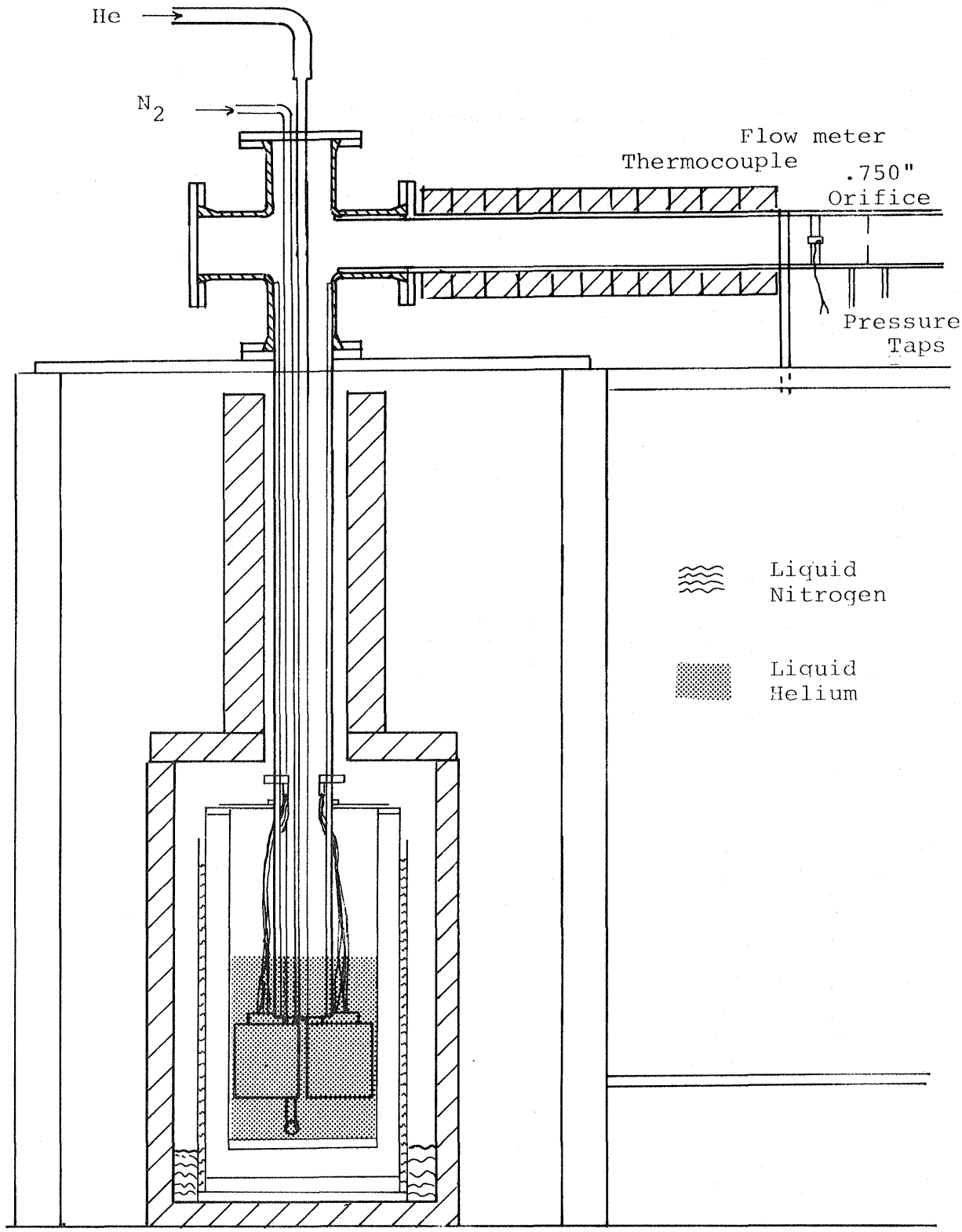

Figure 21 Experimental Schematic

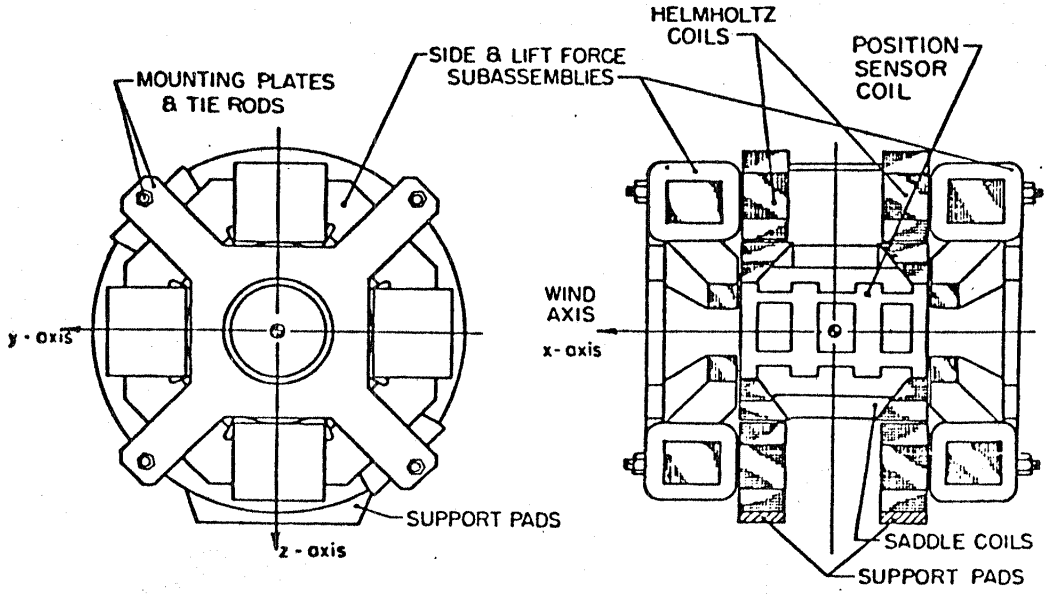

Magnet Assembly

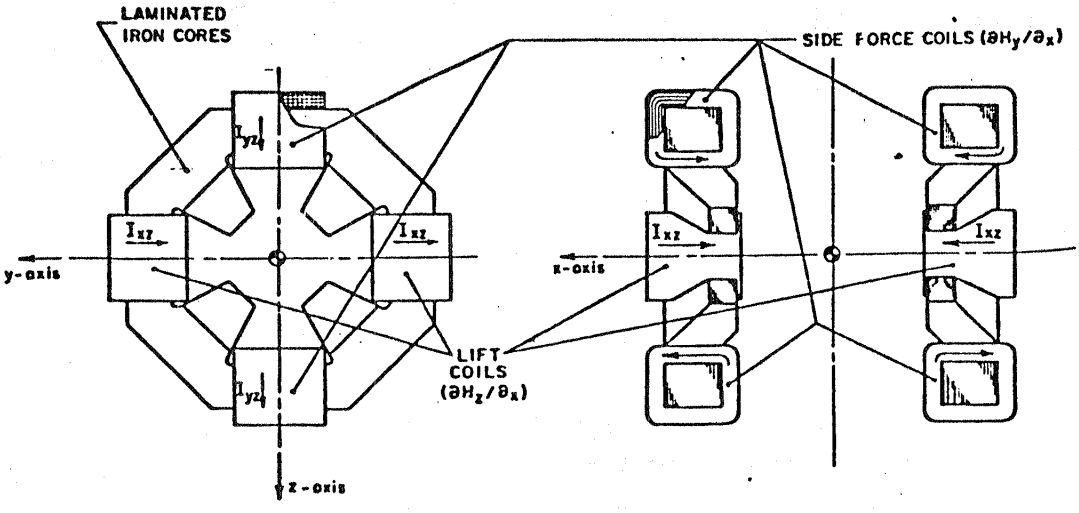

Lift and Side Force System

Figure 22 Present Copper Magnetic Balance Coils after Stephens (33)

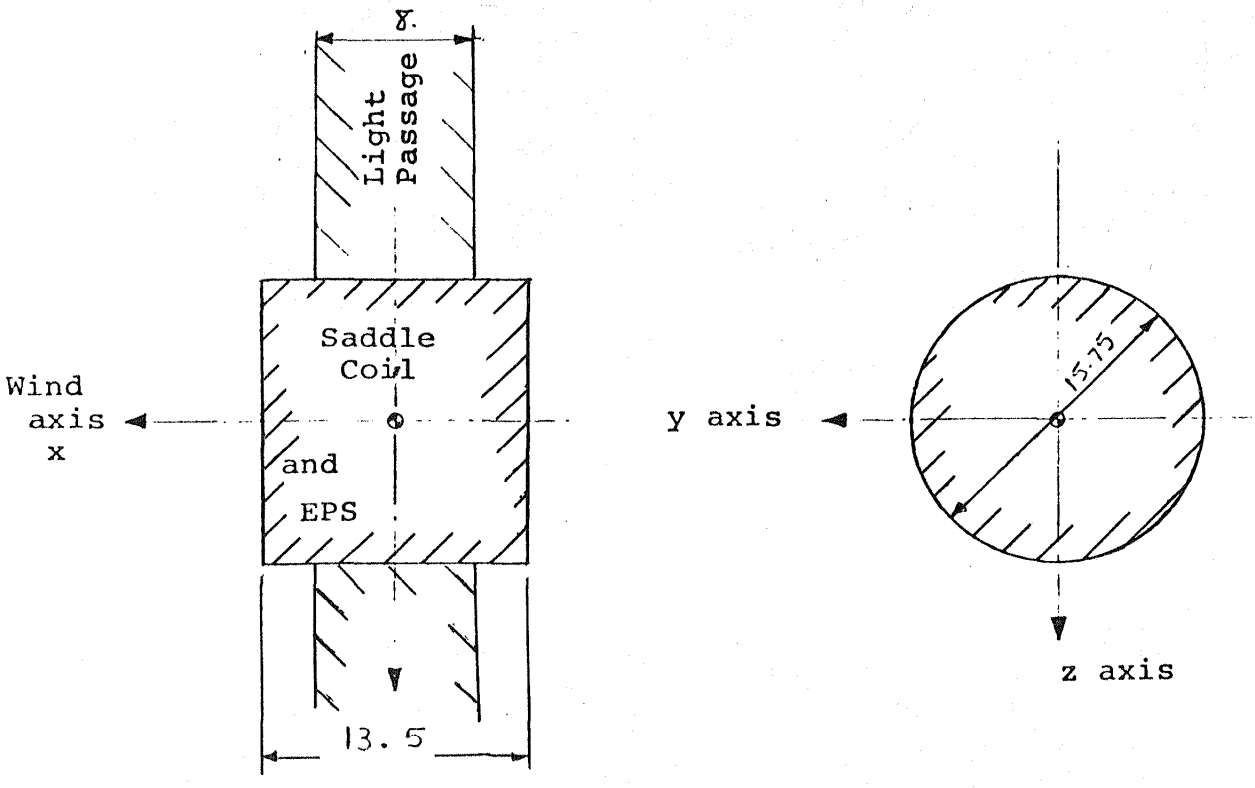

Figure 23 Excluded Volume for Design Dimensions in Inches

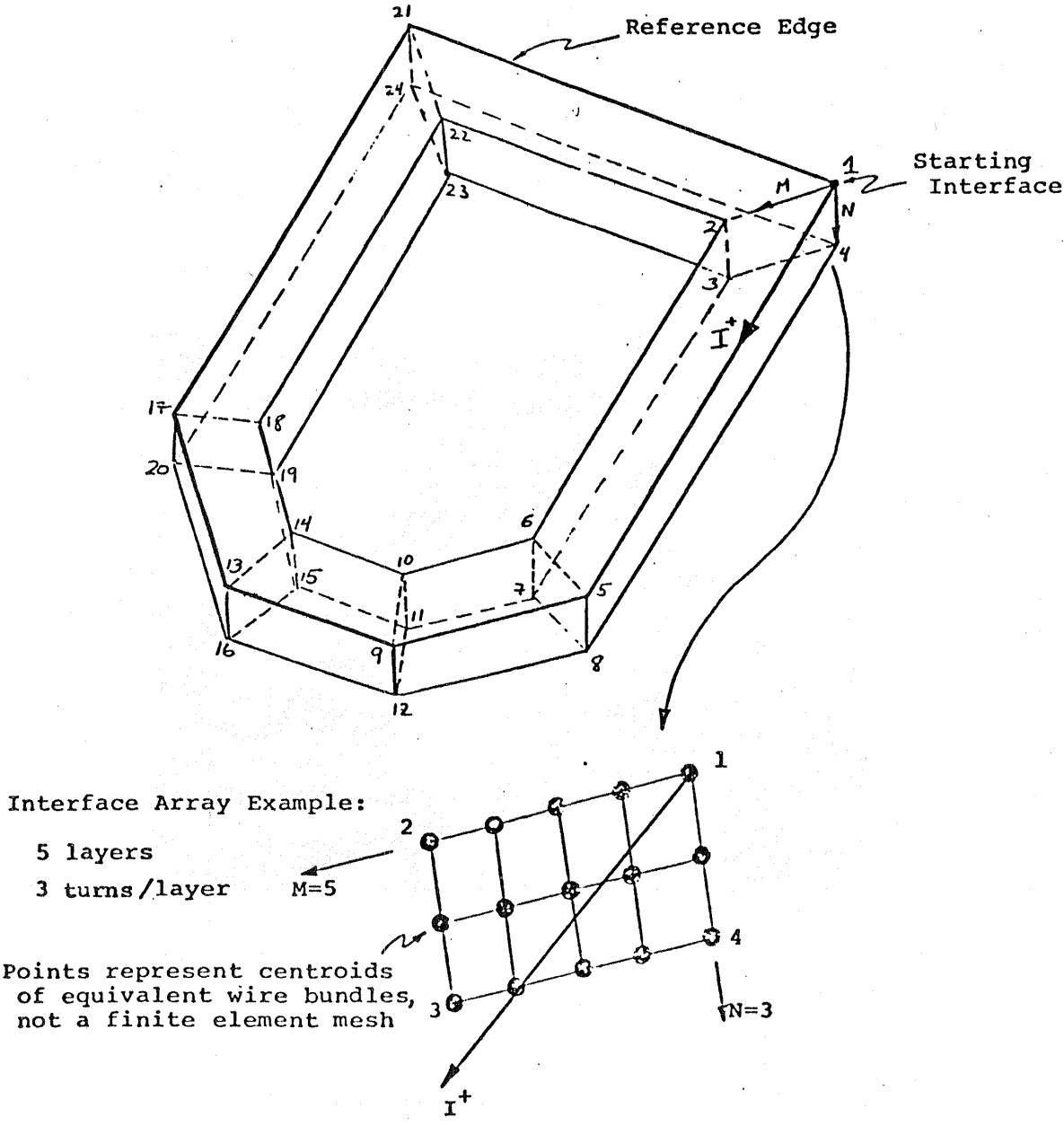

Figure 24 Sample Coil Geometry Specification

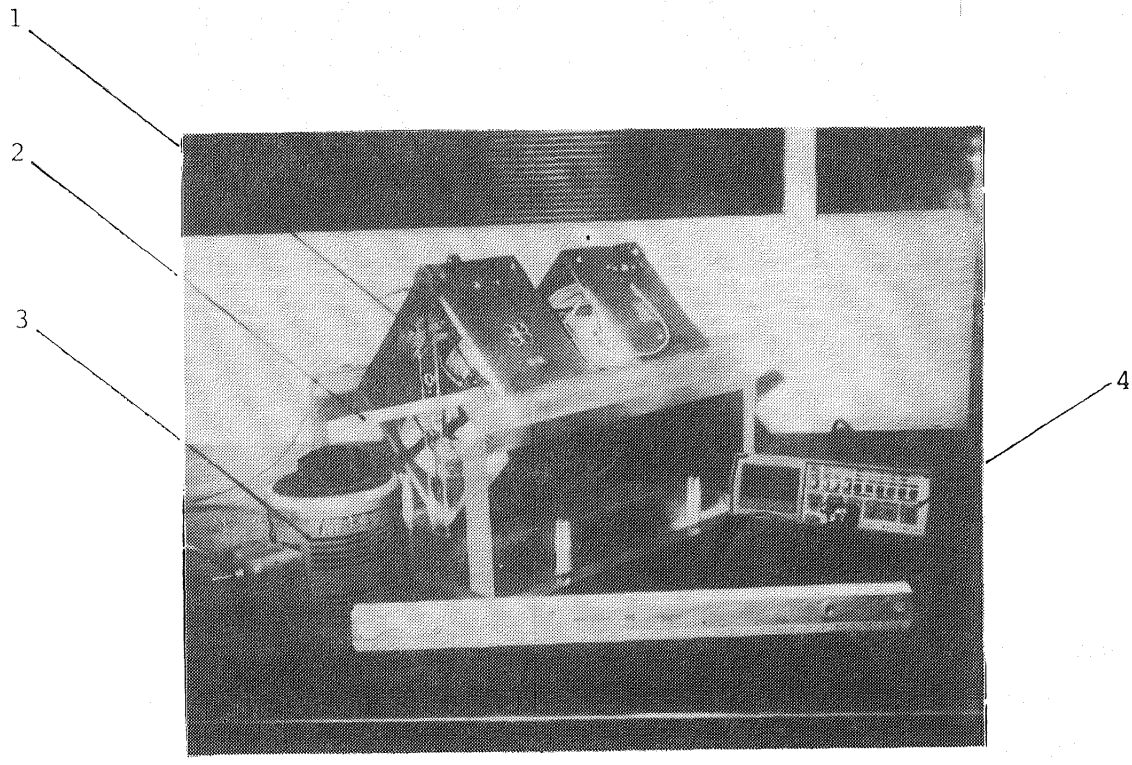

Figure 25 Model Coil for Testing TABLE

1	Model coil	3	A.C. transformer
2	Pick-up coil support	4	Pick-up coil voltmeter

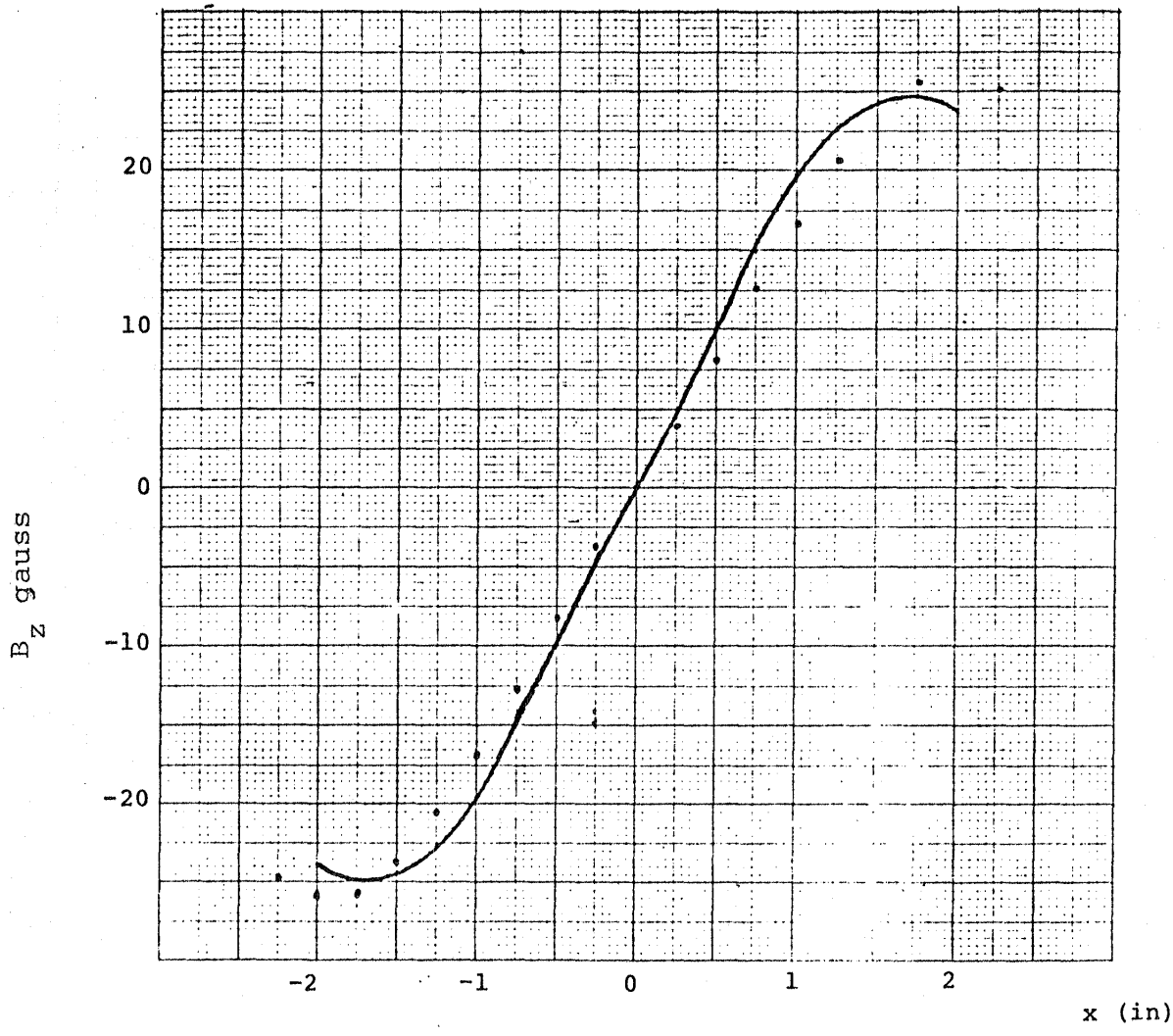

Figure 26 Transverse Field Component vs Axial Distance

Computer Results _____

Model Measurements .

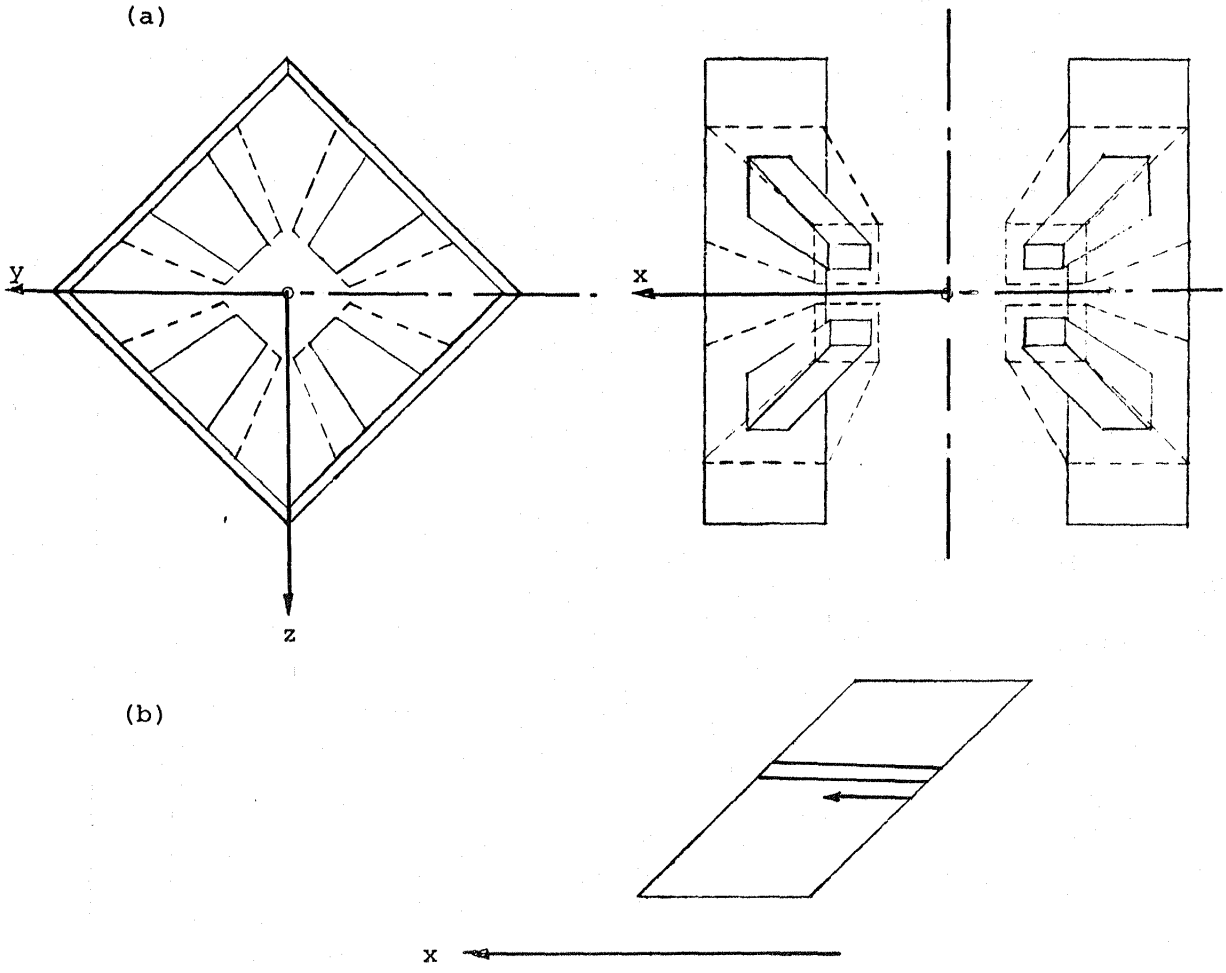

Figure 27 a) Model I
b) Direction of Wires

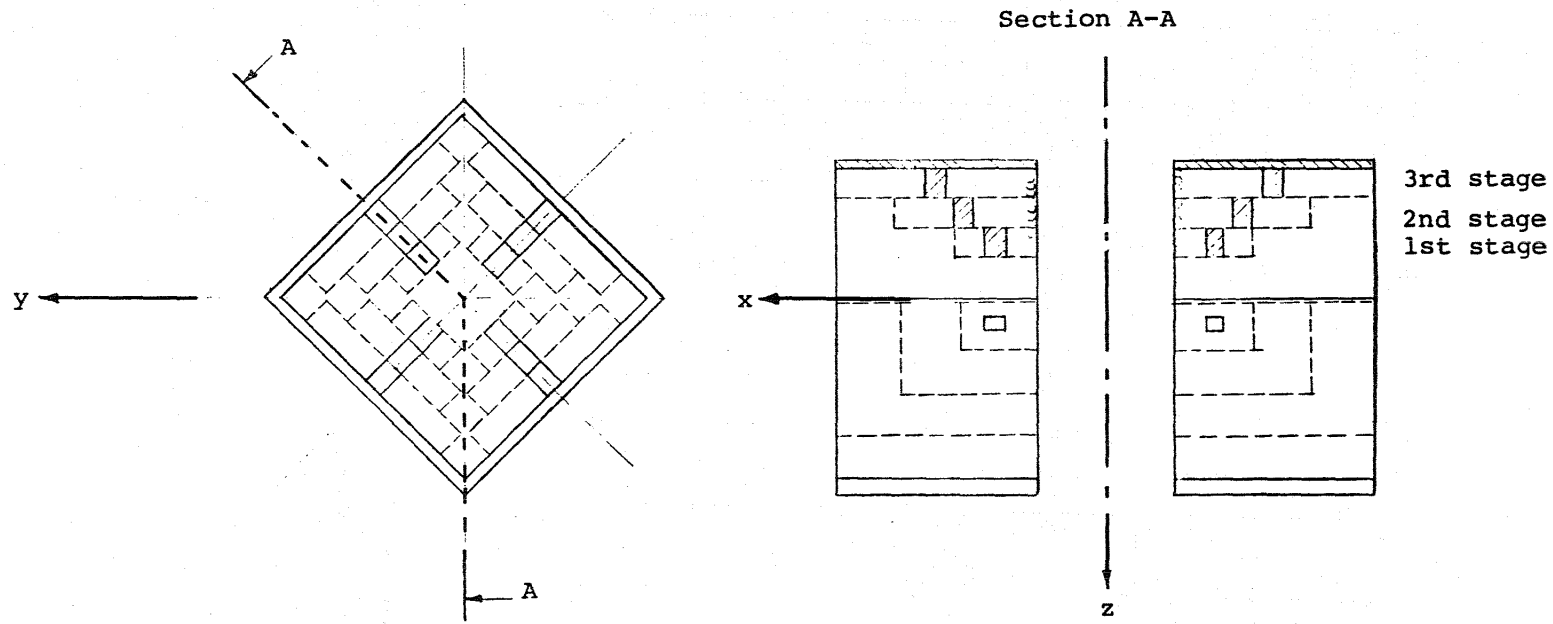

Figure 28 Model III

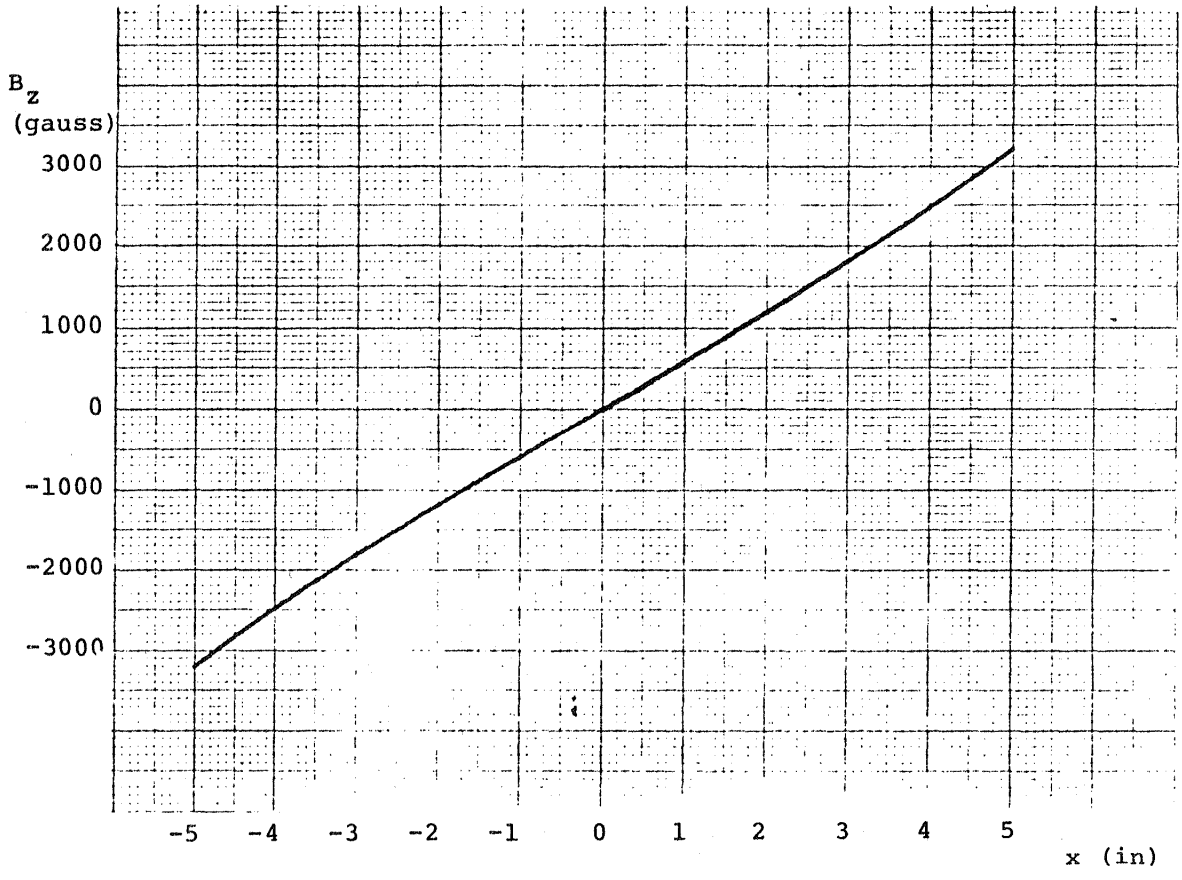

Figure 29 B_z vs Axial Distance x
for Side and Lift Coil

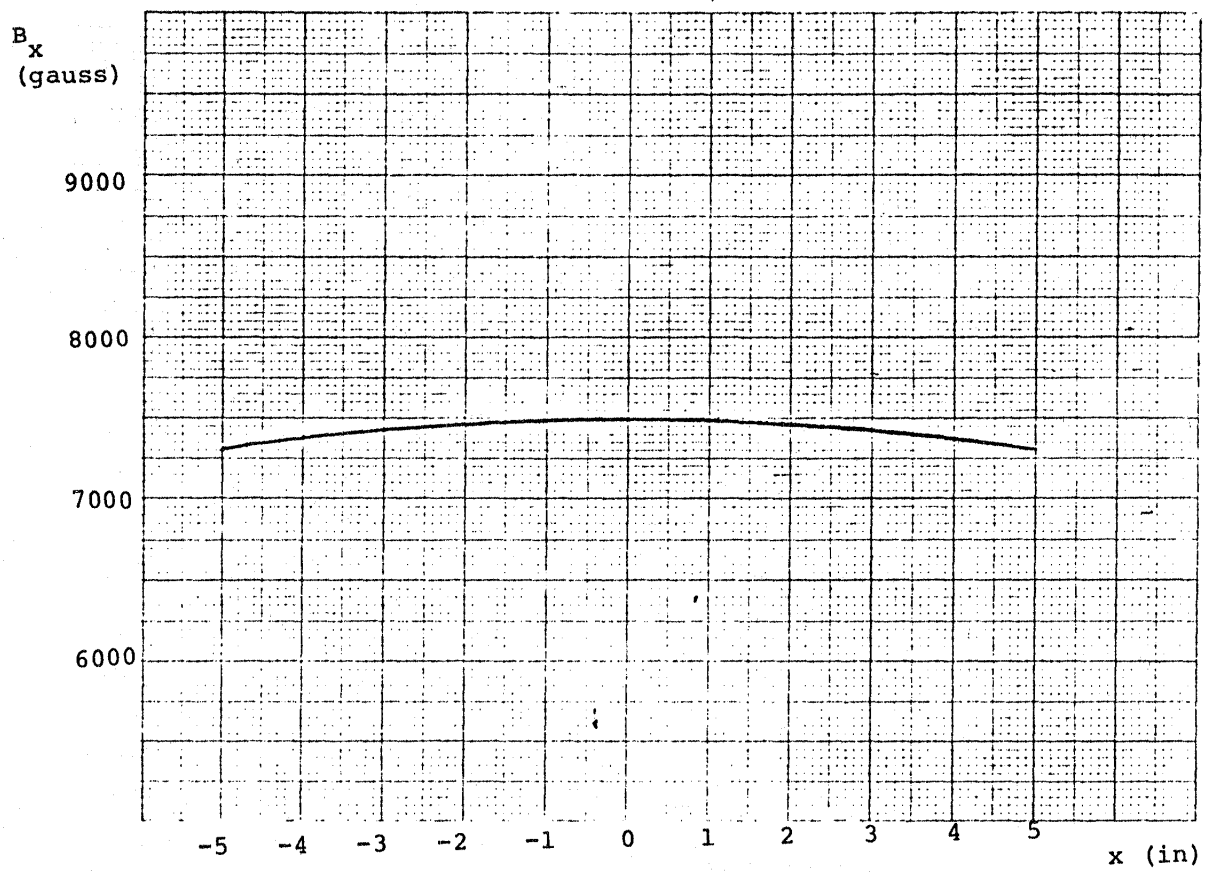

Figure 30 B_x vs Axial Distance x
for Magnetizing Coils

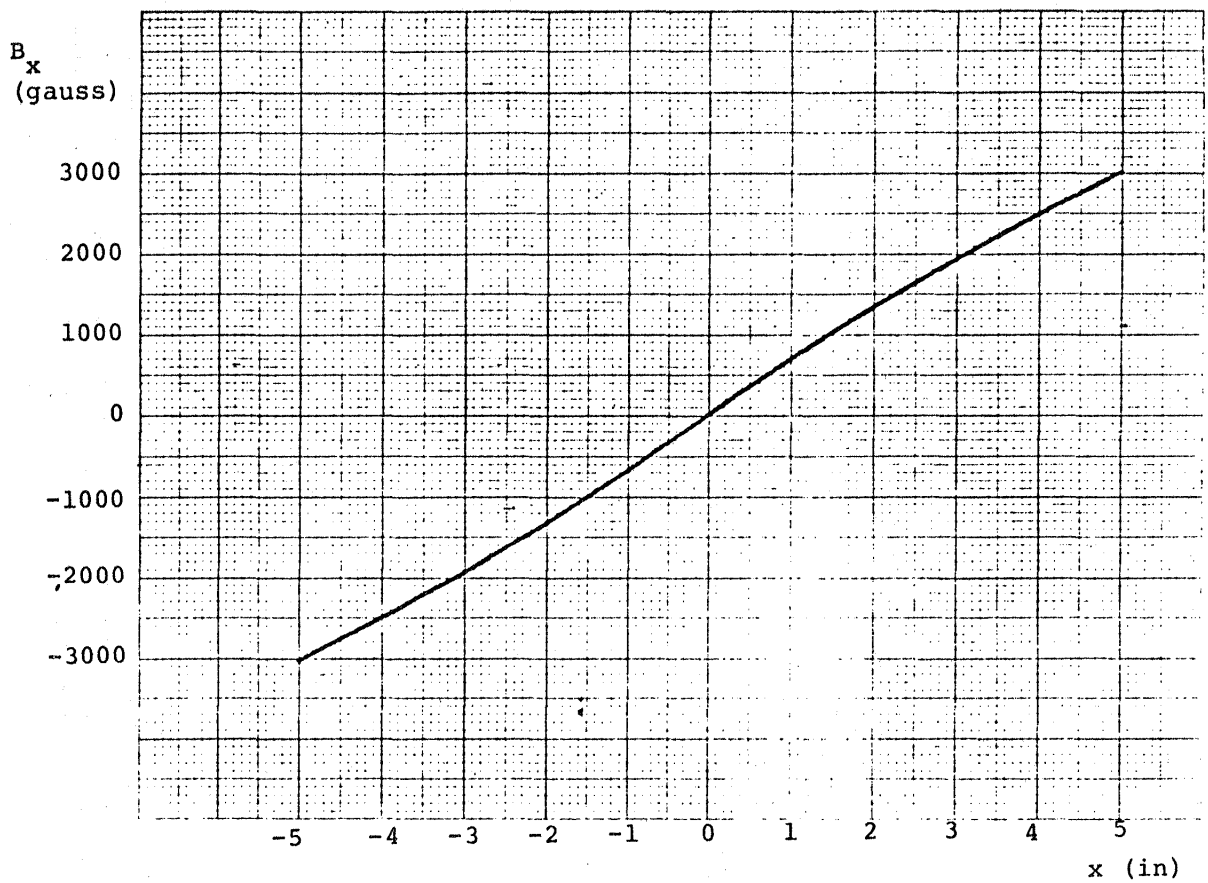

Figure 31 B_x vs. Axial Distance x
for Drag Coils

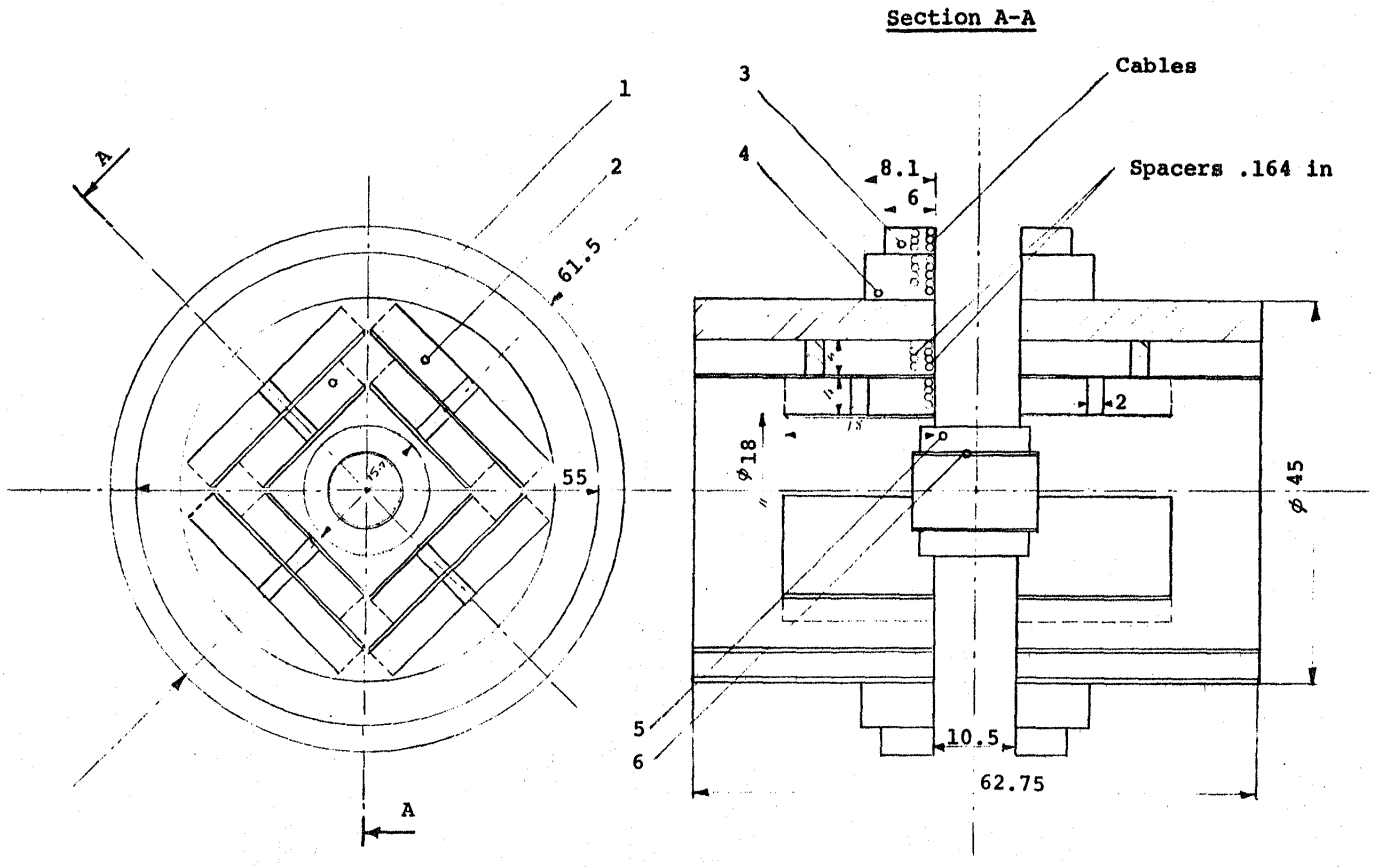

Reference Number	Coil Description	Req No.	Layer*	Turns per Layer*
1	1st stage side and lift	8	36	42
2	2nd stage side and lift	8	52	42
3	Magnetizing	2	38	50
4	Drag	2	52	75
5	Saddle			
6	EPS			

*For side and lift force coils these figures are half the total of number of turns, accounting only for the lift coils.

Figure 32 Assembly of Designed Coils together with Present Saddle and EPS. Dimensions are in inches.

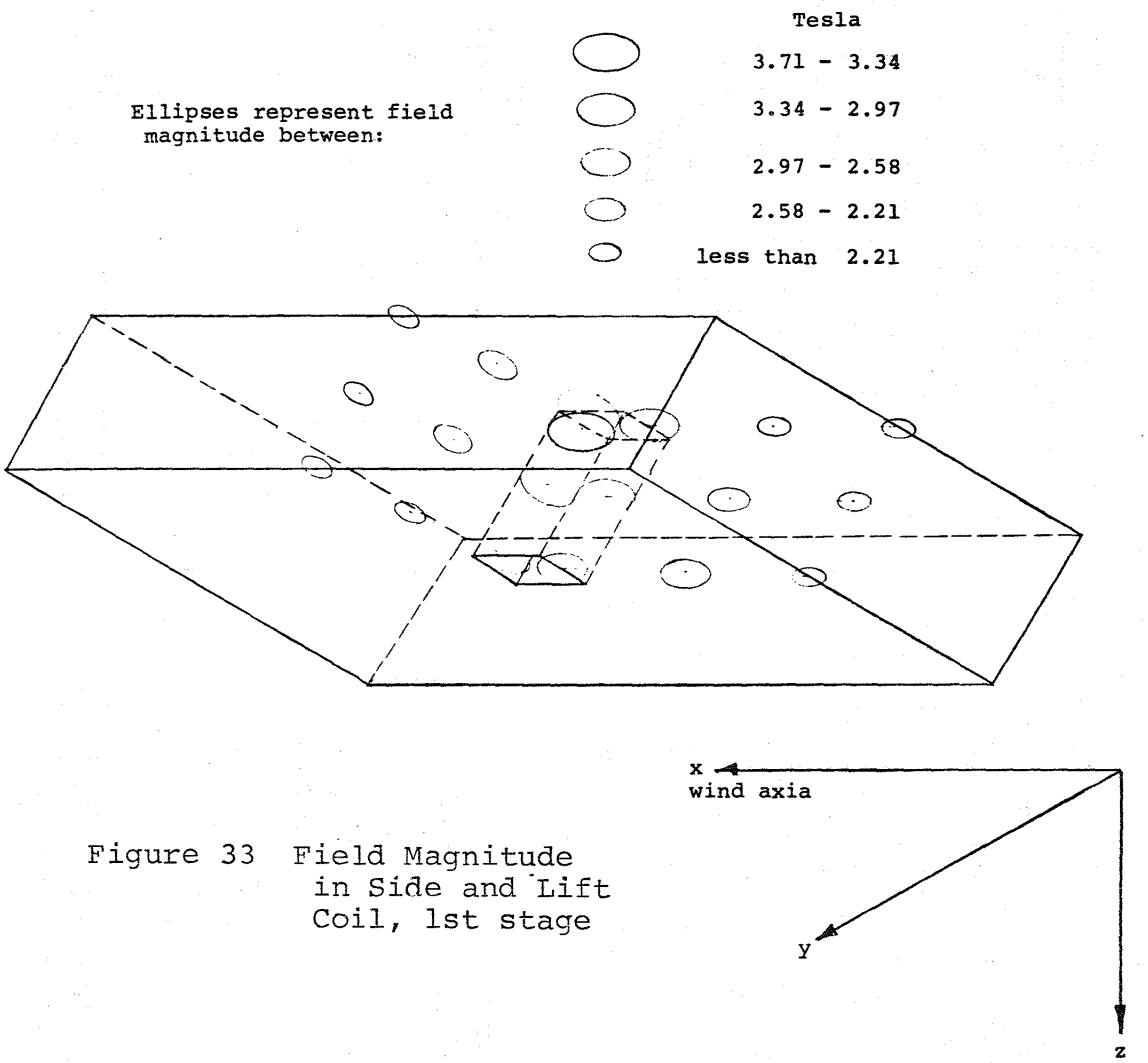

Figure 33 Field Magnitude in Side and Lift Coil, lst stage

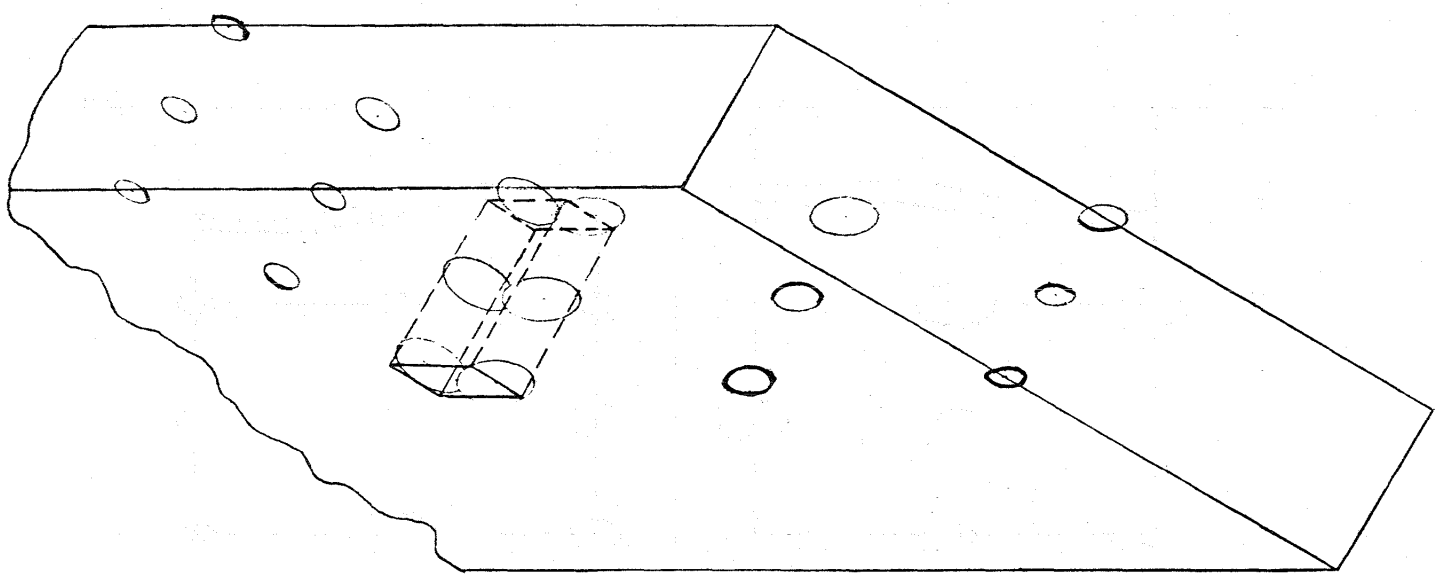

Figure 34 Field Magnitude in Side and Lift Coil, 2nd Stage

Figure 35 Field Magnitude in Drag Coils

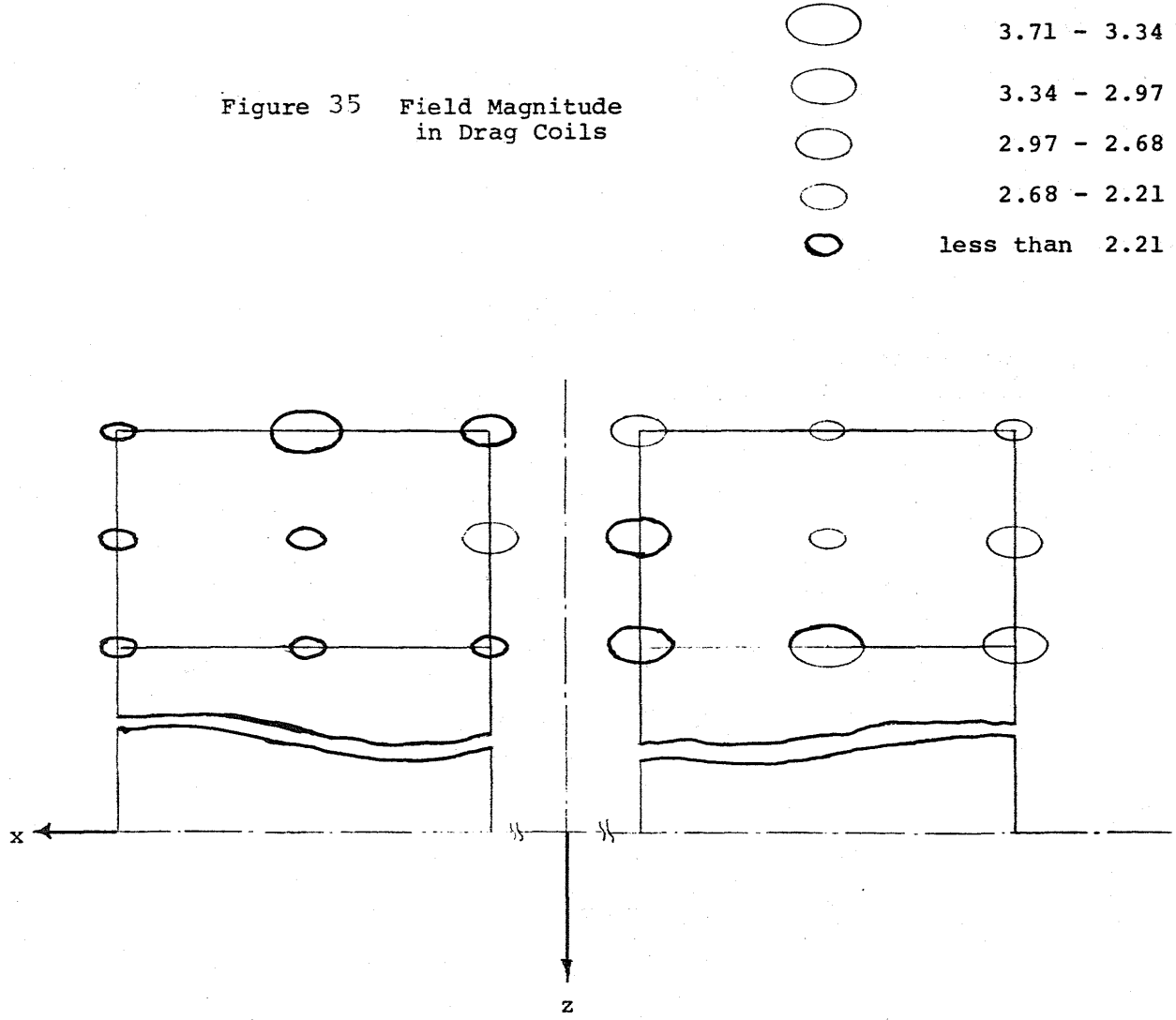

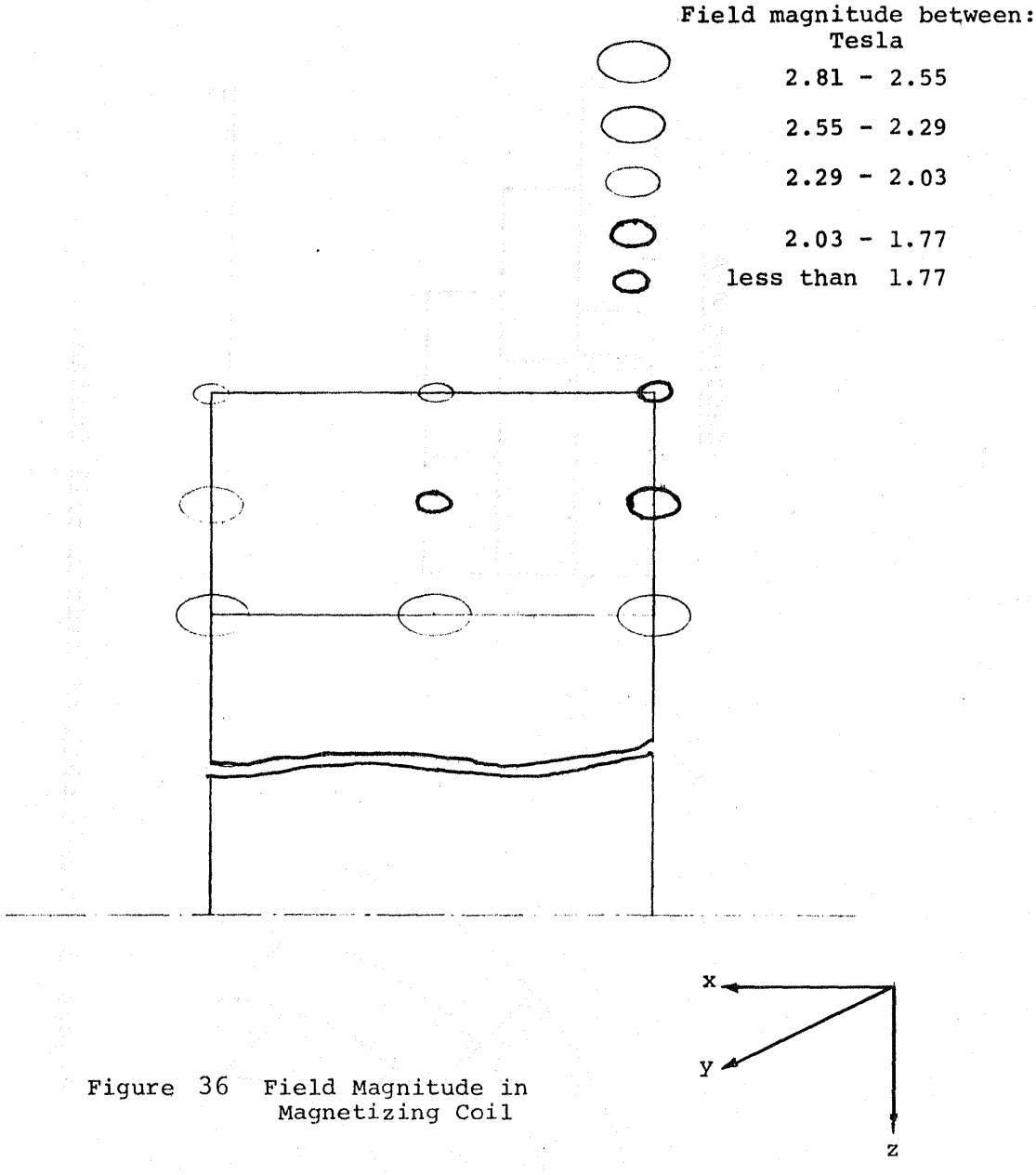

Figure 36 Field Magnitude in Magnetizing Coil

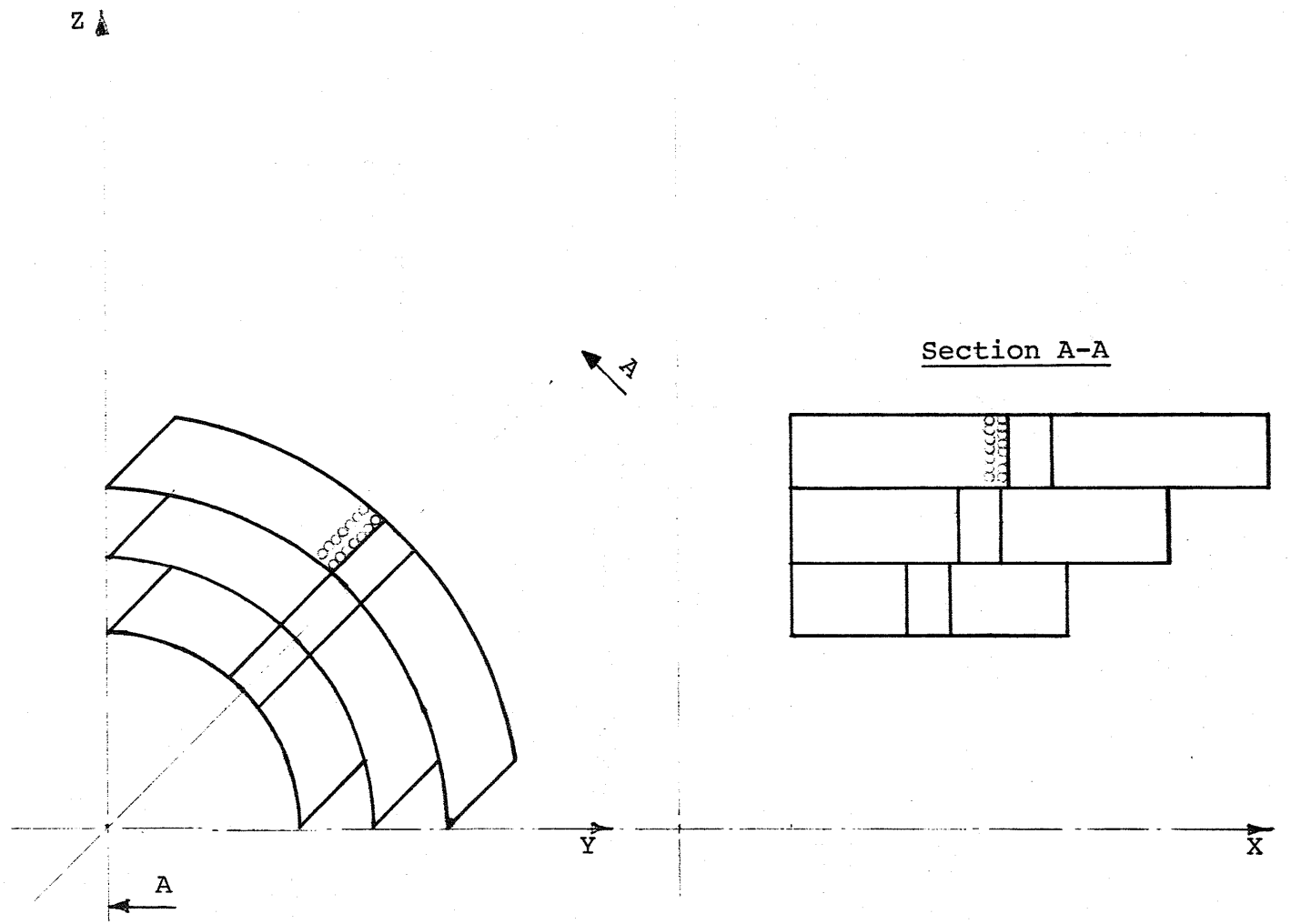

Figure 37 One-eighth of saddle coil design.

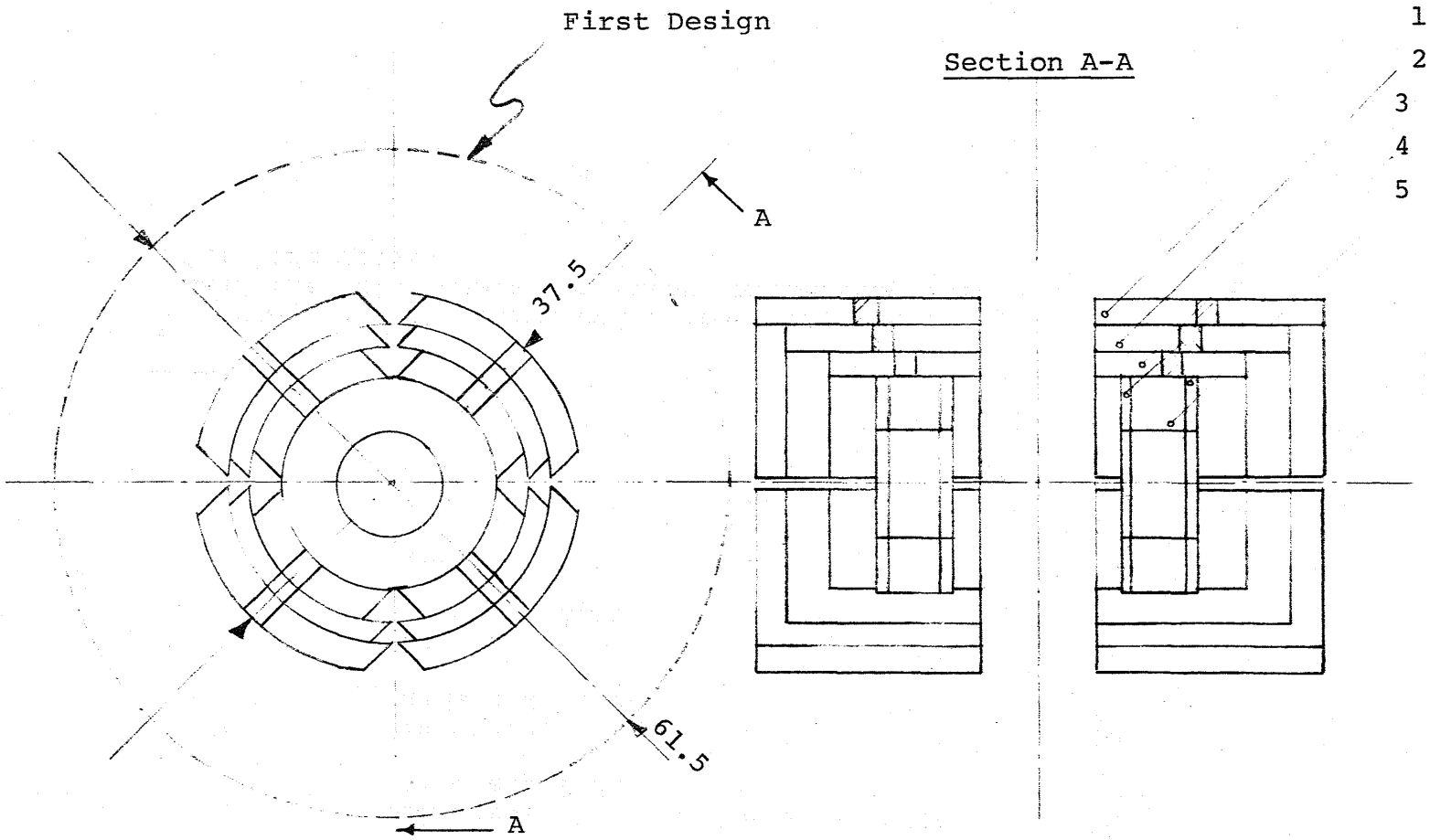

Figure 38 Final design of side force, lift, magnetizing and drag coils.

Figure 38 Legends

Reference Number	Coil Description	Req No.	Layer*	Turns per Layer*
1	3rd stage side and lift	8	44	32
2	2nd stage side and lift	8	35	30
3	1st stage side and lift	8	27	28
4	Drag	4	7	75
5	Magnetizing	2	31	75

*For side and lift force coils these figures are half the total number of turns, accounting only for lift coils.

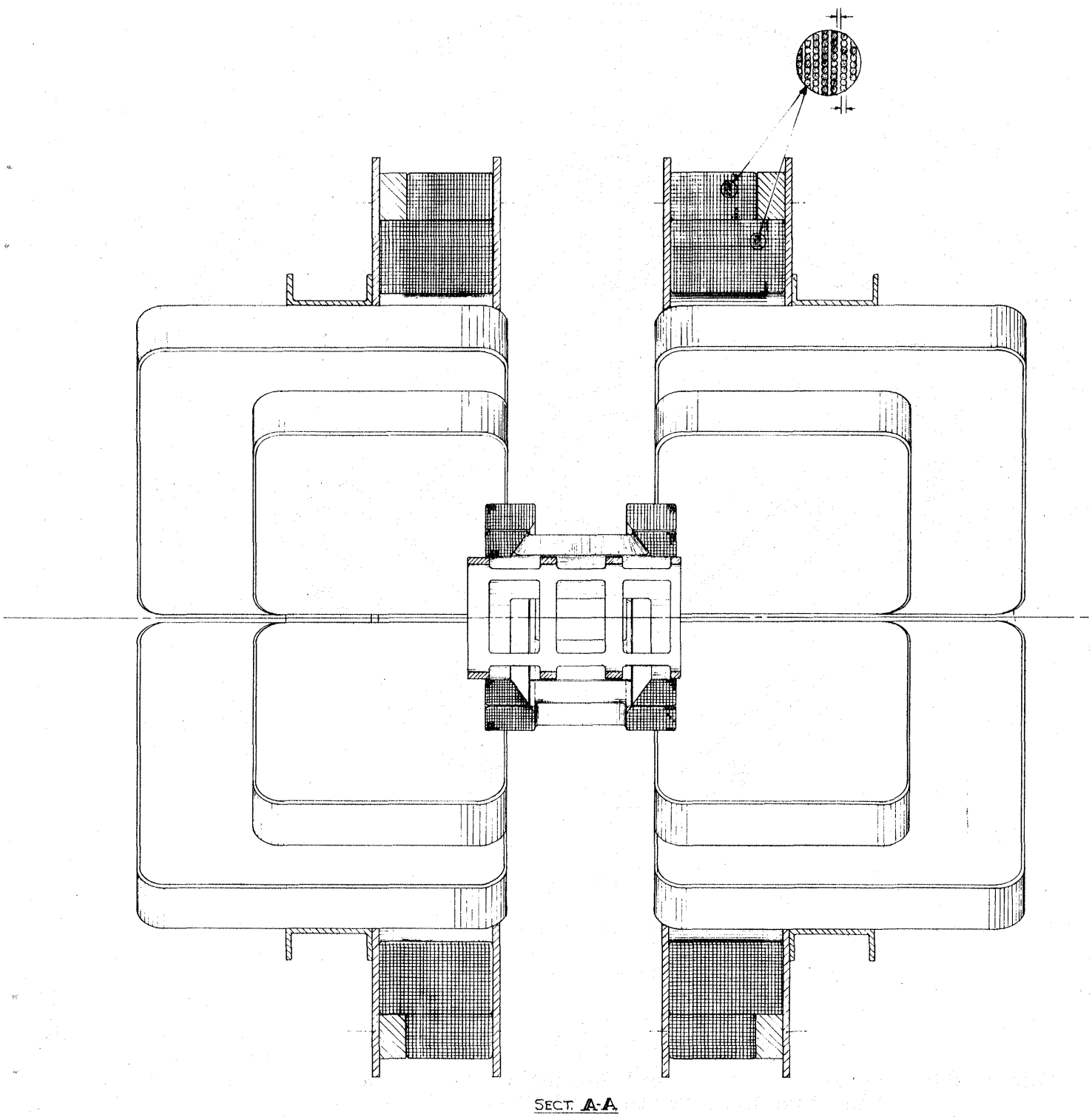

Figure 39a Vertical Section of Superconducting Coil Array using Planar Side and Lift Coils

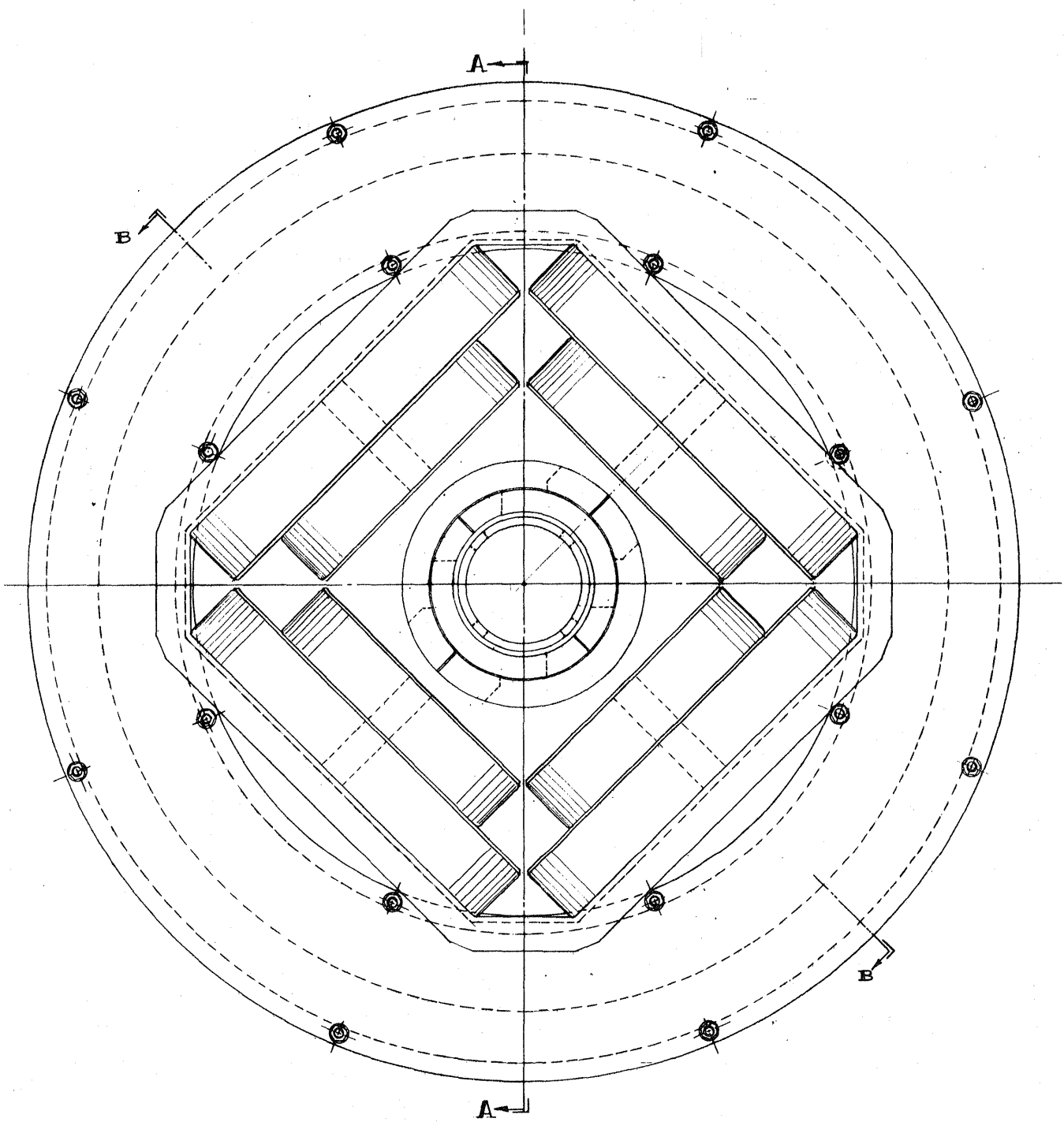

Figure 39b Superconducting Coil Layout using Planar Side and Lift Coils, End View

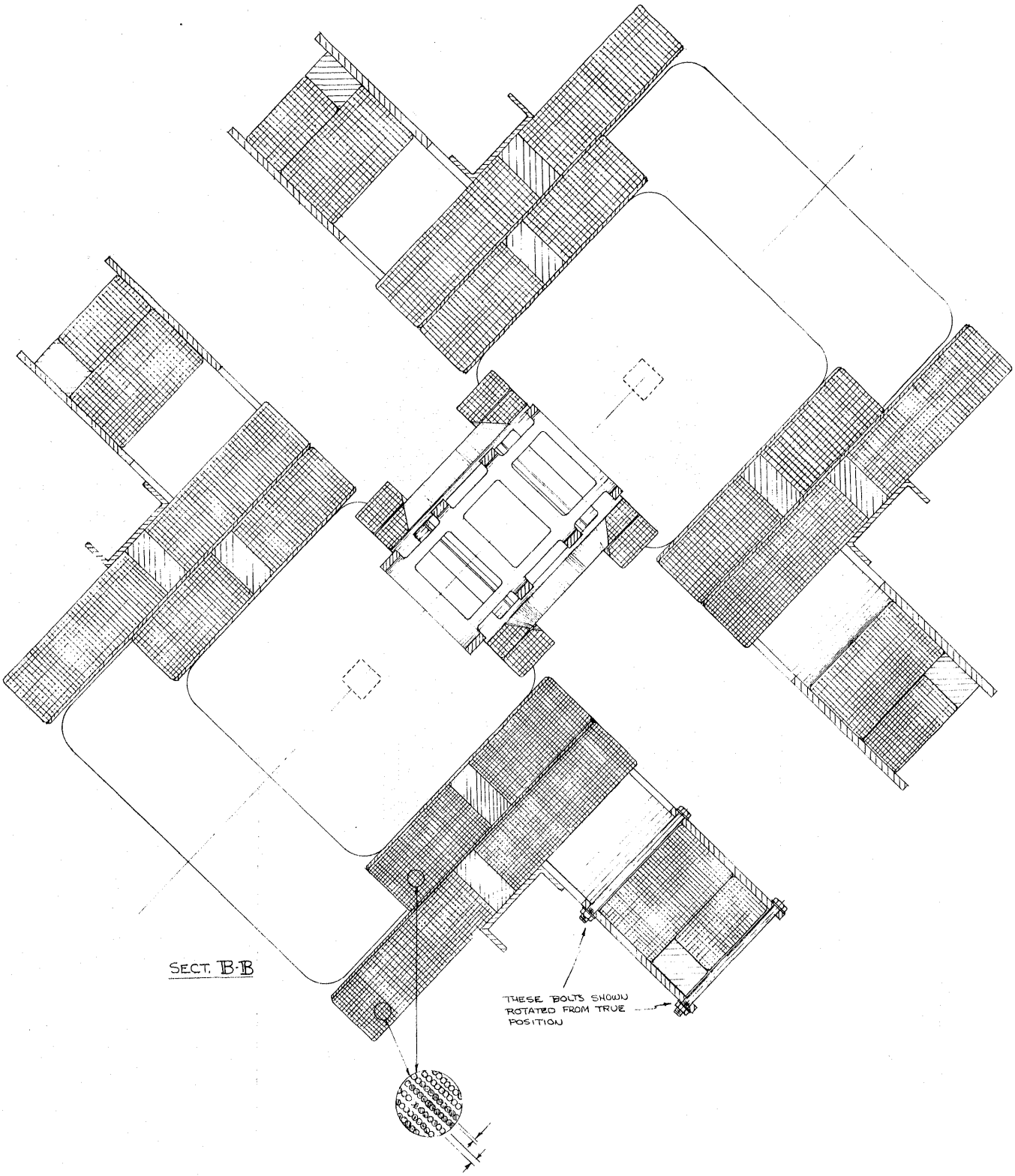

Figure 39c 45-degree Section

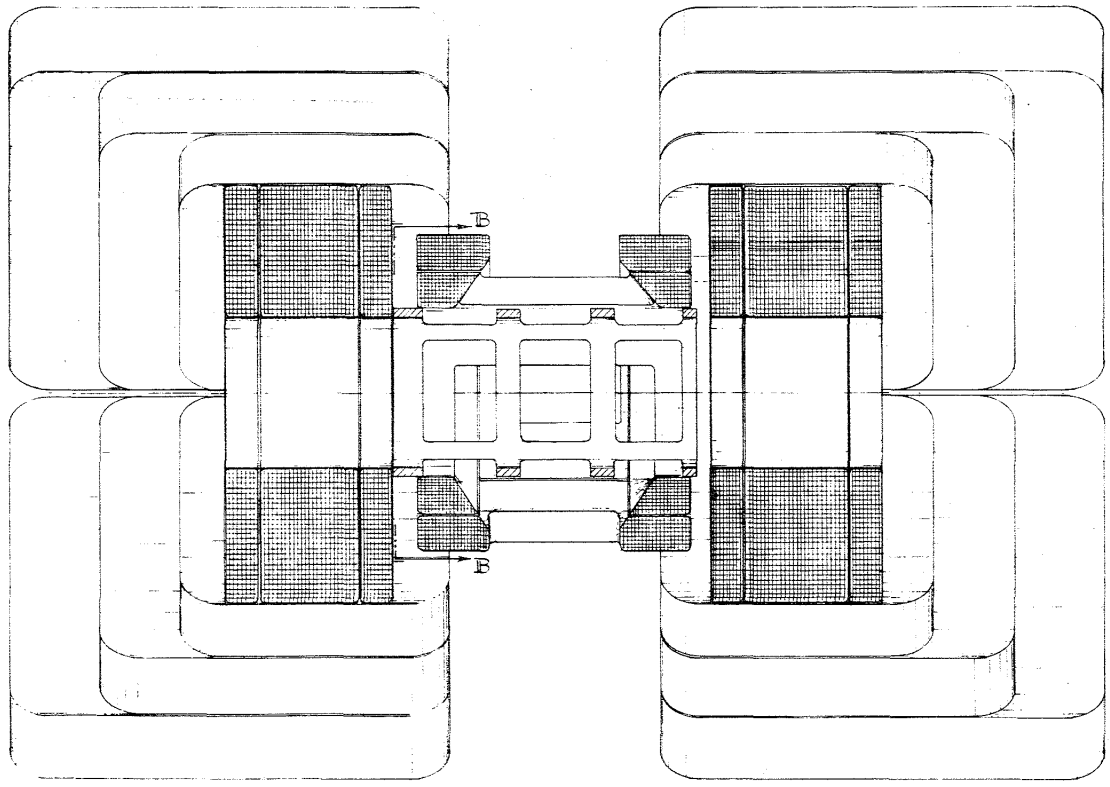

SECTION A-A

Figure 40a Vertical Longitudinal Section
through Saddle-Type Superconducting Magnet Array

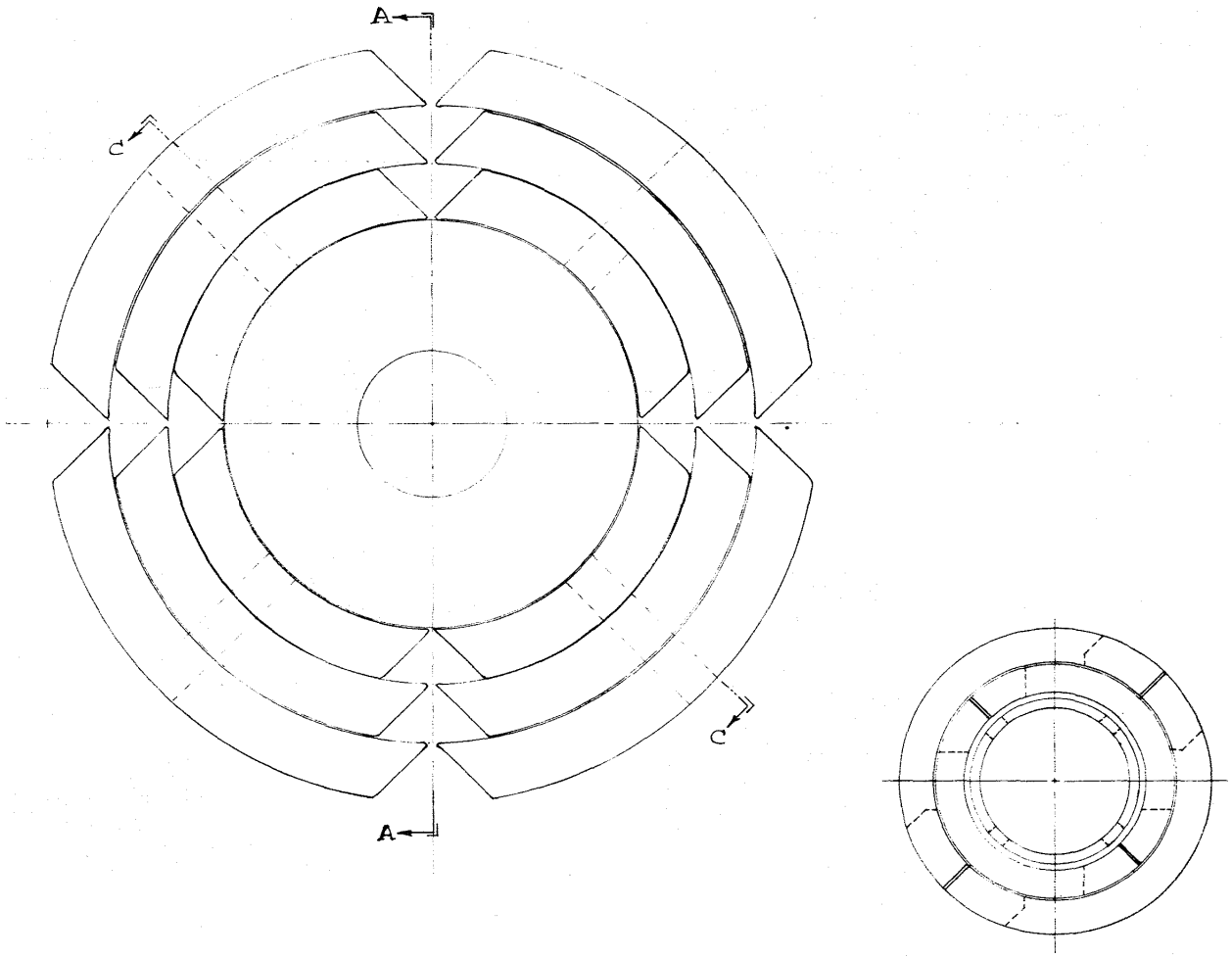

Figure 40b End View of Saddle-Type Superconducting Coil Array

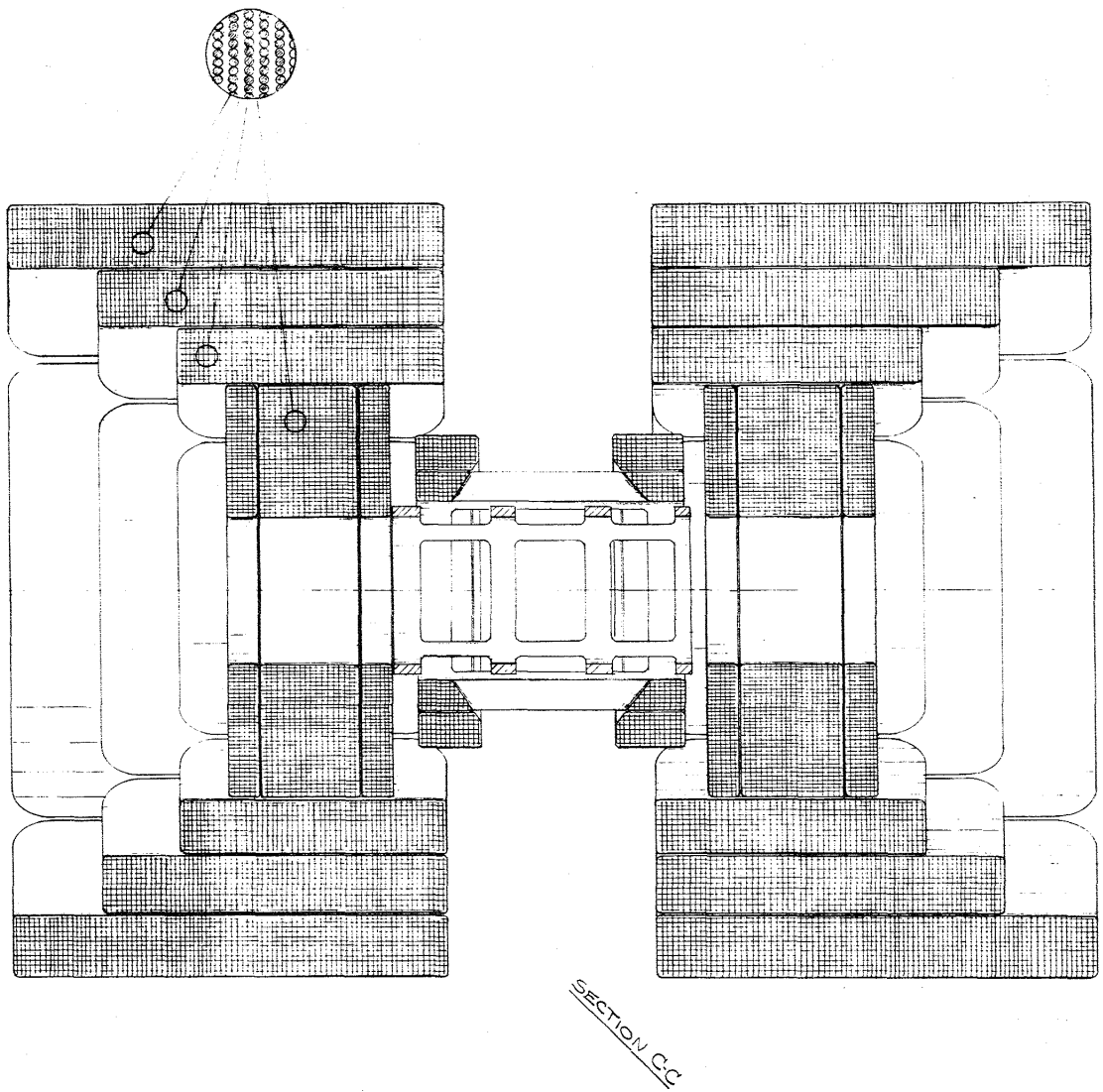

Figure 40c 45° Longitudinal Section of
Saddle-Type Superconducting Coil Array

Appendix A

DEVELOPMENT OF ELECTRONIC POWER METER*

While liquid helium boil-off measurement is the most straightforward means of measuring superconducting coil loss, it has several drawbacks:

1. The measurement is delayed by the time to fill the apparatus with gas and establish a steady state measurement.

2. The tare heat load on the dewar places a lower limit on sensitivity.

3. Losses in the normal leads are to some extent conducted back into the helium volume. This is not objectionable at high losses but can be at high D.C. bias.

In an effort to provide a better means of monitoring dissipation in the sample superconducting coils than provided by helium boil-off, an instantaneous power meter was constructed using an Analogue Device AD435K analogue multiplier.

This meter worked well at room temperature and LN_2 temperature but errors in the pick-up coil caused performance with superconducting coils to be non-quantitative. The meter schematic is shown in Figure A-1 and the connection circuit in Figure A-2. This meter provides the instantaneous (up to about 40 KHz) product of voltage, current and the cosine of the angle between them. When subject to a reactive load at low frequency this device provides an instantaneous record of power flow. When integrated over one cycle, this yields the net power deposited in the coil. Since the reactive voltage component is much larger than the resistive component, a small pick-up coil is provided wound outside the sample coil. The number of turns of this coil is trimmed so the voltage inductively coupled into the coil nearly equals the reactive voltage component. In practice cancellation was achieved within 3 percent at 2000 Hz.**

* The authors would like to acknowledge the work done by Mr Peter Way in testing and debugging of the power meter described in this section.

** Apparently this 3% is partly in phase with the voltage because of electrostatic coupling to the coil.

In principle use of this inductive voltage bucking coil in series with the voltage taps on the sample coil should reduce the out-of-phase voltage component presented to the multiplier to 3 percent of its value at the coil. This removes the problem of multiplier saturation at large reactive voltages. The sample coil test circuit is shown in Figure A-2. Here the controlled generator current (A.C. or D.C.) is fed into the coil through leads B.P. and E.C. These are 880 strand #36 wire used for flexibility and heat exchange with helium. Shunt AB develops the current metering signal for reading by DVM or power meter. Point D is connected to instrument ground with a non-current carrying lead. Point C is connected to the DVM used to read coil voltage and is also connected through the bucking coil to the power meter voltage input. By this means the voltage drop in the input leads BD and EC is not included in any measurement of voltage. The multiplier provided with nine levels of full-scale output derived from three ranges of 20, 200 and 2,000 watts and 3-scale multipliers of x.1 x 1 and x5. That is, set on the x1 scale multiplier and the 20 watt setting, 10 volts at "Z test" and full meter deflection would be obtained at 200 amperes at .1 volt.

When tested at room temperature or with a liquid nitrogen cooled coil, the performance was excellent. However, the power loss with superconducting coils was so small that extraneous effects obscured the power readings. This is believed to be a result of two factors: (1) less than 100% coupling between pick-up coil and primary coil; and (2) capacitive pick-up of coil voltage (which contained in phase voltage drop) by the primarily inductive bucking coil. This was true for both a bucking coil wound outside of the sample coil and one wound with a parallel strand for the whole length of the coil.

It is believed that successful operation could be achieved by developing the bucking signal from a Rogowski coil around one current lead and amplifying it before subtraction. The circuit of Figure A-1 would still be used with the above differential amplifier added to the front end.

FIGURE A-1 POWER METER SCHEMATIC

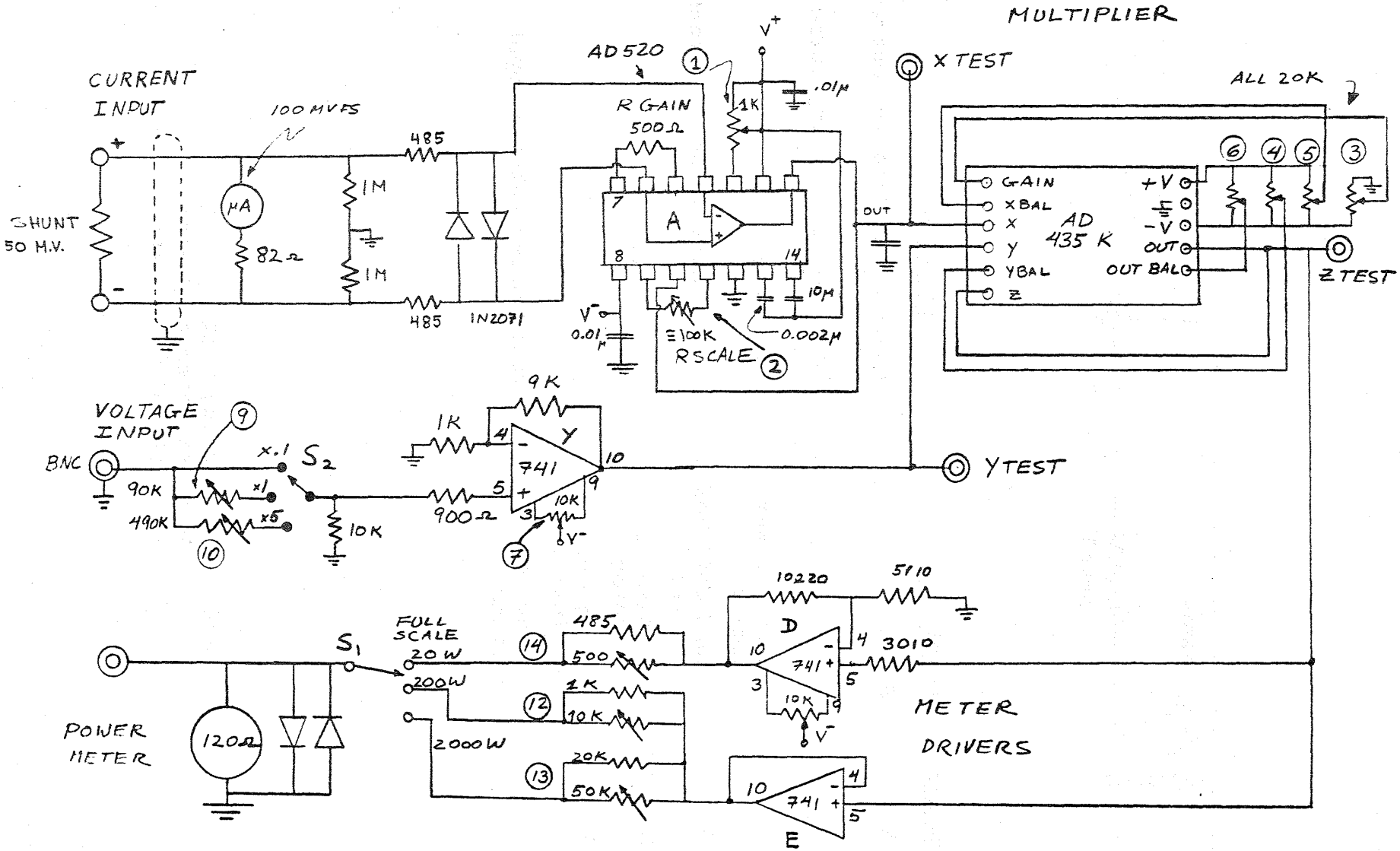

$V^+ = +15$ VOLTS DC

$V^- = -15$ VOLTS DC

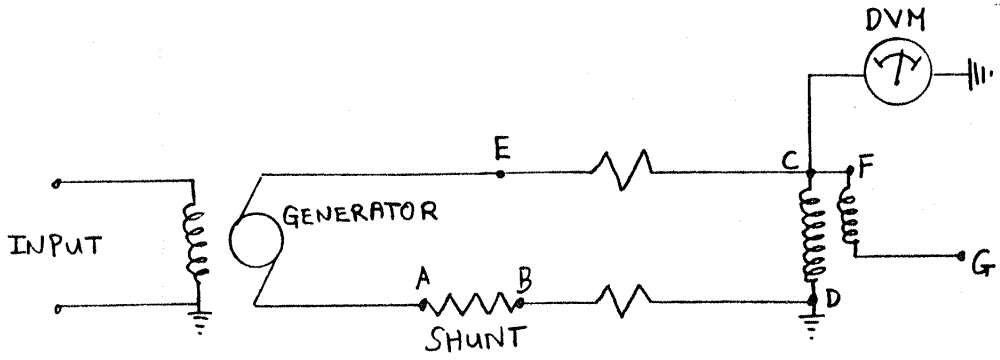

Terminal	Point	Connected to
A	Shunt	Power meter floating current input 1
B	Shunt	Power meter floating current input 2
C	Hot Coil Power Terminal	Coil voltmeter
D	Ground Coil Power Terminal	Power meter ground reference
E	Coil Lead to Generator	Power only
F	Bucking Coil Terminal 1	C
G	Bucking Coil Terminal 2	Power meter voltage input

Figure A-2 Circuit using Bucking Coil and Power Meter to Measure Instantaneous Coil Power

Appendix B

THE LOSS PROGRAM

A computer program was written (13) in Fortran to handle the coil loss calculations. The program consisted of six subroutines to handle the various geometries, and a main program to read input that determines which subroutines are called.

The first subroutine is called POINT. POINT calculates the three components of the magnetic field due to a coil composed of circular turns, assuming a one amp current. This is done by using the equations found in Reference 34 for the field due to one loop of current in terms of the elliptic integrals K and E;

$$H_r = \frac{\mu I}{2\pi} \frac{Z}{r\,[(a+r)^2+Z^2]^{1/2}} \left[-K + \frac{a^2+r^2+Z^2}{(a-r)^2+Z^2} E \right]$$

$$H_Z = \frac{\mu I}{2\pi} \frac{1}{[(a+r)^2+Z^2]^{1/2}} \left[K + \frac{a^2-r^2-Z^2}{(a-r)^2+Z^2} \right]$$

where a is the radius of the loop, and (r,Z) the coordinates of the point called. The field is calculated for all the turns of the coil, and the results summed.

Subroutine LOSS calculates the loss in joules per cycle per meter^3 of superconductor, for a single superconducting filament. Given the diameter of the filament, and the value of the local parallel and transverse field, it calculates the value of the penetration fields, then applies the appropriate loss equations (2.10-2.12) and returns the value to the calling subroutine.

Subroutine LOSSI calculates the loss in joules per cycle for a given coil due to its own field. Taking advantage of symmetry, the subroutine first uses POINT to determine the field strength

at each turn in the lower half of the coil. The losses in each turn are summed and the final result multiplied by two. The value thus obtained is then printed.

Subroutines LOSS2-LOSS4 calculate the interactive loss in a coil due to current in a nearby coil. They work the same as LOSSI, calling POINT, and LOSS, and taking advantage of any symmetries present in each particular geometry.

LOSS2 calculates loss in a coil due to a neighboring coil parallel to it and with the base of each coil on the same plane. The separation between axes is assumed to be the diameter of the coils by the statement; SEP = .140. The program divides the lower from half of the unpowered coil (as looking at both side by side) into discrete volumes, uses POINT and LOSS to calculate loss in each volume, sume them and multiplies the result by four. The result is then written.

LOSS3 calculates loss in a coil due to a neighboring coil adjacent to it, but with the neighboring coil's axis pointing at the center of the unpowered coil. The bottom of the powered coil is assumed to be .070 meters from the axis of the unpowered coil. The loss is calculated as LOSS2.

Finally LOSS4 reverses the roles of LOSS3. The unpowered coil is adjacent to the powered coil and pointing at it. The separation is the same and the computations are performed in the same way.

```
C    SCOTT W. PREY              S.M. THESIS                JUNE, 1979
C
C    PROGRAM TO CALCULATE SUPERCONDUCTING COIL LOSSES DUE TO SELF-FIELD
C    OR DUE TO FIELD GENERATED BY NEARBY COIL
C    TO USE, FIRST INPUT POWERED COIL PARAMETERS; COIL #, INSIDE RADIUS
C    (METERS), OUTSIDE RADIUS, LENGHT, NUMBER OF LAYERS, AND NUMBER OF
C    TURNS PER LAYER
C    SECOND, INPUT LOSS CODE IC;
C      IC=1, SELF FIELD LOSS
C      IC=2, PARALLEL INTERACTIVE LOSS
C      IC=3, PERPENDICULAR LOWER INTERACTIVE LOSS
C      IC=4, PERPENDICULAR UPPER INTERACTIVE LOSS
C    THIRD, INPUT LOSS SUBROUTINE DATA
C      IC=1; INPUT CURRENT, NUMBER OF STRANDS, AND CORE DIAMETER (MM)
C      IC=2,3,4; INPUT UNPOWERED COIL PARAMETERS, THEN INPUT FOR IC=1
C      A NEGATIVE CURRENT SWITCHES TO STEP FOUR
C    FOURTH, INPUT STEP CODE JC
C      JC=1; GOTO STEP ONE
C      JC=2; GOTO STEP TWO
C      JC=3; STOP
C
C
      COMMON RI,RO,XL,LAY,NTL,NTL2
      GOTO 6
   10 WRITE(6,5)
    5 FORMAT(1X,/,/)
    6 READ(5,1) NUM,RI,RO,XL,LAY,NTL
    1 FORMAT(I2,3(F6.4),2I2)
      IF(NUM .LT. 0) GOTO  30
      NTL2=NTL/2
      WRITE(6,2) NUM
    2 FORMAT(1X,'COIL #',I2,' POWERED')
   20 READ(5,3) IC
    3 FORMAT(I1)
      GOTO(11,12,13,14),IC
   11 CALL LOSS1

      GOTO 15
   12 CALL LOSS2
      GOTO 15
   13 CALL LOSS3
      GOTO 15
   14 CALL LOSS4
   15 READ(5,4) JC
    4 FORMAT(I1)
      GOTO(10,20,30),JC
   30 CONTINUE
      END
```

```
      SUBROUTINE POINT(XP,YP,ZP,BX,BY,BZ,ISTEP)
      DOUBLE PRECISION A, RHO, ZZ, XK2, XK, CK2, XKP, XLAM
      COMMON RI,RO,XL,LAY,NTL,NTL2
      REAL K
      DIMENSION R(6), Z(65)
      C=.0000002
      A=LAY-1
      DO 10 I=1,LAY
      B=I-1
   10 R(I)= RI+B*(RO-RI)/A
      AA=NTL
      AA=XL/AA
      DO 20 I=1,NTL
      XI=I
      XI=XI-.5
   20 Z(I)=AA*XI
      BR=0
      BZ=0
      DO 30 I=1,NTL,ISTEP
      DO 30 J=1,LAY
      RHO=SQRT(XP**2+YP**2)
      ZZ=ZP-Z(I)
      A=R(J)
      IF(((XP-A .LE. AA) .AND. (XP-A .GE. -AA)) .OR. ((ZZ .LT. AA)
     1 .AND. (ZZ .GT. -AA))) GOTO 30
      XK2=4.*A*RHO/((A+RHO)**2+ZZ**2)
      IF(XK2 .LT. 1.) GOTO 5
      WRITE (6,1) A,RHO,ZZ
    1 FORMAT(1X,3(F9.6))
    5 CONTINUE
      XK=DSQRT(XK2)
      CK2=1.-XK2
      K=3.14159/2.
      E=K
      IF(XK .EQ. 0.) GOTO  24
      XKP=1.-XK2

      IF(XKP .EQ. 0.0) GOTO 30
      XLAM=DLOG(4./XKP)
      K=XLAM+XKP*(XLAM-1.)/4.+XKP**2*(XLAM-7./6.)*9./64.+
     1 XKP**3*(XLAM-37./30.)*25./256.
      E=1.+XKP*(XLAM-.5)*.5+XKP**2*(XLAM-13./12.)*3./16.+
     1 XKP**3*(XLAM-6./5.)*15./128.
      IF(XK .GT. .95) GOTO 24
      CALL FEC2(XK,1.,1.,RES,IER)
      K=RES
      CALL FEC2(XK,1.,CK2,RES,IER)
      E=RES
   24 CONTINUE
      BR=0
      IF(RHO .EQ. 0.) GOTO 25
      BR=BR+C*ZZ*(-K+(A**2+RHO**2+ZZ**2)*E/((A-RHO)**2+ZZ**2))/
     1 RHO/DSQRT((A+RHO)**2+ZZ**2)
```

```
 25 CONTINUE
    BZ=BZ+C*(K+(A**2-RHO**2-ZZ**2)*E/((A-RHO)**2+ZZ**2))/
   1 DSQRT((A+RHO)**2+ZZ**2)
 30 CONTINUE
    XX=ISTEP
    BZ=BZ*XX
    BR=BR*XX
    BX=0
    BY=0
    IF((XP .EQ. 0.) .AND. (YP .EQ. 0.)) GOTO 40
    THETA=ATAN2(XP,YP)
    BX=BR*COS(THETA)
    BY=BR*SIN(THETA)
 40 CONTINUE
    RETURN
    END



   SUBROUTINE LOSS(C,XN,D,BT,B,WV)
   XJO=6.819E+09
   BO=1.05124
   XMU=1.26E-06
   PI=3.14159
   XJC=XJO*BO/(B+BO)
   BPR=XMU*XJC*D/PI
   BPT=XMU*XJC*D/2.
   IF((BT .GE. BPT) .OR. (B .GE. BPR)) GOTO 10
   WV=(9.054*B**3+(64./9.)*BT**3)/(XMU**2*XJC*D)
   GOTO 20
10 WV=XJC*D*(.8488*B+.6667*BT)
20 RETURN
   END

   SUBROUTINE LOSS1
   COMMON RI,RO,XL,LAY,NTL,NTL2
   DIMENSION X(6),Z(65)
   R=0
   W=0
   XJO=6.819E+09
   BO=1.05124
   XMU=1.26E-06
   PI=3.14159
 5 CONTINUE
   READ(5,1) C,XN,D
 1 FORMAT(2F5.1,F5.4)
   IF(C.LT.0.) GOTO 50
   C=C*.707
   D=D/1000.
   A=LAY-1
   DO 10 I=1,LAY
   BB=I-1
```

```
 10 X(I)=RI+BB*(RO-RI)/A
    A=NTL
    A=XL/A
    DO 20 I=1,NTL2
    X2=I
    X2=X2-.5
 20 Z(I)=X2*A
    DO 40 I=1,LAY
    DO 40 J=1,NTL2
    XP=X(I)
    YP=0
    ZP=Z(J)
    CALL POINT(XP,YP,ZP,BX,BY,BZ,1)
    BR=BX*SQRT(XP**2+YP**2)/XP
    B=SQRT(BR**2+BZ**2)
    B=C*B
    XJC=XJO*BO/(B+BO)
    BP=XMU*XJC*D/PI

    AREA=PI*(D/2.)**2*XN
    F=C/(XJC*AREA)
    BP=BP*(1.-F)
    IF(B .GT. BP) GOTO 30
    WV=9.054*B**3/(XMU**2*XJC*D)
    W=W+2.*PI*X(I)*AREA*WV
    GOTO 40
 30 WV=.8488*B*XJC*D
    W=W+2.*PI*X(I)*AREA*WV
 40 CONTINUE
    W=W*2.*(1.+F**2)
    C=C/.707
    WRITE(6,2) C,W
  2 FORMAT(1X,'SELF FIELD LOSS AT ',F5.1,' AMPS IS ',F8.5,
   1 ' JOULES PER CYCLE')
    GOTO  5
 50 CONTINUE
    RETURN
    END

   SUBROUTINE LOSS2
   DIMENSION X(6),Z(33),DT(3)
   DATA DT /.7854, .5236, .3927/
   READ(5,1) NUM,RI,RO,XL,LAY,NTL
 1 FORMAT(I2,3(F6.4),2I2)
   WRITE(6,5)
 5 FORMAT(1X,/)
   WRITE(6,4)
 4 FORMAT(1X,'PARALLEL COILS')
10 CONTINUE
   READ(5,2) C,XN,D
```

```
 2 FORMAT(2F5.1,F5.4)
   IF(C .LT. 0) GOTO 60
   C=C*.707
   D=D/1000.
   W=0
   SEP=.140
   A=LAY-1
   DC 20 I=1,LAY
   BB=I-1
20 X(I)=RI+BB*(RC-RI)/A
   A=NTL
   A=XL/A
   N2=NTL/2
   DO 30 I=1,N2
   XI=I
30 Z(I)=A*XI
   DO50 I=1,LAY
   DO 50 J=1,N2,4
   K=1
   IF(I .GE. 3) K=2
   IF(I .GE. 5) K=3
   THETA=-DT(K)/2.
40 THETA=THETA+DT(K)
   IF(THETA .GE. 3.14) GOTO 50
   XP=SEP+X(I)*COS(THETA)
   YP=X(I)*SIN(THETA)
   ZP=Z(J)
   CALL POINT(XP,YP,ZP,BX,BY,BZ,4)
   BT=-BX*SIN(THETA)+BY*COS(THETA)
   BR=BX*COS(THETA)+BY*SIN(THETA)
   B=SQRT(BZ**2+BR**2)
   BT=C*BT
   B=B*C
   CALL LOSS(C,XN,D,BT,B,WV)
   AREA=3.14159*(D/2.)**2*XN
   W=W+DT(K)*3.14159*X(I)*AREA*WV
   GOTO 40
50 CONTINUE
   C=C/.707
   W=W*16.
   WRITE(6,3) NUM,C,W
 3 FORMAT(1X,'COIL ',I1,' UNPOWERED LOSS AT ',F5.1,' AMPS POWERED ',
  1'COIL IS ',F9.7,' JOULES PER CYCLE')
   GOTO 10
60 RETURN
   END
```

```
      SUBROUTINE LOSS3
      DIMENSION X(6),Z(33),DT(3)
      DATA DT /.7854, .5236, .3927/
      READ(5,1) NUM,RI,RO,XL,LAY,NTL
    1 FORMAT(I2,3(F6.4),2I2)
      WRITE(6,5)
    5 FORMAT(1X,/)
      WRITE(6,4) NUM
    4 FORMAT(1X,'PERPENDICULAR COILS; COIL ',I1, ' LOWER')
   10 CONTINUE
      READ(5,2) C,XN,D
    2 FORMAT(2F5.1,F5.4)
      IF(C .LT. 0) GOTO 60
      C=C*.707
      D=D/1000.
      W=0
      SEP=.070
      A=LAY-1
      DO 20 I=1,LAY
      BB=I-1
   20 X(I)=RI+BB*(RO-RI)/A
      A=NTL
      A=XL/A
      N2=NTL/2
      DO 30 I=1,N2
      XI=I
   30 Z(I)=A*XI
      DO50 I=1,LAY
      DO 50 J=1,N2,4
      K=1
      IF(I .GE. 3) K=2
      IF(I .GE. 5) K=3
      THETA=-DT(K)/2.
   40 THETA=THETA+DT(K)
      IF(THETA .GE. 3.14) GOTO 50
      XP=X(I)*SIN(THETA)
      YP=Z(J)
      ZP=X(I)*COS(THETA)-SEP
      CALL POINT(XP,YP,ZP,BX,BY,BZ,4)
      BT=-BZ*SIN(THETA)+BX*COS(THETA)
      BR=BZ*COS(THETA)+BX*SIN(THETA)
      B=SQRT(BY**2+BR**2)
      BT=C*BT
      B=B*C
      CALL LOSS(C,XN,D,BT,B,WV)
      AREA=3.14159*(D/2.)**2*XN
      W=W+DT(K)*3.14159*X(I)*AREA*WV
      GOTO 40
```

```
 50 CONTINUE
    C=C/.707
    W=W*16.
    WRITE(6,3) NUM,C,W
  3 FORMAT(1X,'COIL ',I1,' UNPOWERED LOSS AT ',F5.1,' AMPS POWERED ',
   1'COIL IS ',F9.7,' JOULES PER CYCLE')
    GOTO 10
 60 RETURN
    END

    SUBROUTINE LOSS4
    DIMENSION X(6),Z(65)
    READ(5,1) NUM,RI,RO,XL,LAY,NTL
  1 FORMAT(I2,3(F6.4),2I2)
    WRITE(6,5)
  5 FORMAT(1X,/)
    WRITE(6,4)NUM
  4 FORMAT(1X,'PERPENDICULAR COILS; COIL ',I1,' UPPER')
 10 CONTINUE
    READ(5,2) C,XN,D
  2 FORMAT(2F5.1,F5.4)
    IF(C .LT. 0) GOTO 60
    C=C*.707
    D=D/1000.
    W=0
    DT=3.14159/6.
    SEP = .070
    A=LAY-1
    DO 20 I=1,LAY
    BB=I-1
 20 X(I)=RI+BB*(RO-RI)/A
    A=NTL
    A=XL/A
    DO 30 I=1,NTL
    XI=I
 30 Z(I)=A*XI
    DO50 I=1,LAY
    DO 50 J=1,NTL,4
    THETA=-DT/2.
 40 THETA=THETA+DT
    IF(THETA .GE. 1.57) GOTO 50
    XP=Z(J)+SEP
    YP=X(I)*COS(THETA)
    ZP=X(I)*SIN(THETA)
    CALL POINT(XP,YP,ZP,BX,BY,BZ,4)
    BR=BY*COS(THETA)+EZ*SIN(THETA)
```

```
      BT=-BY*SIN(THETA)+BZ*COS(THETA)
      B=SQRT(BX**2+BR**2)
      BT=C*BT
      B=B*C
      CALL LOSS(C,XN,D,BT,B,WV)
      AREA=3.14159*(D/2.)**2*XN
      W=W+DT*3.14159*X(I)*AREA*WV
      GOTO 40
   50 CONTINUE
      C=C/.707
      W=W*16.
      WRITE(6,3) NUM,C,W
    3 FORMAT(1X,'COIL ',I1,' UNPOWERED LOSS AT ',F5.1,' AMPS POWERED ',
     1'COIL IS ',F9.7,' JOULES PER CYCLE')
      GOTO 10
   60 RETURN
      END
```

Appendix C

COMPUTER PROGRAM TABLE AND COMPUTER RESULTS

Computer program TABLE and computer results for the designed lift force, drag and magnetizing coils (Figure 32) are presented. The lift coils' number of turns is half the total available number of turns since the second half belongs to side force coils. Therefore, the side force field component (B_y) distribution is similar to lift force component (B_z) distribution. In practice, they are powered from a single line having the resultant current.

The complete elliptic integrals in Subroutine Circe are computed according to (36).

```
c                                TABLE
c                                -----
c     Program to calculte magnetic field components produced by coils
c     consisting of straight line or circular current elements.
c     Straight line current elements are counted counter-clockwise about
c     the correspondig coordinate directions.All currents are postive
c     counter-clockwise.
c
c                          Input variable list
c
c variable name                          definition
c     im                  number of increments in x direction.
c     jm                  number of increments in y direction.
c     km                  number of increments in z direction.
c     dx                  "delta x"
c     dy                  "delta y"
c     dz                  "delta z"
c     x(1)                x coordinate of starting point for incrementing.
c     y(1)                y coordinate of starting point for incrementing.
c     z(1)                z coordinate of starting point for incrementing.
c     da                  demagnetizing constant for the model.
c     xmu                 magnetic permeablity of free space.
c     coil                indivdual coil description.
c     x1,y1,z1            coordinate of the end points of the straight line
c     x2,y2,z2            current elements making up the coils.
c     ccur                coil current.
c     icoil               numbe of first coil.
c     ncoil               number of last  coil.
c     nint                number of interfaces.
c     mm,nn               dimenssion of interface array.
c     xx,yy,zz            interface endpoints.
c     c1                  axil distance of solenoid from the center.
c     xl                  solenoid length.
c     ri                  solenoid internal dimeter.
c     ro                  solenoid external dimeter.
c     lay                 solenoid number of layers.
c     ntl                 solenoid number of turns per layer.
c
c                               note:
c       In order for coors to work properly,
c     ww,w1,w2,must be dimensioned to at least
c     ww(4,nint),w1(ntot),w2(ntot).xx,yy,zz have the same dimensions
c     as ww.
c
      integer out
      dimension x(50),y(50),z(50),
     1x1(8736),y1(8736),z1(8736),x2(8736),y2(8736),z2(8736)
     2,confg(18),curt(500),coil(18,28),sum(12,50),xx(4,10),yy(4,10),
     3zz(4,10),ww(4,10),w1(8736),w2(8736),ld(50)
      common c1,xl,lay,ntl,ri,ro,curc,kk,ii,jj,nc
4     format(1x,2i2)
5      format(2f10.4,3i5,3f10.4,2i2)
10    format(2f10.4,2f12.10)
11    format(3i4,6f5.3)
12    format(3i3)
18    format(3i3,f8.3)
19    format(3f8.2)
111   format(1x,3f6.2,5x,3f11.2)
113   format(4x,1hX,5x,1hY,5x,1hZ,15x,2hBX,9x,2hBY,9x,2hBZ)
116   format(6x,6hinches,20x,5hgauss)
155   format(/,18a4)
156   format(18a4)
159   format(24x,18a4)
192   format("1",t40,"system summary output")
193   format(//t20,"coil description:",16(/t20,18a4)//)
450   read(1,10,end=420)da,ams,xkt,xmu
c
c     For calculating field inside any coil put the ip equal to the
c     number of that coil.
c
      read(4,4)icoil,ip
      xmp=xmu/(4.*3.1415926)
      read(1,156,end=420) (confg(ic),ic=1,18)
c
c     Input spatial description:
c     maximum number of x,y,and z increments,delta x,delta y,delte z
c     corner points of the plot.
c
      read(1,11)im,jm,km,dx,dy,dz,x(1),y(1),z(1)
c
c     calculate and store the spatial coordinates for this calculation.
      do 2000 i=2,im
2000  x(i)=x(1)-(i-1)*dx
      do 2001 j=2,jm
2001  y(j)=y(1)-(j-1)*dy
      do 50 j=1.100
50    sum(i,j)=0.
      read(1,12)ncoil,inpopt,out
      write(7,159)(confg(ic),ic=1,18)
      do 200 nc=icoil,ncoil
```

```
      write(6,299) nc
c
c     Corresponding values for each 8 coil set should be read from one file.
c
      if(nc.gt.8)go to 28
299   format(1x,"COIL NUMBER",i10)
      read(1,155)(coil(ic,nc),ic=1,18)
      goto 29
28    continue
      if(nc.gt.16)go to 27
      read(2,155)(coil(ic,nc),ic=1,18)
      go to 29
27    if(nc.gt.24)goto26
      read(3,155)(coil(ic,nc),ic=1,18)
      go to 29
26    read(4,155)(coil(ic,nc),ic=1,18)
      read(4,5)c1,xl,lay,ntl,kk,ri,ro,curc,istepx,istepr
      go to 310
29    continue
      if(nc.gt.8)go to 59
      read(1,18)mm,nn,nint,ccur
      go to61
59    continue
      if(nc.gt.16)go to 57
      read(2,18)mm,nn,nint,ccur
      go to 61
57    read(3,18)mm,nn,nint,ccur
61    continue
      do 80 j=1,nint
      do 80 i=1,4
      if(nc.gt.8) goto79
      read(1,19)xx(i,j),yy(i,j),zz(i,j)
      go to 80
79    continue
      if(nc.gt.16)go to 77
      read(2,19)xx(i,j),yy(i,j),zz(i,j)
      go to 80
 77    read(3,19)xx(i,j),yy(i,j),zz(i,j)
80    continue
      ntot=mm*nn*nint
      call coors(nint,mm,nn,ntot,xx,x1,x2,10)
      call coors(nint,mm,nn,ntot,yy,y1,y2,10)
      call coors(nint,mm,nn,ntot,zz,z1,z2,10)
c
c     If the inside field is desired this part will be done defining nn2,mm2.
c
      if(nc.ne.ip) go to 106
      im=0
      mm2=mm/2
      nn2=1
      do 99 n=nn2,nn2
      do 99 m1=mm2,mm,mm2
      do 99 ipp=4,4
      if(m1-2)55,55,56
55    m=1
      go to 58
56    m=m1
58    im=im+1
      ld(im)=4*nn*(m-1)+4*n+ipp
      ldl=ld(im)
      x(im)=(x1(ldl)+x2(ldl))/2
      y(im)=(y1(ldl)+y2(ldl))/2
      z(im)=(z1(ldl)+z2(ldl))/2
99    continue
106   continue
      lm=ntot
310   continue
      ns=0
      do 199 i=1,im
      do 199 j=1,jm
      do 199 k=1,km
      ns=ns+1
      write(6,298) ns
298   format(1x,"NO. OF POINT",i10)
      if(nc.gt.24)go to 201
      bx=0.0
      by=0.0
      bz=0.0
      ll=ld(i)
      do 210 l=1,lm
      if(nc.ne.ip)go to 105
      if(l.eq.ll)go to 198
      go to 105
198   write(7,104) i,x1(l),y1(l),z1(l),x2(l),y2(l),z2(l),l
104   format(2x,i2,2x,6(f7.3,2x),i7)
      go to 210
105   continue
      dk=1
      a=(x1(l)-x(i))/39.37
      b=(x2(l)-x(i))/39.37
```

```
      c=(y1(l)-y(j))/39.37
      d=(y2(l)-y(j))/39.37
      e=(z1(l)-z(k))/39.37
      f=(z2(l)-z(k))/39.37
197   continue
      u=c*f-d*e
      v=e*b-f*a
      w=a*d-b*c
195   format(1x,"ldd=",i3,2x,6(f7.3,2x,"i=",i3),"l=",i3,2x,"i=",i3)
      r1=(a*a+c*c+e*e)**.5
      r2=(b*b+d*d+f*f)**.5
      rs=r1+r2
      rm=r1*r2
      rdr=a*b+c*d+e*f
      rxr=(u**2+v**2+w**2)**.5
194   continue
      h=(rm+rdr)/rm
      if(h-0.01)2,1,1
1     g=rs/(rm*(rm+rdr))
      goto 3
2     g=((rs)*(rm-rdr))/(rm*rxr*rxr)
3     curm=xmp*ccur*g*10000*dk
      bx1=curm*u
      by1=curm*v
      bz1=curm*w
      bx=bx+bx1
      by=by+by1
      bz=bz+bz1
210   continue
      if(nc.le.24) goto 202
201   call circe(x(i),y(j),z(k),bx,by,bz,br,istepx,istepr)
202   continue
      sum(1,ns)=sum(1,ns)+bx
      sum(2,ns)=sum(2,ns)+by
      sum(3,ns)=sum(3,ns)+bz
      if(nc.le.24)go to 203
      sum(6,ns)=sum(6,ns)+bx
      sum(7,ns)=sum(7,ns)+by
      sum(8,ns)=sum(8,ns)+bz
203   continue
199   continue
200   continue
      write(7,192)
      write(7,159) (confg(ioc),ioc=1,18)
      write(7,193) ((coil(ic,ni),ic=1,18),ni=icoil,ncoil)
      write(7,113)
      write(7,116)
      ns=0
      do 410 i=1,im
      do 410 j=1,jm
      do 410 k=1,km
      ns=ns+1
      write(7,111) x(i),y(j),z(k),(sum(ii,ns),ii=1,3)
410   continue
420   continue
      stop
      end

c
c     This subroutine calculates the field of a solenoids due to circular
c     current elements.
c     istepx,istepr are the number of wires in x and r direction which
c     approximated as one wire.
c
      subroutine circe(xp,yp,zp,bx,by,bz,br,istepx,istepr)
      double precision xk1,xk2,k,e
      dimension r(100),xw(100)
      common c1,xl,lay,ntl,ri,ro,curc,kk,ii,jj,nc
      pi=3*atan(sqrt(3.))
      cc=.0000002
      a=ntl-1
      do 10 i=1,ntl
      b=i-1
10    r(i)=(ri+b*(ro-ri)/a)/39.37
      aa=lay
      aa=xl/aa
      do 20 i=1,lay
      xi=i
      xi=xi-.5
20    xw(i)=aa*xi
      br=0
      bx=0
      do 30 i=1,lay,istepx
      do 30 j=1,ntl,istepr
      rho=(sqrt(zp**2+yp**2))/39.37
      c=(xw(i)+c1)*kk
      xx=(xp-c)/39.37
      a=r(j)
      xk2=4.*a*rho/((a+rho)**2+xx**2)
      k=pi/2
      e=k
      if(xk2.eq.0)go to 25
      if(xk2.eq.1)go to 30
      xk1=1-xk2
      g0=13.8629436112d-1
      g1=0.96663442590d-1
      g2=3.590092383d-2
      g3=3.742563713d-2
```

```
      g4=14.51196212d-3
      g5=.5d0
      g6=124.98593597d-3
      g7=.6880248576d-1
      g8=332.8355346d-4
      g9=441.787012d-5
      h0=4432.5141463d-4
      h1=.626060122d-1
      h2=4.757383546d-2
      h3=1.736506451d-2
      h4=24.99836831d-2
      h5=.9200180037d-1
      h6=40.69697526d-3
      h7=.526449639d-2
      k=g0+g1*xk1+g2*xk1**2+g3*xk1**3+g4*xk1**4+(g5+g6*xk1+g7*xk1**2
     1+g8*xk1**3+g9*xk1**4)*(log(1./xk1))
      e=1+h0*xk1+h1*xk1**2+h2*xk1**3+h3*xk1**4+(h4*xk1+h5*xk1**2+h6*xk1
     1**3+h7*xk1**4)*(log(1./xk1))
      br=cc*curc*xx*10000/(rho*((a+rho)**2+xx**2)**.5)*(-k+(a**2+
     1rho**2+xx**2)*e/((a-rho)**2+xx**2))+br
25    continue
      bx=bx+cc*curc*10000/(((a+rho)**2+xx**2)**.5)*(k+(a**2-rho**2-
     1xx**2)*e/((a-rho)**2+xx**2))
30    continue
      xs=istepx
      rs=istepr
      br=br*xs*rs
      bx=bx*xs*rs
      by=0
      bz=0
      if(rho.eq.0)go to 40
      theta=atan(yp/zp)
      bz=br*cos(theta)
      by=br*sin(theta)
40    continue
      return
      end


c
c     This subroutine calculates the endpoints of wire filaments
c     in a coil. The coil is approximated by a series of quadrilateral
c     interfaces.
c  variable           definition
c    ww(i,)        vertex coordinates for each interface.
c    w1(ind)       first endpoint of filament.
c    w2(ind)       second endpoint of filament.
c    lim           second dimension of ww array.
c
      subroutine coors(nint,m,n,ntot,ww,w1,w2,lim)
      dimension ww(4,lim),w1(ntot),w2(ntot)
      if(m.gt.1.and.n.gt.1) go to 100
      ind=0
      if(m+n.ne.2) go to 110
      write(7,200)
200   format("the filament coordinates are already specified")
      return
110   if(m.ne.1) go to 120
      do 40 j=1,n
      do 40 k=1,nint
      ind=ind+1
      w1(ind)=(ww(1,k)*(n-j)+(j-1)*ww(4,k))/float(n-1)
40    continue
      go to 130
120   do 50 i=1,m
      do 50 k=1,nint
      ind=ind+1
      w1(ind)=(ww(1,k)*(m-i)+(i-1)*ww(2,k))/float(m-1)
50    continue
      go to 130
100   ind=0
      do 10 i=1,m
      do 10 j=1,n
      do 10 k=1,nint
      ind=ind+1
      w1(ind)=(ww(1,k)*(n-j)*(m-i)+ww(4,k)*(j-1)*(m-i)+
     1        ww(2,k)*(i-1)*(n-j)+ww(3,k)*(i-1)*(j-1))
     2        /float((m-1)*(n-1))
10    continue
c
c     w2 is generated from w1 so that the endpoints for each coil
c     are together.
c
130   k=m*n


      nn=nint-1
      do 20 l=1,k
      ll=(l-1)*nint
      w2(l*nint)=w1(ll+1)
      do 20 i=1,nn
      w2(i+ll)=w1(i+1+ll)
20    continue
      return
      end
```

Side and Lift Force Coils Magnetic Field system summary output

coil description:
lift coil x(+) y(-) z(-)
lift coil x(+) y(+) z(+)
lift coil x(+) y(-) z(+)
lift coil x(+) y(+) z(-)
lift coil x(-) y(+) z(-)
lift coil x(-) y(-) z(-)
lift coil x(-) y(+) z(+)
lift coil x(-) y(-) z(+)
lift coil 2 x(+) y(-) z(-)
lift coil 2 x(+) y(+) z(+)
lift coil 2 x(+) y(-) z(+)
lift coil 2 x(+) y(+) z(-)
lift coil 2 x(-) y(+) z(-)
lift coil 2 x(-) y(-) z(-)
lift coil 2 x(-) y(+) z(+)
lift coil 2 x(-) y(-) z(+)

X	Y	Z	BX	BY	BZ
inches			gauss		
5.00	0.00	0.00	0.00	0.00	3210.41
4.00	0.00	0.00	0.00	0.00	2498.65
3.00	0.00	0.00	-0.00	0.00	1827.49
2.00	0.00	0.00	-0.00	0.00	1194.03
1.00	0.00	0.00	0.00	-0.00	589.29
0.00	0.00	0.00	-0.00	-0.00	0.00
-1.00	0.00	0.00	-0.00	-0.00	-589.29

Drag Coils Magnetic Field system summary output

coil description:
drag coil 1
drag coil 2

X	Y	Z	BX	BY	BZ
inches			gauss		
5.00	0.00	0.00	-2986.28	0.00	0.00
4.00	0.00	0.00	-2441.84	0.00	0.00
3.00	0.00	0.00	-1862.83	0.00	0.00
2.00	0.00	0.00	-1257.09	0.00	0.00
1.00	0.00	0.00	-633.15	0.00	0.00
0.00	0.00	0.00	0.00	0.00	0.00
-1.00	0.00	0.00	633.15	0.00	0.00

Magnetizing Coils Magnetic Field system summary output

coil description:
Magnetizing coil 1
Magnetizing coil 2

X	Y	Z	BX	BY	BZ
inches			gauss		
5.00	0.00	0.00	-7258.84	0.00	0.00
4.00	0.00	0.00	-7326.72	0.00	0.00
3.00	0.00	0.00	-7379.74	0.00	0.00
2.00	0.00	0.00	-7417.71	0.00	0.00
1.00	0.00	0.00	-7440.53	0.00	0.00
0.00	0.00	0.00	-7448.14	0.00	0.00
-1.00	0.00	0.00	-7440.53	0.00	0.00

Appendix D

COMPUTER PROGRAM TABLE MODIFIED FOR SADDLE COIL CALCULATIONS

Side and lift coils field components on X axis.

Magnetizing coils field components on X axis.

Drag coils field components on X axis.

Since this uses a close approximation to the circular arc, the convergence of the results with increasing the number of divisions was studied and is shown in Figure D-1. For this computation choosing a division of 15 degrees results in a .5% error or less. Thus increments of 15 percent should be conservative for most design calculations.

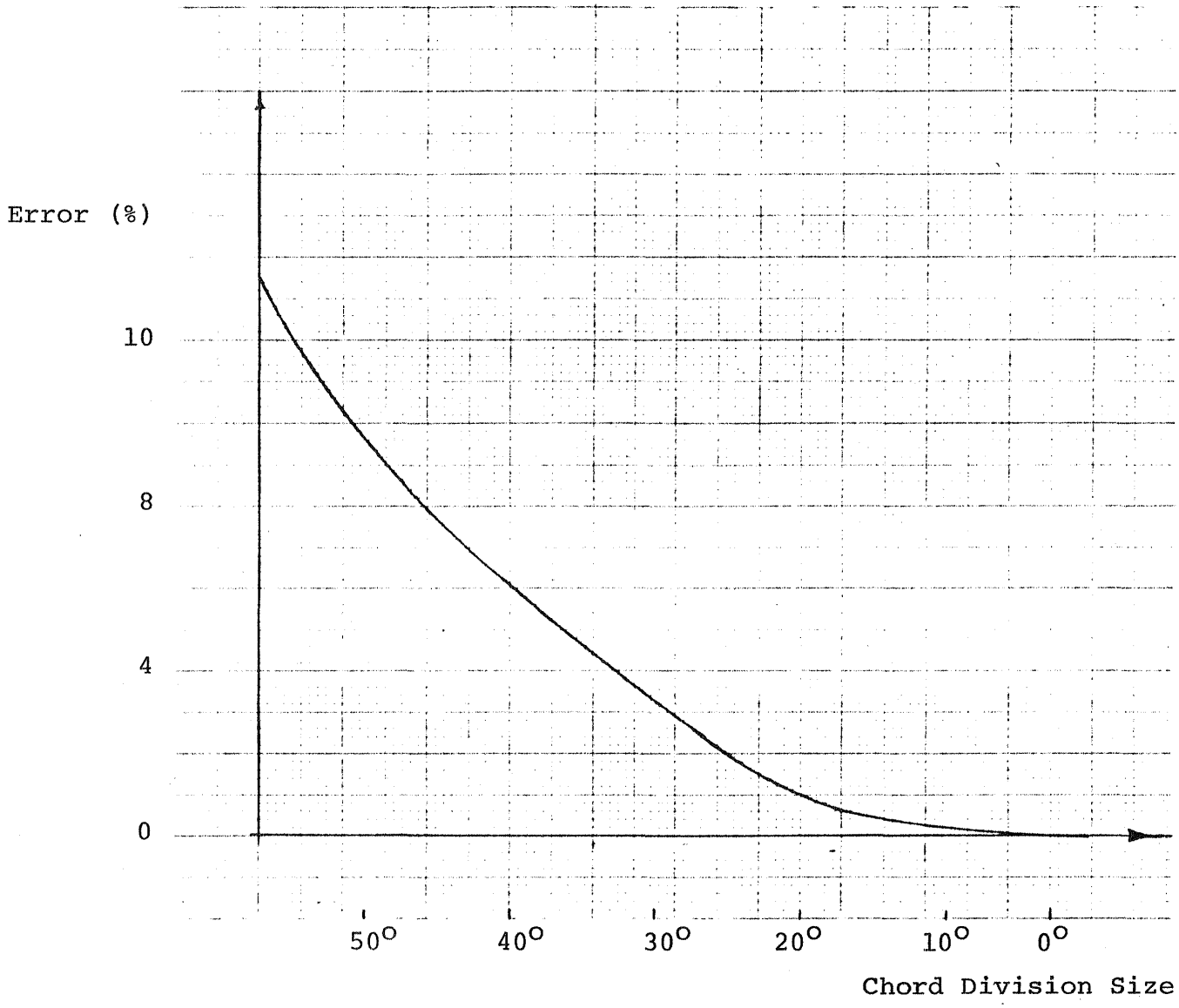

Figure D-1 Convergence characteristic of saddle coil computer results for chord approximation to circular arc.

```
c
c                                TABLE
c                           ---------------
c
      integer out
      dimension x(50),y(50),z(50),yc(5632),zc(5632),
     1x1(5632),y1(5632),z1(5632),x2(5632),y2(5632),z2(5632)
     2,confg(18),coil(18,30),sum(12,50),xx(4,10),yy(4,10),
     3zz(4,10),ld(50)
      common c1,xl,lay,ntl,ri,ro,curc,kk,ii,jj,nc
4     format(1x,3i2,f5.3,i2)
5     format(2f10.4,3i5,3f10.4,2i2)
10    format(2f10.4,2f12.10)
11    format(3i4,3f5.3,3f5.2)
12    format(3i3)
18    format(3i3,f8.3)
19    format(3f8.2)
111   format(1x,3f6.2,5x,3f11.4)
113   format(4x,1hX,5x,1hY,5x,1hZ,15x,2hBX,9x,2hBY,9x,2hBZ)
116   format(6x,6hinches,20x,5hgauss)
155   format(/,18a4)
156   format(18a4)
159   format(24x,18a4)
192   format("1",t40,"system summary output")
193   format(//t20,"coil description:",16(/t20,18a4)//)
450   read(1,10,end=420)da,ams,xkt,xmu
      read(4,4)icoil,ip,isad,dalfa1,kcoil
      xmp=xmu/(4.*3.1415926)
      read(1,156,end=420) (confg(ic),ic=1,18)
      read(1,11)im,jm,km,dx,dy,dz,x(1),y(1),z(1)
      do 2000 i=2,im
2000  x(i)=x(1)-(i-1)*dx
      do 2001 j=2,jm
2001  y(j)=y(1)-(j-1)*dy
      do 2002 k=2,km
2002  z(k)=z(1)-(k-1)*dz
      do 50 j=1,50
      do 50 i=1,12
 50   sum(i,j)=0.
      read(1,12)ncoil,inpopt,out
      write(7,159)(confg(ic),ic=1,18)
      do 200 nc=icoil,ncoil,kcoil
      write(6,299) nc
      if(nc.gt.8)go to 28
299   format(1x,"COIL NUMBER",i10)
      read(1,155)(coil(ic,nc),ic=1,18)
      goto 29
28    continue
      if(nc.gt.16)go to 27
      read(2,155)(coil(ic,nc),ic=1,18)
      go to 29
27    if(nc.gt.24)goto26
      read(3,155)(coil(ic,nc),ic=1,18)
      go to 29
26    read(4,155)(coil(ic,nc),ic=1,18)
      read(4,5)c1,xl,lay,ntl,kk,ri,ro,curc,istepx,istepr
      go to 310
29    continue
      write(6,155) (coil(ic,nc),ic=1,18)
      if(nc.gt.8)go to 59
      read(1,18)mm,nn,nint,ccur
      go to61
59    continue
      if(nc.gt.16)go to 57
      read(2,18)mm,nn,nint,ccur
      go to 61
57    read(3,18)mm,nn,nint,ccur
61    continue
      do 80 j=1,nint
      do 80 i=1,4
      if(nc.gt.8) goto79
      read(1,19)xx(i,j),yy(i,j),zz(i,j)
      go to 80
79    continue
      if(nc.gt.16)go to 77
      read(2,19)xx(i,j),yy(i,j),zz(i,j)
      go to 80
77    read(3,19)xx(i,j),yy(i,j),zz(i,j)
80    continue
      ntot=mm*nn*nint
      call coors(nint,mm,nn,ntot,xx,x1,x2,10)
c
c     if isad=0      regular coil
c     if isad=1      saddle  coil
c
      if(isad.eq.0)go to 75
      i1=2
      if(xx(1,2).ne.xx(1,1))i1=3
      call saddle(mm,nn,ntot,yy,zz,y1,z1,y2,z2,i1)
      go to 76
75    continue
      call coors(nint,mm,nn,ntot,yy,y1,y2,10)
      call coors(nint,mm,nn,ntot,zz,z1,z2,10)
76    continue
      if(nc.ne.ip) go to 106
      im=0
      m2=4*nn-7
      mi=2*nn-4
      do 99 m=1,m2,mi
      im=im+1
      ld(im)=4*nn*(mm-1)+m
      ld1=ld(im)
      x(im)=(x1(ld1)+x2(ld1))/2
      y(im)=(y1(ld1)+y2(ld1))/2
      z(im)=(z1(ld1)+z2(ld1))/2
```

```
99    continue
106   continue
310   continue
      lm=ntot
      ns=0
      do 199 i=1,im
      j=i
      k=i
      ns=ns+1
298   format(1x,"NO. OF POINT",i10)
      if(nc.gt.24)go to 201
      bx=0.0
      by=0.0
      bz=0.0
      ll=ld(i)

      do 210 l=1,lm
      if(nc.ne.ip)go to 105
      if(l.eq.ll)go to 198
      go to 105
198   write(7,104) i,x1(l),y1(l),z1(l),x2(l),y2(l),z2(l),l
104   format(2x,i2,2x,6(f7.3,2x),i7)
      go to 210
105   continue
      dk=1
      a=(x1(l)-x(i))/39.37
      b=(x2(l)-x(i))/39.37
      c=(y1(l)-y(j))/39.37
      d=(y2(l)-y(j))/39.37
      e=(z1(l)-z(k))/39.37
      f=(z2(l)-z(k))/39.37
c
c     This part divides each arc into predetermined
      divisions and computes
c     field due to the chords of those arcs.
c     dalfa1 is the arbitrary arc division in radians.
c
      if(isad.eq.0)go to 74
      if(x2(l).ne.x1(l))go to 74
      if(y1(l).eq.0)y1(l)=0.0001
      if(z1(l).eq.0)z1(l)=0.0001
      alfa1=atan(y1(l)/z1(l))
      alfa=(3.14159/4.-abs(alfa1))*2
      nalfa=abs(alfa)/dalfa1
      if(nalfa.eq.0)nalfa=1
      dalfa=alfa/nalfa

      ky=yy(1,1)/abs(yy(1,1))
      kz=zz(1,1)/abs(zz(1,1))
      r=((y1(l))**2+(z1(l))**2)**.5
      do 73 ii=1,nalfa+1
      beta=abs(alfa1)+(ii-1)*dalfa
      yc(ii)=r*ky*abs(sin(beta))
      zc(ii)=r*kz*abs(cos(beta))
73    continue
      do 72 ii=1,nalfa
      a=(x1(l)-x(i))/39.37
      b=(x2(l)-x(i))/39.37
      c=(yc(ii)-y(j))/39.37
      d=(yc(ii+1)-y(j))/39.37
      e=(zc(ii)-z(k))/39.37
      f=(zc(ii+1)-z(k))/39.37
74    continue
      u=c*f-d*e
      v=e*b-f*a
      w=a*d-b*c
195   format(1x,"ldd=",i3,2x,6(f7.3,2x,"i=",i3),
       "l=",i3,2x,"i=",i3)
      r1=(a*a+c*c+e*e)**.5
      r2=(b*b+d*d+f*f)**.5
      rs=r1+r2
      rm=r1*r2
      rdr=a*b+c*d+e*f
      rxr=(u**2+v**2+w**2)**.5
194   continue
      h=(rm+rdr)/rm
      if(h-0.01)2,1,1
1     g=rs/(rm*(rm+rdr))
      goto 3
2     g=((rs)*(rm-rdr))/(rm*rxr*rxr)
3     curm=xmp*ccur*g*10000*dk
      bx1=curm*u
      by1=curm*v
      bz1=curm*w
      bx=bx+bx1
      by=by+by1
      bz=bz+bz1
72    continue
210   continue
      if(nc.le.24) goto 202
201   call circe(x(i),y(j),z(k),bx,by,bz,br,istepx,istepr)
```

```
202   continue
      sum(1,ns)=sum(1,ns)+bx
      sum(2,ns)=sum(2,ns)+by
      sum(3,ns)=sum(3,ns)+bz
      if(nc.le.24)go to 203
      sum(6,ns)=sum(6,ns)+bx
      sum(7,ns)=sum(7,ns)+by
      sum(8,ns)=sum(8,ns)+bz
203   continue
      write(7,111) x(i),y(j),z(k),bx,by,bz
199   continue
200   continue
      write(7,88) dalfa1
88    format(5x,"DALFA = ",f15.5)
      write(7,192)
      write(7,159) (confg(ioc),ioc=1,18)
      write(7,193) ((coil(ic,ni),ic=1,18),ni=icoil,ncoil)
      write(7,113)
      write(7,116)
      ns=0
      do 410 i=1,im
      ns=ns+1
      j=i
      k=i
410   write(7,111) x(i),y(j),z(k),(sum(ii,ns),ii=1,3)
      write(6,86)
86    format("DO YOU WANT TO REPEAT ? ENTER NONZERO DALFA")
      read(5,83) dalfa1
83    format(1x,f5.3)
      if(dalfa1.eq.0)go to 420
      do 84 i=1,3
      do 84 n=1,ns
84    sum(i,n)=0
      go to 310
420   continue
      stop
      end
      subroutine circe(xp,yp,zp,bx,by,bz,br,istepx,istepr)
      double precision xk1,xk2,k,e
      dimension r(100),xw(100)
      common c1,xl,lay,ntl,ri,ro,curc,kk,ii,jj,nc
      pi=3*atan(sqrt(3.))
      cc=.0000002
      a=ntl-1
      do 10 i=1,ntl
      b=i-1
10    r(i)=(ri+b*(ro-ri)/a)/39.37
      aa=lay
      aa=xl/aa
      do 20 i=1,lay
      xi=i
      xi=xi-.5
20    xw(i)=aa*xi
      br=0
      bx=0
      do 30 i=1,lay,istepx
      do 30 j=1,ntl,istepr
      rho=(sqrt(zp**2+yp**2))/39.37
      c=(xw(i)+c1)*kk
      xx=(xp-c)/39.37
      a=r(j)
      xk2=4.*a*rho/((a+rho)**2+xx**2)
      k=pi/2
      e=k
      if(xk2.eq.0)go to 25
      if(xk2.eq.1)go to 30
      xk1=1-xk2
      g0=13.8629436112d-1
      g1=0.9666344259Od-1
      g2=3.590092383d-2
      g3=3.742563713d-2
      g4=14.51196212d-3
      g5=.5d0
      g6=124.98593597d-3
      g7=.6880248576d-1
      g8=332.8355346d-4
      g9=441.787012d-5
      h0=4432.5141463d-4
      h1=.6260601220-1
      h2=4.7573835460-2
      h3=1.7365064510-2
      h4=24.9923823 1d-2
      h5=.9200180037d-1
      h6=40.6969752 6d-3
      h7=.526449639d-2
      k=g0+g1*xk1+g2*xk1**2+g3*xk1**3+g4*xk1**4+(g5+g6*xk1+g7*xk1**2
     1+g8*xk1**3+g9*xk1**4)*(log(1./xk1))
      e=1+h0*xk1+h1*xk1**2+h2*xk1**3+h3*xk1**4+(h4*xk1+h5*xk1**2+h6*xk1
     1**3+h7*xk1**4)*(log(1./xk1))
      br=cc*curc*xx*10000/(rho*((a+rho)**2+xx**2)**.5)*(-k+(a**2+
     1rho**2+xx**2)*e/((a-rho)**2+xx**2))+br
25    continue
      bx=bx+cc*curc*10000/(((a+rho)**2+xx**2)**.5)*(k+(a**2-rho**2-
     1xx**2)*e/((a-rho)**2+xx**2))
      go to 30
```

```
30    continue
      xs=istepx
      rs=istepr
      br=br*xs*rs
      bx=bx*xs*rs
      by=0
      bz=0
      if(rho.eq.0)go to 40
      theta=atan(yp/zp)
      bz=br*cos(theta)
      by=br*sin(theta)
40    continue
      return
      end
                subroutine coors(nint,m,n,ntot,ww,w1,w2,lim)
      dimension ww(4,lim),w1(ntot),w2(ntot)
      if(m.gt.1.and.n.gt.1) go to 100
      ind=0
      if(m+n.ne.2) go to 110
      write(7,200)
200   format("the filament coordinates are already specified")
      return
110   if(m.ne.1) go to 120
      do 40 j=1,n
      do 40 k=1,nint
      ind=ind+1
      w1(ind)=(ww(1,k)*(n-j)+(j-1)*ww(4,k))/float(n-1)
40    continue
      go to 130
120   do 50 i=1,m
      do 50 k=1,nint
      ind=ind+1
      w1(ind)=(ww(1,k)*(m-i)+(i-1)*ww(2,k))/float(m-1)
50    continue
      go to 130
100   ind=0
      do 10 i=1,m
      do 10 j=1,n
      do 10 k=1,nint
      ind=ind+1
      w1(ind)=(ww(1,k)*(n-j)*(m-i)+ww(4,k)*(j-1)*(m-i)+
     1         ww(2,k)*(i-1)*(n-j)+ww(3,k)*(i-1)*(j-1))
     2         /float((m-1)*(n-1))
10    continue
130   k=m*n
      nn=nint-1
      do 20 l=1,k
      ll=(l-1)*nint
      w2(l*nint)=w1(ll+1)
      do 20 i=1,nn
      w2(i+ll)=w1(i+1+ll)
20    continue
      return
      end
```

This subroutine calculates current element endpoints of a saddle type coil. Saddle is consistent with the subroutine Coors as long as numbering and direction of current elements is concerned. (refer to (3)).

Inputs are the interface coordinates.

```
      subroutine saddle (m,n,ntot,u,v,u1,v1,u2,v2,i1)
      dimension v(4,4),u(4,4),u1(ntot),v1(ntot),u2(ntot),
     1          v2(ntot)
      ro=sqrt(u(1,1)**2+v(1,1)**2)
      ri=sqrt(u(3,1)**2+v(3,1)**2)
      q=sqrt(2.)
      ind=0
      ku=u(1,1)/abs(u(1,1))
      kv=v(1,1)/abs(v(1,1))
      d1=1.
      d2=ri*q/2.
      r4=sqrt(u(4,1)**2+v(4,1)**2)
      if(abs(r4-ro)-.1)5,7,7
```

```
7     continue
      do 1 i=1,m
      do 1 j=1,n
      do 1 k=1,4
      ind=ind+1
      r=ro-(ro-ri)/(n-1)*(j-1)
      a=(d2-(d2-d1)/(m-1)*(i-1))*q
      u1(ind)=(sqrt(2*r**2-a**2)-a)/2.
      if(u1(ind).eq.0.0) u1(ind)=.0001
      v1(ind)=(abs(u1(ind))+a)
      if(abs(u(1,1)).le.abs(v(1,1)))go to 8
      temp=u1(ind)
      u1(ind)=v1(ind)
      v1(ind)=temp
8     u1(ind)=u1(ind)*ku
      v1(ind)=v1(ind)*kv
1     continue
      go to 4
5     continue
         nm=n
      n=m
      m=nm
      do 6 j=1,n
       do 6 i=1,m
       do 6 k=1,4
      ind=ind+1
      r=ro-(ro-ri)/(n-1)*(j-1)
      a=(d2-(d2-d1)/(m-1)*(i-1))*q
      u1(ind)=(sqrt(2*r**2-a**2)-a)/2.
      if(u1(ind).eq.0.0) u1(ind)=.0001
      v1(ind)=(abs(u1(ind))+a)
      if(abs(u(1,1)).le.abs(v(1,1)))go to 9
      temp=u1(ind)
      u1(ind)=v1(ind)
      v1(ind)=temp
9     u1(ind)=u1(ind)*ku
      v1(ind)=v1(ind)*kv
6     continue
4     continue
      do 2 i=i1,ind,4
      u1(i)=abs(v1(i-1))*ku
      v1(i)=abs(u1(i-1))*kv
      u1(i+1)=abs(u1(i))*ku
      v1(i+1)=abs(v1(i))*kv
```



```
2     continue
      do 3 i=1,ind
      u2(i)=u1(i+1)
      v2(i)=v1(i+1)
      if(i/4*4.ne.i)go to 3
      u2(i)=u1(i-3)
      v2(i)=v1(i-3)
3     continue
      return
      end
aaaaaa
```

system summary output

```
coil description:
lift coil x(+) y(-) z(-)
lift coil x(+) y(+) z(+)
lift coil x(+) y(-) z(+)
lift coil x(+) y(+) z(-)
lift coil x(-) y(+) z(-)
lift coil x(-) y(-) z(-)
lift coil x(-) y(+) z(+)
lift coil x(-) y(-) z(+)
lift coil 2 x(+) y(-) z(-)
lift coil 2 x(+) y(+) z(+)
lift coil 2 x(+) y(-) z(+)
lift coil 2 x(+) y(+) z(-)
lift coil 2 x(-) y(+) z(-)
lift coil 2 x(-) y(-) z(-)
lift coil 2 x(-) y(+) z(+)
lift coil 2 x(-) y(-) z(+)
lift coil 3 x(+) y(-) z(-)
lift coil 3 x(+) y(+) z(+)
lift coil 3 x(+) y(-) z(+)
lift coil 3 x(+) y(+) z(-)
lift coil 3 x(-) y(+) z(-)
lift coil 3 x(-) y(-) z(-)
lift coil 3 x(-) y(+) z(+)
lift coil 3 x(-) y(-) z(+)
```

X	Y	Z	BX	BY	BZ
inches			gauss		
5.00	0.00	0.00	-0.8278	1.0990	2888.2894
4.00	0.00	0.00	-0.9422	0.9798	2279.5496
3.00	0.00	0.00	-1.0103	0.8412	1686.3673
2.00	0.00	0.00	-1.0309	0.6968	1110.9974
1.00	0.00	0.00	-1.0097	0.5584	550.6235
0.00	0.00	0.00	-0.9571	0.4335	-1.3004
-1.00	0.00	0.00	-0.8839	0.3266	-553.2781

The results are not symmetrical exactly because of different layer and turn per layer for each coil set while having the same ampere turns.

1 **system summary output**

coil description:
drag coil 1-a
drag coil 2-a
drag coil 1-b
drag coil 2-b

X	Y	Z	BX	BY	BZ
inches			gauss		
5.00	0.00	0.00	-3866.7193	0.0000	0.0000
4.00	0.00	0.00	-2983.0098	0.0000	0.0000
3.00	0.00	0.00	-2155.8302	0.0000	0.0000
2.00	0.00	0.00	-1393.5434	0.0000	0.0000
1.00	0.00	0.00	-682.8394	0.0000	0.0000
0.00	0.00	0.00	0.0000	0.0000	0.0000
-1.00	0.00	0.00	682.8394	0.0000	0.0000

1 **system summary output**

coil description:
Magnetizing coil 1
Magnetizing coil 2

X	Y	Z	BX	BY	BZ
inches			gauss		
5.00	0.00	0.00	10736.4222	0.0000	0.0000
4.00	0.00	0.00	9353.5276	0.0000	0.0000
3.00	0.00	0.00	8309.1200	0.0000	0.0000
2.00	0.00	0.00	7586.6281	0.0000	0.0000
1.00	0.00	0.00	7164.1253	0.0000	0.0000
0.00	0.00	0.00	7025.2583	0.0000	0.0000
-1.00	0.00	0.00	7164.1253	0.0000	0.0000

1. Report No.	2. Government Accession No.	3. Recipient's Catalog No.
NASA CR-165660		

4. Title and Subtitle	5. Report Date
APPLICATION OF SUPERCONDUCTING COILS TO THE NASA PROTOTYPE MAGNETIC BALANCE	January 1981
	6. Performing Organization Code
7. Author(s) C. W. Haldeman, R. A. Kraemer, S. W. Prey, M. M. Alishahi and E. E. Covert	8. Performing Organization Report No. MIT TR 207
	10. Work Unit No.
9. Performing Organization Name and Address Massachusetts Institute of Technology Aerophysics Laboratory Cambridge, Ma 02139	11. Contract or Grant No. NSG 1356
	13. Type of Report and Period Covered Contractor Report 1-1-77 to 8-31-80
12. Sponsoring Agency Name and Address National Aeronautics and Space Administration Washington, DC 20546	14. Sponsoring Agency Code 505-31-53-02

15. Supplementary Notes

Langley Technical Monitor: Richmond P. Boyden

16. Abstract

Application of superconducting coils to a general purpose magnetic balance is studied. Under the conditions of operation with fields of 1 or 2 Tesla and frequencies of 20-40 Hz as well as D.C., the most suitable currently available superconducting cable for coils appears to be a bundle of many fine wires which are transposed and are mechanically confined. Sample coils were constructed and tested using such a cable of 220 strands of varnish insulated .064 mm O.D. copper stabilized Nb-Ti superconductor and cables of the same superconducting area, but 55 .122 mm diameter strands. Sample coils were tested at central A.C. fields up to .5 Tesla, slewing rates up to 53 Tesla/sec and frequencies up to 30 Hz. A.C. losses were measured from helium boil-off and were approximately 20 percent higher than those calculated. Losses were dominated by hysteresis and a model for loss calculation which appears suitable for design purposes is presented along with computer listings.

Combinations of two coils were also tested and interaction losses are reported. Again, the proposed loss models appear adequate at high currents for which design calculations would be carried out.

Two feasible geometries are presented for a version of the NASA-MIT prototype magnetic balance using superconductors.

17. Key Words (Suggested by Author(s))	18. Distribution Statement
Magnetic suspension Superconducting coils Litz wire A.C. superconductors Interaction losses A.C. losses	Unclassified - Unlimited Star Category - 09

19. Security Classif. (of this report)	20. Security Classif. (of this page)	21. No. of Pages	22. Price*
Unclassified	Unclassified	142	A07

For sale by the National Technical Information Service, Springfield, Virginia 22161

End of Document